Imperial College London

Renewable Chitin Based Nanomaterials from Fungi

Wan Mohd Fazli Wan Nawawi

June 2016

A dissertation submitted in partial fulfillment of the requirement for the degree of Doctor of Philosophy of Imperial College London

Department of Chemical Engineering,
Imperial College London, South Kensington Campus,
SW7 2AZ London, UK

DECLARATION & COPYRIGHT

This dissertation is a description of the work carried out by the author in the Department of Chemical Engineering, Imperial College London between June 2012 to June 2016 under the supervision of Prof Alexander Bismarck and Prof Richard Murphy. Except where acknowledged, the material presented is the original work of the author and no part of it has been submitted for a degree at this or any other university.

Wan Mohd Fazli Wan Nawawi

June 2016

ABSTRACT

Fungal cell walls are rich in structural fibers made of chitin and glucan. These fibers were covalently linked, forming a ready-made nanocomposite fabric which is potentially useful in the development of a single-sourced bioreinforcement material that combines the strength of chitin and the toughness of glucan. In this study, chitin-glucan material was extracted from common mushroom (*Agaricus bisporus*) and tree bracket fungi (*Daedaleopsis confragosa*). Animal chitin extracted from crab shells (*Cancer pagurus*) was used as a comparison. We adopted mild extraction process to preserve the native quality of chitin-glucan within the fungal source.

Six themes will be discussed: (1) comparison between fungal-based and animal-based chitin, (2) the effect of grammage on fungal chitin film, (3) the effect of blending time on fungal chitin film, (4) composite preparation using combination of different fungal extracts, (5) preparation of high volume fraction fungal-based chitin laminates, and (6) utilization of fungal chitin nanofiber as a natural binder for loose flax fiber.

Extracts from common mushroom were found to be (1) readily disintegrated into nanofiber dimension (10–20 nm wide, several micrometers long) without any post-mechanical treatment, (2) more hydrophobic than animal based chitin, and (3) possess a film forming capability. Extracts from tree bracket fungi assumes microfiber dimension (1–2 μm wide, several micrometers long) and require specialized equipment for further nanofibrillation. Chitin to glucan ratio in common mushroom was found to be nearly equal at 40:50, while glucan predominates in bracket fungi (chitin to glucan, 1:99). This translates to distinct mechanical properties, in which strong films having tensile strength of ~200 MPa were produced from common mushroom extract, while tough films with elongation at break exceeding 10% were produced from bracket fungi. The strength of common mushroom nanofibers is further extended as a reinforcement in epoxy laminated composite and as a binder for nonwoven flax preform.

ACKNOWLEDGEMENTS

In the Name of Allah, Most Gracious, Most Merciful

All praise to God for giving me this opportunity to conduct and complete my PhD study at Imperial College London – a world class institution renowned for its research excellence.

My wholehearted thank to my dear wife, Norul Najwa Arshad, for all her sacrifices and patience during the whole course of my study. Thank you for keeping me motivated, listening to my ramblings, and all your encouragements which had kept me going. I also would like to express my highest gratitude to my mom, Nora Nawawi, my dad, Wan Nawawi, and my mom-in-law, Siti Aminah, for their unconditional love and support – and by extension to all my family members.

I would like to express my special gratitude to my supervisors, Prof. Alexander Bismarck and Prof. Richard Murphy for their superb guidance and continuous support towards my research. Especially for Alex, thank you being so kind and understanding, and allowing me to work in your Vienna lab during the final phase of my research. Hopefully we can continue to work and collaborate in the forthcoming future.

Further thanks to all personnel in PaCE group (both at Imperial and Vienna): Koon Yang Lee, Siti Rosminah Shamsuddin, Shukor Zainol Abidin, Ain Kamal, Min Tang, Jing Li, Andreas Mautner, Marta Fortea-Verdejo, Dmitrii Rusakov, Hele Diao, Henry Maples, Michael Tebboth, Robert Woodward, Francois de Luca, Natasha Shirshova, Ling Ching Wong, Jonny Blaker, and Tomi Herceg. Special thanks also to Eero Kontturi, Katri Kontturi , Umang Shah, and David Anthony. Not to forget the lab technicians and admin/support staffs who had helped me during my study, namely: Patricia Carry, Andrew Macey, Chin Lang, Claudia Mitterer (Vienna), Alex Hubner (Vienna), Susi Underwood, Claudia Weber (Vienna), Severine Toson, Sarah Payne, Ben Kistnah, and Keith Walker. Special thanks also to my PhD thesis examiner, Prof. Alain Dufresne from Grenoble INP, France, and Dr. Jerry Heng from Imperial College London,UK.

Finally, I would like to thank my sponsor, International Islamic University Malaysia and Ministry of Education Malaysia for granting me the opportunity to study in such highly regarded establishment and pursuing my passion in academia.

Thank you

TABLE OF CONTENTS

LIST OF FIGURES

Chapter 2

Chapter 3

Chapter 4

Chapter 5

Chapter 6

LIST OF TABLES

Chapter 6

CHAPTER ONE
INTRODUCTION

1.1 Background of the Study

Natural fibers, are an attractive, widely available and relatively cheap reinforcing agent who received much renewed interest in recent years due to public demand for eco-friendly products and intensifying legislative pressure for greener, sustainable and carbon neutral materials. Their increased use was also encouraged by the fear of depleting fossil resources, which is the largest source of monomers from which the majority of polymers are generated. Common synthetic polymers, such as polyethylene terephthalate (PET), polyethylene (PE), polyvinyl chloride (PVC), polypropylene (PP), polystyrene (PS) and many others are mostly non-biodegradable thus contributing to piles of wastes not only on overflowing landfill sides but also in the environment.

However, biopolymers, such as starch, lignocellulose, casein and polyhydroxylalkanoates (PHA) or bio-derived polymers, such polylactic acid (PLA), just to name a few, have often inferior properties compared to their synthetic counterparts. Developing composites is thus a vital strategy to enhancing their mechanical performance. The addition of reinforcing agents or fillers into renewable polymers in the form of fibers, which are inherently stiff and strong has given rise to a unique family of materials that combine the properties of the reinforcement with the processability of plastics.

One interesting way to improve the properties of biopolymers is to introduce nanoscale biofillers for even better reinforcement. This is expected to eventually give rise to polymers with much improved load bearing capacity because of the larger filler and polymer interface. Natural fibers have a lower density than widely used glass fibers, a parameter that is particularly important when the part weight of a structure needs to be reduced. But the greatest appeal in using natural fibers lies in their renewability, sustainability and biodegradability. Thus, the challenge in substituting conventional polymer composites with composites created from naturally available feedstock is to design materials that exhibit structural and functional integrity during use and are only susceptible to microbial and environmental degradation after disposal (or triggered treatment) and without any significant negative environmental impact.

1.2 Problem Statements

Chitin nanoparticles (nanofibers or whiskers) have been viewed as a promising renewable nanoreinforcement for composite production. However, most studies are using crustacean shells as chitin source. It is known that chitin is the structural element in fungi and, therefore, fungal derived chitin could offer a valuable source to new chitin based materials. The uncertainty and inconsistency of shellfish which is subject to seasonal and regional supply fluctuations coupled with increasing levels of heavy metals (and radioactive pollution) of the sea intensify the need of viewing fungal chitin as a viable alternative to animal-based chitin.

1.3 Research Objectives

The primary aim of this research is to develop an effective extraction procedure of fungal chitin nanofibers and to prepare chitin films and chitin base composites. The specific objectives include:

1. To extract chitin nanofibers from fungi. Common mushroom, *A. bisporus*, was chosen as typical example. In order to access the quality of the chitin, it has to be extracted from different parts, i.e. stalk, cap, and whole fruiting body of the mushroom. Chitin nanofiber films made from common mushroom are to be compared with films made from chitin nanofibers extracted from crab shells, *C. pagurus*.
2. To evaluate the effect of grammage on the properties of chitin films made from common mushroom nanofibers.
3. To extract chitin microfibers from tree bracket fungi, *D. confragosa* and to prepare and characterize the films made from it. Films made from extracted fibers will be compared with films made from non-purified tree bracket fungi fiber extract.
4. To prepare and characterize thin film composites made from common mushroom nanofibers and tree bracket fungi microfibers.
5. To prepare and characterize high reinforcement volume fraction chitin film base laminated epoxy composites.
6. To prepare and characterize flax nonwoven preforms using common mushroom nanofibers as a binder.

1.4 Structure of the Thesis

This thesis is divided into 7 chapters. The introduction (Chapter 1) includes the background and objectives of the research, as well as an overview of the thesis. Chapter 2 reviews the trends in chitin nanoparticle research with emphasis on chitin films and nanocomposites. This chapter also reviews the difference between animal-based chitin and fungal-based chitin. Chapter 3 describes the materials and methodology used for this research and the produced results are covered in the following three experimental chapters (Chapter 4, 5, and 6). Chapter 4 compares chitin nanofibers isolated from crab and chitin nanofibers isolated from different parts of common mushrooms. The effect of grammage on the properties of mushroom chitin films will be discussed at the end of this chapter. In Chapter 5, the discussion revolves around the extracts from tree bracket fungi. This extract has been used to produce film and composites which will be compared to common mushroom nanofibers. The prospects of using mushroom chitin nanofibers to prepare high volume fraction chitin film base epoxy (thermosetting) laminated composites and to bind loose flax fibers will be evaluated in Chapter 6. The conclusions drawn from this research and suggestions for future work are presented in Chapter 7.

CHAPTER TWO
LITERATURE REVIEW

2.1 Introduction

Chitin is a fibrous biopolymer that makes up the crustacean shell, the insect exoskeleton, and the fungal cell wall. It is a renewable, biodegradable, and non-toxic material with abundance second only to cellulose. In the coming sections, we will first look at the parallel history between chitin and cellulose. Next, we will discuss chitin in terms of its structure, origin and extraction process. The role of chitin nanofibers and whiskers in film and nanocomposite fabrication will be further elucidated. Finally, we will discuss the advantages and disadvantages of using fungal-based chitin over animal-based chitin.

2.2 Brief History of Chitin

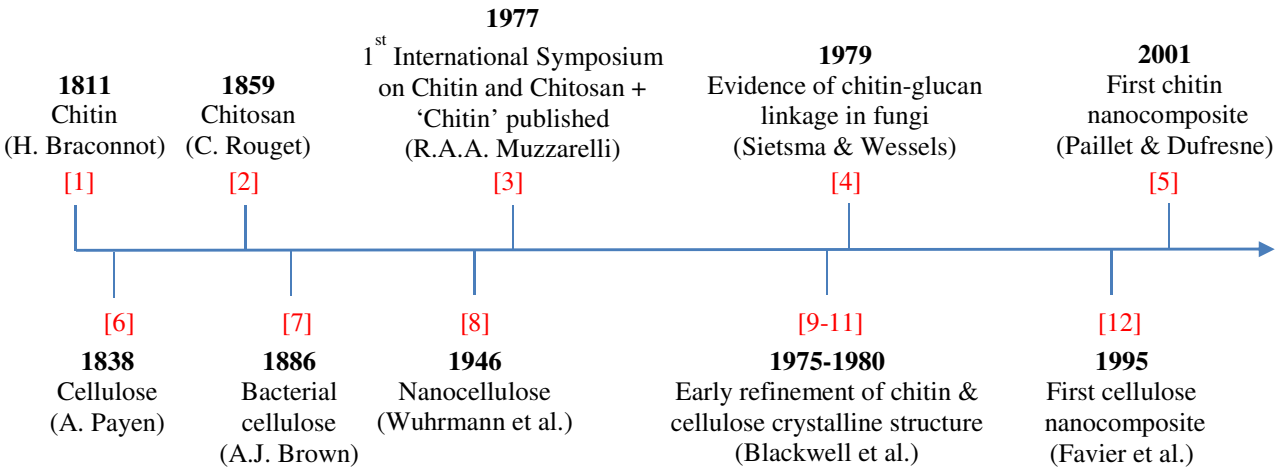

Figure 2.1 Timeline of early discoveries and breakthrough in chitin and cellulose field.

Figure 2.1 depicts major discoveries and the early breakthrough in the field of chitin and cellulose. Interested reader can obtain additional details elsewhere [13-15]. Although Braconnot's isolation of chitin preceded Payen's isolation of cellulose by almost 30 years, research and

industrial application of chitin has much lagged behind to that of cellulose. Upsurge of interest in chitin only started in the 70s, where at least three factors help to contribute: (1) publication of '*Natural Chelating Polymer*'[16] and '*Chitin*'[3] by Muzzarelli, (2) organization of 1st International Conference on Chitin and Chitosan in 1977 – now in its 13th edition, and (3) growth of aquaculture and shellfish consumption in Asia [15]. Nowadays, the momentum continues with dedicated societies like Japanese Society for Chitin & Chitosan (established in 1989), European Chitin Society (established in 1996) and Indian Chitin Society (established in 2010). More and more dedicated symposiums have been organized across the globe such as Japanese Chitin & Chitosan Symposium (2016 = 30th edition), International Conference of the European Chitin Society (2015 = 12th edition), The Asia-Pacific Chitin & Chitosan Symposium (2016 = 11th edition), Iberoamerican Chitin Symposium (2015 = 7th edition), and Indian Chitin & Chitosan Symposium (2016 = 5th edition).

We will now take a brief walk into the parallel history of chitin and cellulose in recent years: the pioneering works and the breakthroughs. The focus will be directed on nanofiber-based sheets and nanocomposites.

Unlike starch which is granular in nature, both cellulose and chitin are fibrous. Hence, they are prime candidates for sheets, films, or paper-making. A stronger paper can be made by fibrillating the fibers into nanofibers. Smaller fibers provide bigger surface area, creating more hydrogen bonding and entanglement which consequently leads to stronger sheets. Yamanaka et al. [17] was the first to demonstrate in 1983 that bacterial nanocellulose sheets possess a remarkable tensile modulus (E) and tensile strength (σ) of 15–18 GPa and ~250 MPa, respectively. The first study on strong sheets from kraft pulp nanocellulose was carried out in 2008 by Lars Berglund's group in Sweden (E = 13.2 GPa, σ = 214 MPa) [18]. By orienting the fiber by a means of cold drawing [19], they managed to produce the highest value for cellulose nanopaper so far : E = 24.6 GPa, σ = 428 MPa. This is 13 times stiffer and 13 times stronger than standard A4 paper[1].

The first report on chitin nanofiber sheets comes in 1992 [20], in which sheets made from crab chitin (α-chitin) were compared to sheets made from squid pen chitin (β-chitin). However, the nanofibers used in that study had a relatively large diameter (~100 nm in width). Research

[1] Based on tensile test of standard office A4 paper with 80 g/m^2 grammage, measured in our laboratory: E = 1.9 GPa, σ = 31.9 MPa, tensile strain at maximum strength = 1.41%, tensile toughness = 0.5 MJ/m^3.

with smaller chitin nanofibers (10–20 nm in width) was started more recently in 2010 by a Japanese team led by Shinsuke Ifuku [21-24]. Their chitin sheet has decent mechanical properties (E = 2.5 GPa, σ = 42 MPa) [25]. In 2014, Berglund's group [26] managed to obtain substantial improvement (E = 7.3 GPa, σ = 153 MPa) which is the highest reported value for chitin sheets in literature so far.

When Turbak et al. [27] first demonstrated that large quantities of cellulose nanofibers can be obtained by homogenizing kraft pulp at high pressure, scientists started to play with the idea of using natural fibers as a potential nanoreinforcement in composite materials. Pioneering works in 1995 by a group of scientists at CERMAV[2] have led the way [12]. At first, they used the crystalline part of the cellulose nanofiber called whiskers (or cellulose nanocrystals) to reinforce a latex polymeric matrix. By adding 6% tunicin whiskers [12] or 30% wheat straw whiskers [28, 29], they observed a 1000-fold improvement in storage modulus. Later, they used cellulose nanofibers to reinforce a starch-based matrix [30, 31]. By adding 5% potato pulp nanofibers, they observed a significant improvement (at least two orders of magnitude) in storage modulus compared to a neat starch film.

Inspired by the reinforcing effect provided by cellulose, these CERMAV scientists started to do pioneering work on nanocomposite reinforced by chitin. They have used chitin whiskers isolated from squid pen [5], *Riftia* tube [32], and crab shells [33-35]. The first report on chitin nanofiber as reinforcement in composite comes much more recently. In 2011, a Japanese team led by Ifuku impregnated chitin nanofiber film in eleven different types of thermoplastic (meth)acrylic resin to obtain transparent nanocomposite films – all of which show great improvement in mechanical properties compared with the neat resin [25].

All aforementioned nanocomposite studies deal with water-based or thermoplastic resins. Thermoset matrix like epoxy or phenol-formaldehyde is often favored when a high performance material is required. In 2000, CERMAV scientists once again published a pioneering study by using cellulose tunicin whiskers to reinforce a waterborne epoxy resin [36]. However, a major breakthrough was made 5 years later by Yano and co-workers in Japan [37]. They demonstrated that a strong nanocomposite with a bending modulus (E_b) of 19 GPa and a bending strength (σ_b) of 370 MPa can be made when kraft pulp nanofibers were used as a reinforcement in a phenolic resin. An even higher modulus and strength (E_b = 28 GPa, σ_b ~410 MPa) was obtained when

[2] Centre de Recherches sur les Macromolécules Végétales, Grenoble, France.

bacterial cellulose nanofibers were used in the same resin [38]. This is the highest reported value in cellulose nanocomposite field so far and to put this into perspective, the measured strength is almost comparable to structural steel [39]. It is worth noting that Yano used a high cellulose content (>80%) and a very high compressive pressure (50–100 MPa) to prepare their nanocomposite. Research involving nanoscale chitin with thermoset matrix is much rarer. The first study was published in 2013, when Shao et al. [40] impregnated 40% chitin nanofibers in epoxy resin. No data on mechanical properties were presented. Just recently in 2016, Shibata et al. [41] reinforced their waterborne epoxy resin with 3% chitin nanofiber, but their nanocomposite performance (E = 2.4 GPa, σ = 50 MPa) is nowhere near to cellulose nanocomposites prepared by Yano. The author (Shibata) claimed that their nanocomposite performance was actually reduced at higher loadings of chitin. As for chitin whiskers in a thermoset matrix, we are yet to find a single study about it.

Our brief walk into the history of cellulose and chitin shows one undeniable fact: progress in chitin follows the footsteps of cellulose. We can attribute this to the rich history of cellulose itself, spanning over millennia as a source for clothing, building materials, and energy. Abundance and readily available source enables the prosperity of textile and paper industry, which further catalyzes research in cellulose. When the numbers of scientific publication of cellulose, chitin, and chitosan were combined, Scopus database[3] reveals the following order: cellulose (71%) > chitosan (19%) > chitin (10%). If chitin researchers can equip themselves with some knowledge about cellulose, at least by following its research trend, they will be much better prepared in their own chitin study. In the coming sections, we will focus more on chitin. Readers who are interested in nanocellulose and their nanocomposite are referred to an excellent monograph written by Alain Dufresne in 2012 [42] and the following recent reviews: [43-48].

[3] As on June 2016. Search is based on 'title, abstract and keyword' for 'cellulose', 'chitin', and 'chitosan'.

2.3 Structure and Source of Chitin

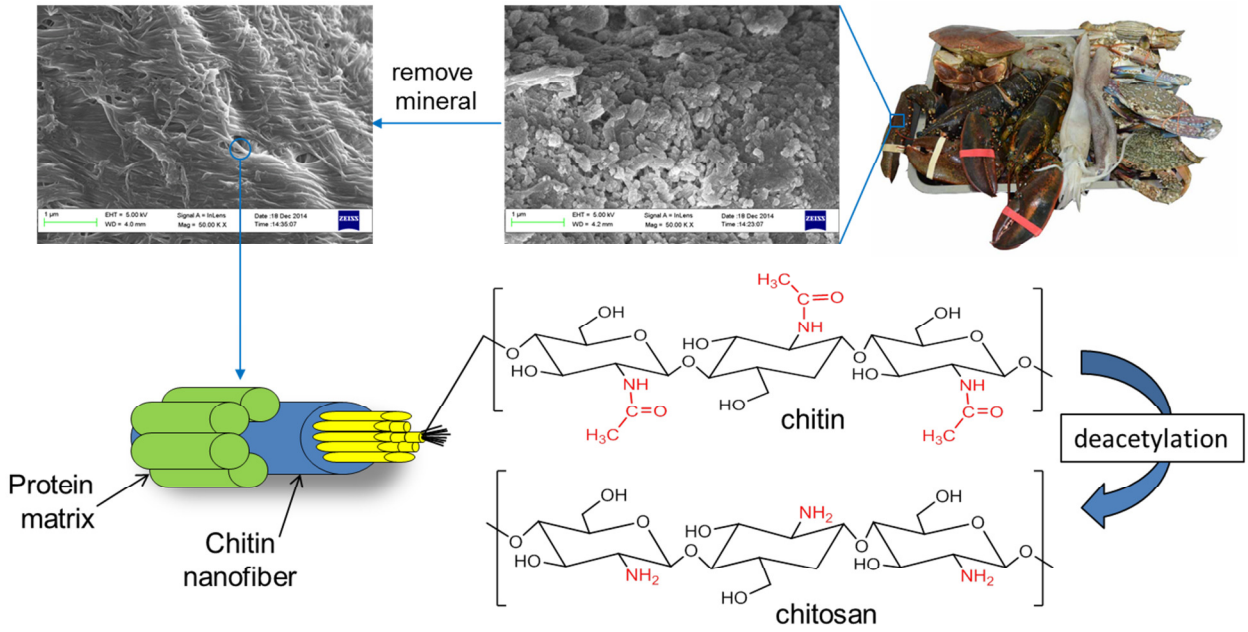

Figure 2.2 Chitin and chitosan structure.

Chitin is structurally similar to cellulose except that the C2-hydroxl group of cellulose is replaced by an acetamide group (see Figure 2.2, shown as red in chitin structure). If this group is deacetylated, the polymer becomes chitosan. Primary amine groups in chitosan can be protonated in dilute acid, thus it is more soluble than chitin and can: (1) confer antibacterial properties when it is in gel form [49, 50], (2) chelate heavy metal and dye in wastewaters more efficiently than chitin [51-53], and (3) be manipulated more easily than chitin for added functionality [54]. Given these factors, it is not surprising that more research has been done on chitosan than on chitin. Nevertheless, the susceptibility of chitosan in dilute acid makes it unsuitable for applications that require durability such as strong films or composites.

Chitin exist in two major polymorphic forms, α and β. Their sources and related properties are given in Table 2.1, while their molecular packing is depicted in Figure 2.3. It has been suggested that the third polymorph, γ-chitin, may be a distorted version of either α- or β-chitin rather than true third polymorphic form [55].

Table 2.1 Sources and properties of α-chitin and β-chitin

	α-chitin	**β-chitin**
Sources	Shells of crustaceans Lobster [56] Crab [21] Shrimp [57] Krill [58] Cuticle of insects [59] Cell wall of fungi Mushroom [60] Yeast [61] Mold [62] Marine alga *Phaeocystis* [63] → highly crystalline Grasping spine of arrow worms *Sagitta* [64] → most crystalline	Squid pen [65] Sea tubeworms [66] Centric diatom, *Thalassiosira* [67] → most crystalline
Molecular packing	Orthorhombic [63, 68] (a: 4.75 Å, b: 18.89 Å, c:10.33 Å, γ: 90°)	Monoclinic [67, 69] (a: 4.82 Å, b: 9.25 Å, c:10.39 Å, γ: 97.2°)
Chain arrangement	Anti-parallel; analogous to mercerized or regenerated cellulose (cellulose II)	Parallel; analogous to native cellulose (cellulose I)
Hydrogen bonding	Has intersheet bonding Has intrasheet, interchain, and intrachain bonding	No intersheet bonding Has intrasheet, interchain, and intrachain bonding
Polymorph stability	Stable	Metastable, converted into α-chitin by 25–30% NaOH [70] 8% HCl [71] More easily deacetylated [65]
Thermal stability	Isotropic lateral expansion when heated [72] Compared with cellulose, chitin has: Lower expansion coefficient Higher degradation temperature [73]	Anisotropic lateral expansion when heated [72]
Lattice modulus (axial)	Theoretical (calculation) : ~ 150 GPa [59] Experimental (XRD) : 59.3 GPa [74] Compare with cellulose (experimental) [75] Cellulose I = 110 –220 GPa Cellulose II = 70–112 GPa	Not reported
Solubility	Stable, not soluble in most organic solvent	Soluble in formic acid [76] Susceptible to swell in water [77]

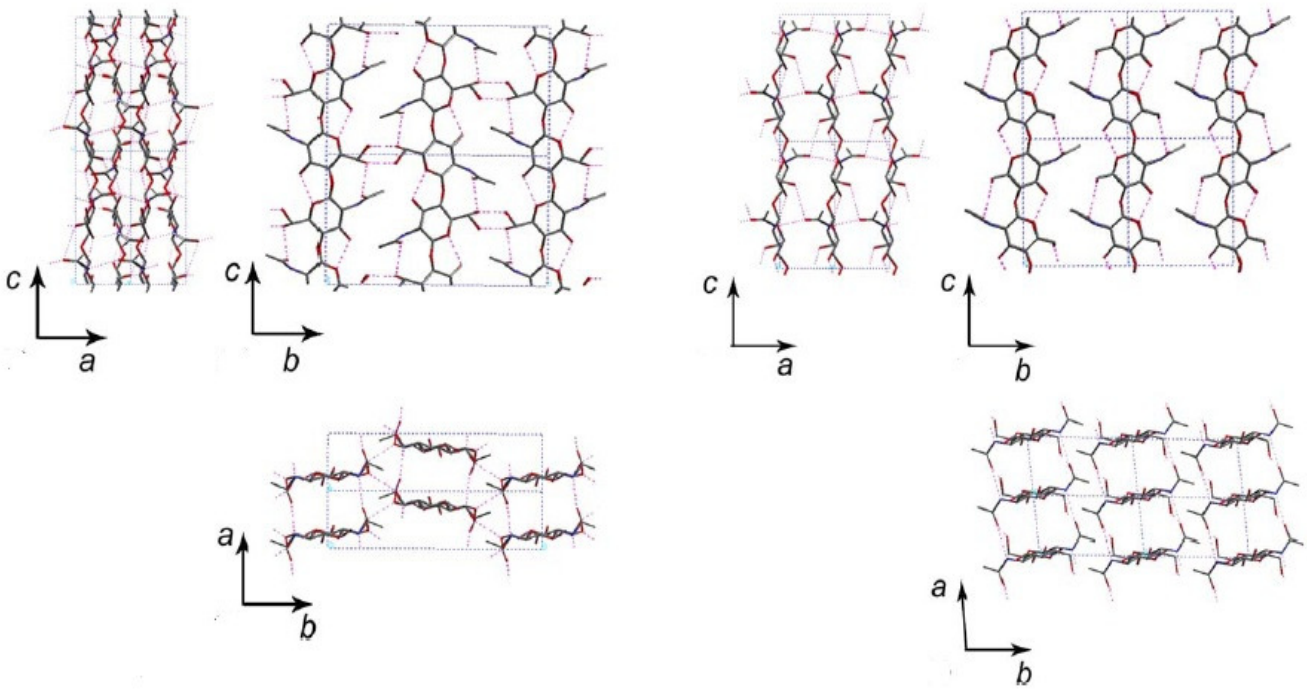

α-chitin β-chitin

Figure 2.3 α- and β-chitin structures with c axis representing the fiber direction. From ref. [78].

Zooplankton cuticles (in particular Antarctic krill, with the estimated biomass of 379 million tons [79]), constitutes the largest source of chitin on earth [80]. However, fishing of these tiny organisms (a few millimeters in length) is too difficult to consider for any industrial use. Waste from shellfish industry (shrimp, crab, and lobster shells) in which the chitin content ranges between 8 to 40% [33, 81, 82] constitutes the main source of commercial chitin production nowadays. The chitin content in fungi is usually lower than in the crustacean source, and the content for few selected species is tabulated in Table 2.2.

The primary biological function of crustacean chitin and fungal chitin is to provide structural scaffold in support of the animal exoskeleton or fungal cell wall. However, this function is fulfilled differently due to their different physiochemical properties. Shellfish chitin normally binds with sclerotized proteins and minerals, while fungal chitin is associated with other polysaccharides such as glucan and mannan [83].

Table 2.2 Chitin content in selected fungi species[a]

Fungi	Per dry weight		Per AIM[b]		
	Chitin (%)	Ref.	Chitin (%)	Glucan (%)	Ref.
A.bisporus (Common mushroom)					
Whole	3–9	[60, 84, 85]	36		[87]
Stalk	7–19	[84, 86]	34–44	18–36	[86, 88]
Cap	6–7	[84]			
Mycelium			31	27	[88]
L. edodes (Shiitake mushroom)	1–10	[60, 84, 85]	28	68	[89]
P. ostreatus (Oyster mushroom)	2–15	[84, 85, 90]			
P. eryngii (King trumpet mushroom)	3–9	[60, 85, 90]			
S.commune (Split gill mushroom)			22	68	[91]
A. niger (Black mold)	8–27	[92, 93]	24	40	[92]
S. cerevisae (Baker yeast)	1–3	[94]	3	37	[95]
M. rouxii (White mucor)	8–9	[92, 96]			

[a]The values from literatures were rounded to nearest decimal. Only the lowest and the highest value are presented.
[b]AIM = alkali insoluble material.

During the extraction process – even if the treatment is very harsh – not all non-chitinous content can be eliminated, suggesting the existence of covalent-like crosslinks between chitin polymers and other substances. This is quite different than interaction between cellulose-hemicellulose-lignin in woody biomass. Cellulose is hydrogen bonded (rather than covalently bonded) to the rest, while hemicellulose and lignin is covalently linked [97]. This fact cause it is much easier to obtain better quality cellulose than better quality chitin (in term of crystallinity). However, we should point out, that it is very difficult, if not impossible, to extract all non-cellulosic materials from the plant fiber matrix. Traces of hemicellulose (<1%) for example, prevail even in the purest form like Whattman filter paper. In animal chitin, unless if the sources are from diatom *Cyclotella* or *Thalassiosisira* – which is pure chitin, no associated protein [98] – residual protein will always co-exist with chitin polymer.

In crustacean shells and insect cuticles, the crosslinks between chitin and protein is well known. However, it is still debatable whether the bridging is covalent in nature [76, 99, 100] or not [101, 102]. Given that the amount of residual protein is very low, it is often negligible. Thus, if the reader, while reading animal-based chitin literature, comes across the following sentence

"…*x* have 35% chitin", they can be confident that the stated value is close enough to the actual chitin content.

In fungi, covalent linkages between chitin and glucan have been evidenced by chemical hydrolysis and enzymatic dissection [4, 103], gene disruption [104], and solid state NMR [105]. The initial study was done on *S. commune* (split gill mushroom)[4], but similar results were also found for other fungi [106-109]. Unlike animal chitin where the residual protein is minimal, fungal chitin contains a higher proportion of glucan, often higher than that of chitin itself. Thus, any literature citing the percentage of chitin from fungi should be treated with caution, especially if the works is not directly related to mycology[4]. More often than not, the stated chitin value represents the alkali insoluble material (AIM), in which chitin and glucan co-exist. Alkali insoluble glucan exists in β-form, often called as β-glucan.

There are numerous entries discussing fungal β-glucan and its structure diversity [110]. However, most of them refer to the water soluble part only. For example, lentinan is β-glucan obtained from the hot water extract of *L. edodes* (shiitake mushroom), schizophyllan from *S.commune* (split gill mushroom), zymosan from *S. cere*viase (baker yeast), pleuran from *P. ostreatous* (osyter mushroom), grifolan from *G. frondosa* (maitake mushroom) and ganoderan from *G.lucidum* (lingzhi or reishii mushroom). All these glucans were studied mainly because the human innate immune system can recognize them [111], hence they boast remarkable potential in application such as immune stimulator, antibacterial, antitumor, anticancer, antioxidant and other health related benefits. In our study, we were only interested in alkali insoluble β-glucan, thus we will not further discuss the soluble glucans and an interested reader is referred to these three recent critical reviews: [112-114].

Association with chitin makes β-glucan insoluble. When the alkali resistant part of the cell wall is extensively treated with glucanase (glucan degrading enzyme), 16% of glucan still retained in the insoluble form [91]. But when the same resistant part is treated with chitinase (chitin degrading enzyme), all glucan became soluble [4]. Both of these results indicated a crosslink between chitin and glucan. Insolubility during the glucanase treatment is due to crystalline chitin, while total solubilization after chitinase treatment reflects the collapse of the crystalline structure. Thus, logic dictates, if some glucan is still in the insoluble form after extensive glucanase treatment, then it must somehow be linked to chitin. It is worth noting that

[4] Dedicated field that study fungi.

the glucanase action is highly specific and was carried out on the alkali resistant part, so typical alkali extraction will leave more glucan connected to chitin.

Insoluble β-glucan usually consists of (1→3) backbone with (1→6) branches (see Figure 2.4a). Its proportion and branching is highly dependent on the species and the extraction process. Harsh acid treatments will degrade most of the glucan, causing the X-ray diffraction pattern of the sample resemble to that of crustacean chitin [91].

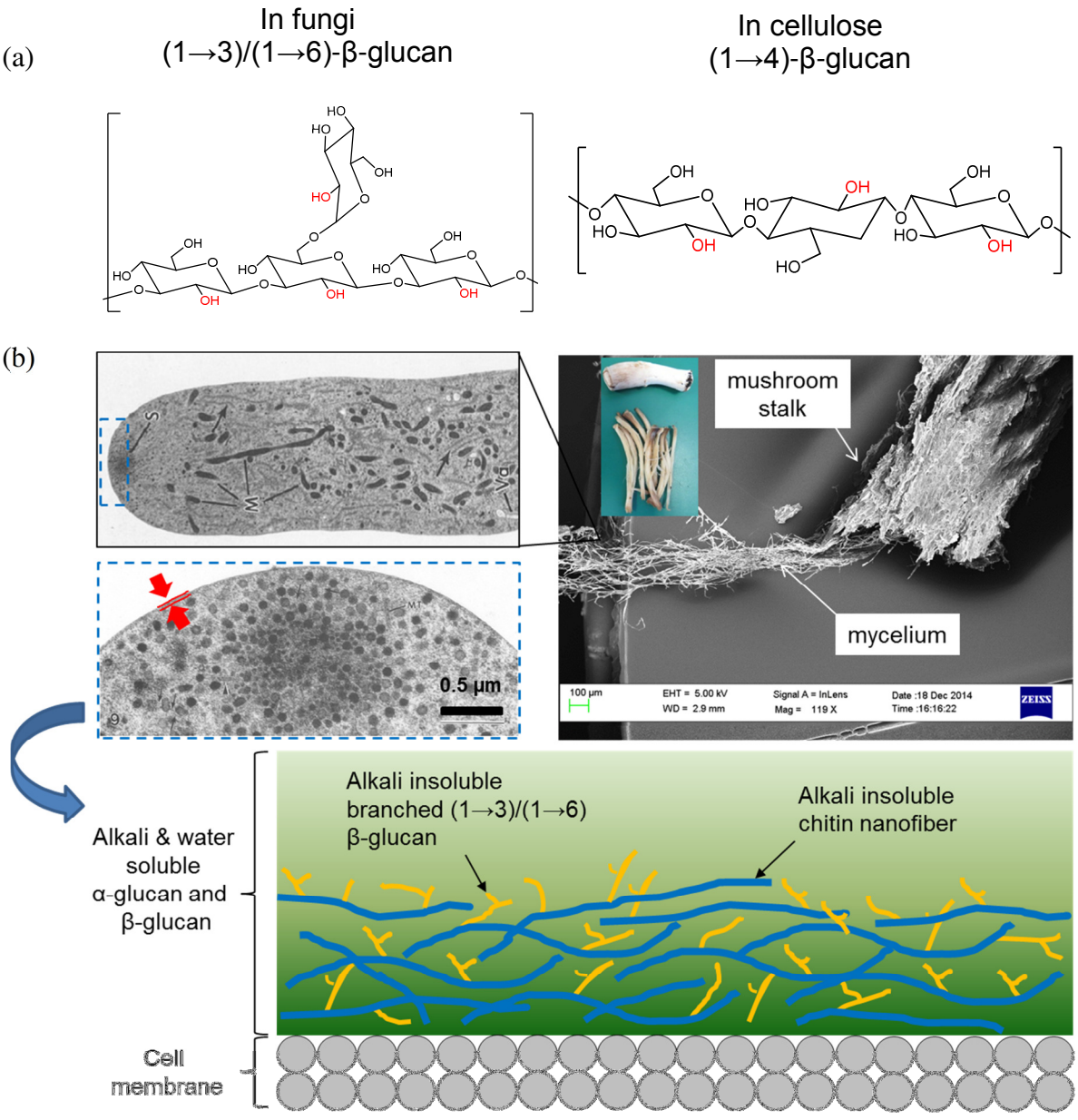

Figure 2.4 (a) the difference between glucan structures in fungi and cellulose, (b) where chitin resides in mushroom? ; TEM image represents hyphal tip of *S. rolfsii* from ref. [115].

The relation between chitin and insoluble glucan in the fungal cell wall is depicted in Figure 2.4b. Extensive studies have been carried out to elucidate the architecture of chitin-glucan linkages in Ascomycete phyla (yeast and filamentous fungi). However, similar studies with basidomycete (mushroom) are still lacking. Figure 2.5 illustrates the chitin-glucan model gathered from literature. There are small difference between the insoluble part of glucan among mushrooms, yeast and filamentous fungi. Nevertheless in most part, all of them bear the common motif: β-glucan which is associated with chitin is predominately having (1→3) backbone with (1→6) branching [116]. In yeast, most of the chitin is concentrated at the bud scar, while for the other fungi, chitin is present throughout the cell wall. All fungi group synthesize chitin in their cell wall, but only zygomycete (mucor species) are known to be able to co-synthesize chitin and chitosan simultaneously [96, 117].

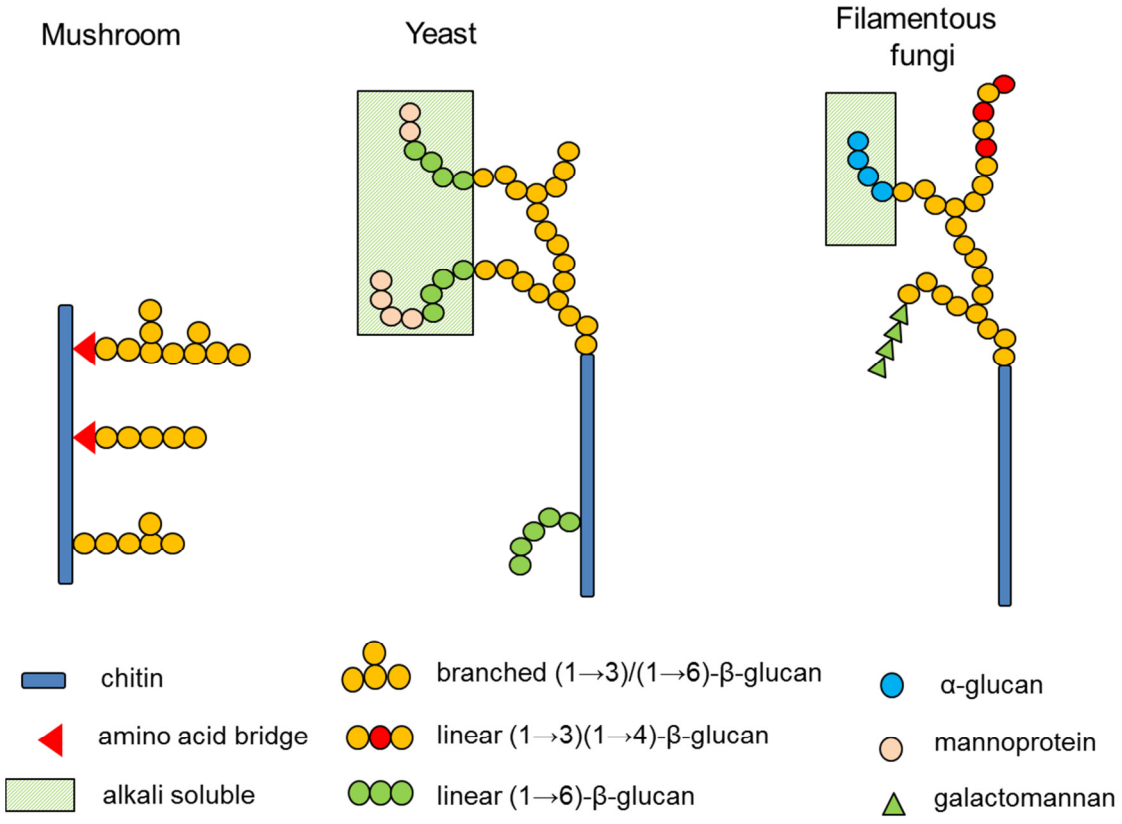

Figure 2.5 Architecture of chitin-glucan complex in fungi. The mushroom model is based on *S. commune* [4], the yeast model is based on *S. cerevisae* and *C. albicans* [61, 103, 118], and the filamentous fungi model is based on *A. fumigatus* [108].

2.4 Extraction of Chitin and Preparation of Chitin Nanofibers/Whiskers

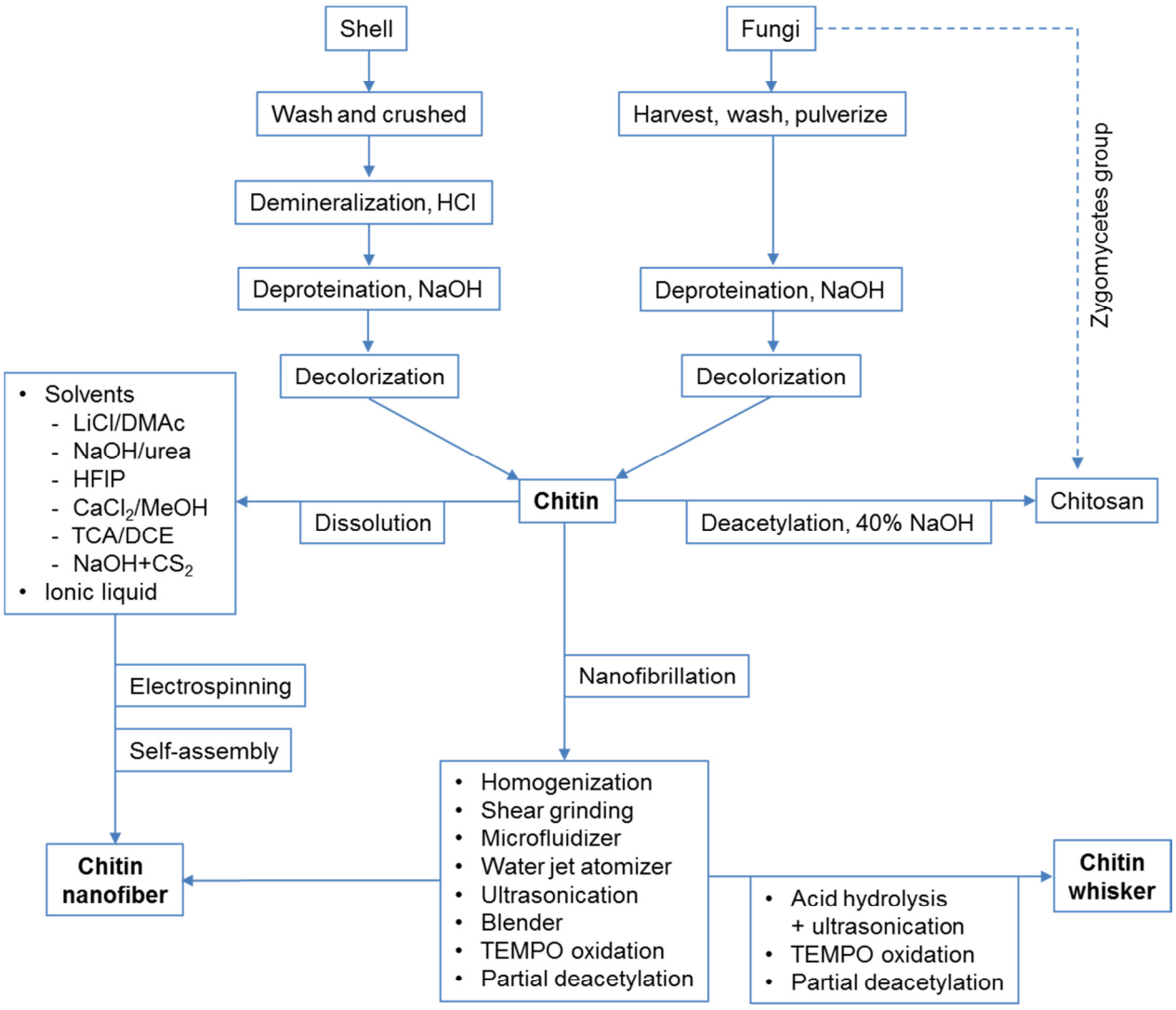

HCl = hydrochloric acid, NaOH = sodium hydroxide, LiCl/DMAc = Lithium chloride / N,N-dimetyhlacetamide, HFIP = 1,1,1,3,3,3-hexafluoro-2-propanol, CaCl2/MeOH = calcium chloride/methanol, TCA/DCE = trichloroacetic acid / 1,2-dichloroethane, $NaOH+CS_2$ = sodium hydroxide + carbon disulfide (xanthate or viscose process), TEMPO = 2,2,6,6-tetramethylpiperidine-1-oxyl

Figure 2.6 Isolation of chitin and chitosan from crustacean shells and fungi, and preparation of chitin nanofiber and chitin whisker.

There are three main steps usually carried out for chitin extraction from the crustacean shells: demineralization, deproteination, and decoloration [119]. Because fungi are not calcified, the demineralization step is unnecessary [86, 120]. A deacetylation step is added if a chitosan product is preferred.

Demineralization removes inorganic material in calcified crustacean shells. It is usually carried out using dilute acid, commonly hydrochloric acid (HCl), at room temperature. Care must be taken as acid can both deacetylate and depolymerize the chitin chain [121, 122]. Percot et al. [123] in his optimization study reported that shrimp shells are completely demineralized within 15 minutes of 0.25 M HCl treatment at room temperature. Longer treatment times, higher concentrations of acid, or higher extraction temperatures will all cause a substantial reduction in chitin molecular weight. Although HCl is relatively expensive and detrimental to chitin, it remains the most commonly used decalcifying agent in both laboratory and industrial scale production of chitin. Weak synthetic amino acids like ethylenediaminetetraacetic acid (EDTA) at controlled pH have been proposed as non-degradative demineralization reagents [124]. However, elimination of inorganic salts was found to be incomplete [119].

Deproteination, that is the removal of protein, is a crucial step in chitin extraction for both crustacean and fungal sources. Sodium hydroxide (NaOH) and potassium hydroxide (KOH) are preferred reagents. They are typically used at 1 M concentration with variations in temperature and extraction time. Deproteination is less damaging to chitin compared to demineralization, but prolonged treatments and high temperatures can lead to deacetylation [123]. Higher deacetylation leads to: (1) decrease in hydrophobicity, (2) decrease in film tensile strength, (3) increase in film ductility, (4) increase in solubility, (5) increase in cell adhesion and proliferation, and (5) increase in the rate of biological degradation [125-128]. The more deacetylated the chitin, the more it resembles chitosan. The use of proteolytic enzymes [129] provides an alternative to the harsh chemical treatments, minimizing the effect of deacetylation and depolymerization. However, there are cost-related problems associated with enzyme usage. To bring down the production costs associated with the deproteination step, Ifuku et al. [130] forewent the whole process and came up with a chitin-protein nanofibers product. They found that the composite film (with acrylic) have an almost similar mechanical properties compared to the composite made from fully deproteinatized chitin nanofibers.

More greener and cost effective extraction processes can be achieved via biological fermentation [131]. For example, Jung et al. [132] used lactic acid producing bacteria, *Lactobacillus paracasei*, to produce acid for the demineralization step, and protease producing bacteria, *Serratia marcesens* to remove protein during their deproteination step. Compared to the chemical process, biological treatment can result in higher crystallinity and higher molecular weight in the chitin or chitosan product [133].

Acid and alkaline treatment alone produces colored chitin. Decoloration step is added when a bleached product is desired. Pigment can be removed using ethanol or acetone after the demineralized step. Alternatively, the coloring matters may be destroyed by bleaching using sodium hypochlorite (NaOCl) or an oxidation process using hydrogen peroxides (H_2O_2).

The deacetylation step of chitin into chitosan is usually achieved by treating chitin with 40–50% NaOH at 95–100 °C for 2–3 hours, followed by neutralization. The chitosan is then extracted with 2% acetic acid solution, filtered and precipitated in distilled water. If the deacetylation process is carried out at room temperature, it yields a water soluble form of chitin, i.e. alkali-chitin, instead of chitosan [125, 134-136].

2.5 Chitin Nanofiber and Whisker

In recent years, there have been increased focus on chitin nanomaterials, either as nanofibers [24] or whiskers [137]. Whiskers are crystalline part of fibers, often termed nanocrystals that are devoid of amorphous regions. They are shorter and have more defined dimensions. Regardless of its form, most studies utilize animal-based chitin as their starting material. To the best of our knowledge, only two studies[5] related to the extraction of fungal-based chitin nanomaterials have been conducted so far [60, 138].

[5] Chitin as nanofibrilliar substance in fungi is well studied by mycologist, but they are mostly focusing on structure in vivo and its role during fungal morphogenesis.

2.5.1 Chitin Nanofiber

Table 2.3 summarizes the width of chitin nanofibers obtained from different nanofibrillation processes. All nanofibers in the table are several micrometers in length.

Table 2.3 Diameter of chitin nanofiber from different nanofibrillation process

Source	Method	Width (nm)	Ref.
Crab shell	Grinding + homogenization	<50	[139]
	Grinding, pH 3–4	10–20	[22]
	Microfluidizer	20–30	[140]
	Ultrasonication, 24 kHz, 120 min, pH 3–4	2–20	[141]
	20% NaOH → grinding, pH 3–4[a]	10	[142, 143]
	Water jet atomizer "Star Burst"		
	(5 or 10 pass), neutral pH	17.3–18.2	[144]
	(1, 5, or 10 pass), pH 3	16.5–19.0	[144]
	High speed blender, 10 min		
	37000rpm, neutral pH	77 ± 37	[145]
	37000rpm, pH 3–4	20–30	[145]
	15000 rpm, pH 3–4	20–30	[146]
	11000rpm, pH 3–4	20–30	[146]
	4000rpm, pH 3–4	~100	[146]
Shrimp shell	Grinding, neutral pH	10–20	[57]
	Ultrasonication, 60 kHz, 30 min + pulse sonication	20	[147]
	Electrospinning	670–µm	[148]
	Domestic blender, 30 min, pH 3–4[b]	<50	[149]
Squid pen	Grinding, pH 3	12–20	[150]
	Ultrasonication, 19.5 kHz, 2 min, pH 3–4	3–4	[151]
	Self-assembly[c]		
	Dissolution in HFIP → solvent evaporation	3	[152, 153]
	Dissolution in LiCl/DMAc → precipitation	10	[152]
Lobster shell	Homogenization	80–100	[154]
Mushroom	Grinding, pH 3	20–28	[60]

[a]α-chitin is partially deacetylated with 20% NaOH (the surface of nanofiber behave like chitosan, but its core is chitin) followed by grinding in acidic condition.
[b]Typical maximum rotational speed for conventional food mixer or kitchen blender is between 11000–15000 rpm.
[c]HFIP = 1,1,1,3,3,3-hexafluoro-2-propanol, LiCl/DMAc = lithium chloride / N,N-dimethylacetamide

Chitin nanofibers can be prepared by subjecting extracted chitin to various mechanical nanofibrillation process such as: high pressure homogenization [154], wet shear grinding [21], water jet atomization [144], microfluidization [140], ultrasonication [147, 155], or high speed blending [146]. All these treatment are similar to nanofibrillation treatments used for cellulose, except that in cellulose, cyrocrushing [156] has also been tried. All nanofibrillation process,

except for ultrasonification, rely on high shearing and high impact force generated onto a chitin fiber bundle, causing weak interfaces among nanofibers to be broken. In ultrasonification, high frequency oscillation creates a localized high pressure region, resulting in cavitation and impaction which ultimately loosen the fibers.

Chitin nanofiber can also be prepared by a chemical method via TEMPO[6]-mediated oxidation in the presence of a catalyst (TEMPO), sodium bromide (NaBr), and an oxidizer, sodium hypochlorite (NaClO) [157, 158]. NaClO with TEMPO oxidizes the primary C6-hydroxyl groups of polysaccharides into carboxylic acid moieties via an aldehyde intermediate. The charges brought in by the carboxylates promote anionic electrostatic repulsion that separate individual fibers apart. This method of nanofibrillation was first demonstrated for cellulose by Isogai and co-workers in 2006 [159]. Total oxidation of native cellulose cannot be achieved by TEMPO even after addition of large amount of NaClO [160], but in the case of chitin, total oxidation can occur [161, 162], hence the oxidation process for chitin must be strictly controlled. Unlike cellulose, TEMPO for chitin has a different effect on different polymorph type. TEMPO for squid pen β-chitin produces neither nanofiber nor whiskers [163], TEMPO for highly crystalline tube worm β-chitin produces nanofiber (20–50 nm in width, several microns in length) [163], and TEMPO for crab α-chitin produces only whiskers (8 nm width, 340 nm in length) [164].

In 2008, Fan et al. [151] reported a much simpler and faster way to produce chitin nanofiber from squid pen β-chitin (3–4 nm in width and several micron in length) by treating the sample with 2 min ultrasonication under acidic conditions. The idea is based on cationization of free amine groups on the chitin crystallite surface at pH 3–4. Cationization leads to electrostatic repulsion, similar to what happens during TEMPO oxidation; but in this case it is a cationic repulsion instead of an anionic repulsion. In the aforementioned study, ultrasonication works with squid pen β-chitin, but it did not work with tubeworm β-chitin or crab α-chitin due to higher crystallinity. Crab α-chitin can be fibrillated into uniform nanofibers with 10–20 nm diameter by subjecting a never-dried sample to a grinding treatment [21]. Drying causes the fibers to collapse and lose their swelling capability, thus making it harder to defibrillate. Later it was found that it was possible to obtain nanofibers of similar width using dried chitin by a means of grinding in acidic conditions [22]. Treatment with 33% NaOH, cause α-chitin to be partially deacetylated,

[6] 2,2,6,6-tetramethylpiperidine-1-oxyl

resulting in chitosan-like surface with a chitin core. Because chitosan is protonated in acid, nanofibers from partially deacetylated chitin can be easily individualized at pH 3–4 as a result of cationic repulsion of the positively charged amino group [165].

In 2010, Rolandi group [152] found that when squid pen β-chitin dissolved in HFIP[7], it can reassemble itself into α-chitin nanofibers (3 nm width) during solvent evaporation. β-chitin dissolved in LiCl/DMAc[8] can also self-assembled during precipitation process, but it produces larger diameter nanofibers (10 nm width).

2.5.2 Chitin Whisker

Table 2.4 summarizes the dimensions of chitin whiskers obtained from different processing methods.

Table 2.4 Dimensions of chitin whiskers from different processing methods

Source	Method	Length (nm)	Width (nm)	Ref.
Crab shell	3 M HCl, 1.5 h, boiling	100–600	4–40	[33]
	3 M HCl, 6 h, boiling	100–500	10–50	[166]
	3 M HCl, 3 h, boiling	300	20	[167]
	33% NaOH → pH 3–4[a]	250 ± 140	6.2 ± 1.1	[165]
	TEMPO oxidation	50–500	8–10	[164]
	TEMPO oxidation	250	15	[168]
	TEMPO oxidation	150–500	20–55	[169]
	Ionic liquid/methanol	several 100	20–60	[170]
Shrimp shell	3 M HCl, 1.5 h, boiling	150–800	5–70	[171]
	3 M HCl, 6 h, reflux at 120 °C	231–969	12–65	[172]
	3 M HCl, 1.5 h, 90 °C	200–500	10–15	[173]
Squid pen	3 M HCl, 1.5 h, boiling	50–300	10	[5]
Riftia tube	3 M HCl, 1.5 h, boiling	500–10000	18	[32]

[a]α-chitin is partially deacetylated by 33% NaOH (i.e. the crystallite surface behave like chitosan, but its core still chitin) followed by 1 min ultrasonication at pH 3–4 to promote cationization.

Chitin whiskers (also known as chitin nanocrystals or chitin crystallites) are usually prepared by boiling chitin sample in hydrochloric acid (HCl) followed by ultrasonication. These

[7] 1,1,1,3,3,3-hexafluoro-2-propanol
[8] Lithium chloride / N,N-dimethylacetamide

whiskers form stable colloidal suspensions due to the presence of cationic surface charge on its crystallite surface and they can rearrange themselves in a helicoidal fashion at certain concentrations [174]. Stable colloidal whiskers for cellulose, on the other hand, can be achieved by using sulfuric acid (H_2SO_4) instead of HCl. Although the presence of sulfate groups on cellulose crystallites induce anionic electrostatic repulsion [175], they are also detrimental for the thermal stability of cellulose [176]. This is one of the advantages of chitin over cellulose in the whisker form, as the use of HCl does not affect the thermal stability of chitin. The yield and the dimensions of either chitin or cellulose whiskers is highly dependent on the acid concentration and the duration of hydrolysis. Higher acid concentrations and longer treatment times will cause substantial reduction in whiskers' length to width ratio [177].

TEMPO mediated oxidation is another method for whisker production. This method offers several advantages over the conventional acid hydrolysis: (1) the process is more controllable by the amount of oxidizer added, (2) whisker recovery can reach 90%, and (3) no deacetylation of chitin occurs during TEMPO mediated oxidation [137]. More recently, Kadokawa et al. [170] has found that chitin regenerated from an ionic liquid can reassemble into a whisker form when the resulting chitin-ionic liquid gel is soaked in methanol.

2.6 Chitin Film and Its Nanocomposite

In the earlier section (Section 2.2), we have discussed briefly chitin based films and their related nanocomposite with comparison to cellulose. Hereby, we will extend our knowledge by looking at the diverse studies that have been performed on chitin nanofibers or whiskers in terms of film and nanocomposite preparation.

2.6.1 Chitin Film

There are three different methods to prepare a chitin film: (1) by first dissolving the chitin in an appropriate solvent or in an ionic liquid, and then regenerate it, (2) by evaporating chitin nanofibers suspension, and (3) by evaporating chitin whiskers suspension. Generally, the first method produces a weak gel without any defined fiber morphology, hence, the film made from it does not possess nanofiber or whisker features. However, if an ionic liquid with methanol is used, it is possible to regenerate chitin whiskers [170]; and if hexafluoro-2-propanol solvent (HFIP) is

used, it is possible to regenerate chitin nanofibers [152]. The common method to prepare 100% nanochitin films is by evaporating chitin nanofibers or chitin whiskers suspension. The evaporation process can be done by solution casting, hot pressing, or by using dedicated sheet making equipment (e.g. Rapid-Köthen). Films made from nanofiber usually have better mechanical properties than films made from whisker as a result of more extensive fiber entanglement. Table 2.5 tabulates the tensile properties of the films made from chitin nanofibers, chitin whiskers, and regenerated chitin.

Table 2.5 Tensile properties of chitin film prepared via different process[a]

Source	Morphology	Process	*E* (GPa)	σ (MPa)	ε (%)	Ref.
Crab shell	Nanofiber	Microfluidizer → Rapid-Köthen	8.2	77	1.4	[140]
	Nanofiber	Acidic grinding → hot press	2.5	42		[25]
	Nanofiber	Partial deacetylation → casting	8.8	157	5.4	[143]
	Whisker	TEMPO oxidation → casting	5.3	110	5	[178]
	Whisker	Partial deacetylation → casting	4.9	140	9.7	[178]
	Whisker	HCl hydrolysis → casting	5.7	49	1.2	[178]
	Whisker	Ionic liquid/methanol → casting		~4.4	~0.2	[170]
Lobster shell	Nanofiber	Microfluidizer → Rapid-Köthen	7.3	153	8	[26]
	Regenerated	TCA/DCE solvent → casting	3.1	95	10.9	[179]
Squid pen	Nanofiber	Self-assembly from HFIP solvent				
		Cold press	~1.6	147	~29	[180]
		Vacuum dry	~1.8	111	~15	[180]
		Vacuum filter	~1.9	123	~19	[180]
		Centrifugal casting	4.3	~130	~14	[181]
Shrimp shell	Regenerated	Xanthate process → casting	1.97	51	7.1	[182]
α-chitin[b]	Regenerated	NaOH/urea solvent → casting	4.7	111	6.1	[183]
	Regenerated	LiCl/DMAc solvent → cold press	2.7	77	20	[184]

[a] *E* = Tensile modulus, σ = tensile strength, ε = tensile strain at failure, TEMPO = 2,2,6,6-tetramethylpiperidine-1-oxyl, HCl = hydrochloric acid, TCA/DCE = trichloroacetic acid / 1,2-dichloroethane, HFIP = 1,1,1,3,3,3-hexafluoro-2-propanol, NaOH = sodium hydroxide, LiCl/DMAc = lithium chloride / N,N-dimethylacetamide

[b] Commercial chitin, but the source was not stated. It is either from crab shell or from shrimp shell.

2.6.2 Chitin Nanocomposite

Composite is a hybrid material having two or more different constituents which is different in their physical and chemical characteristic, that when combined, produce synergistic effect towards the engineering performance of the end product. It is generally composed of two phases: the matrix and the reinforcement (also known as filler). The matrix dictates the composite shape by holding the reinforcement phase together, protecting them from adverse environment and transferring the external load between the reinforcing components. The reinforcement, being stiffer than the matrix, offers strength and rigidity to the composite while stopping any crack in the matrix from propagating. The smaller the reinforcement, the higher the surface area and the more contacts it can make with the matrix. If these contacts – often referred as fiber/matrix interface – are good, external load can be transferred efficiently across the whole composite.

Chitin nanofibers or nanowhiskers, with estimated fiber modulus of at least 150 GPa [59] (experimentally it was found to be 59.3 ± 11.3 GPa [74]), should offer a green and renewable alternative nanoreinforcement in a common plastic polymeric matrix that commonly have a modulus at around 3 GPa. In general, nanofibers can offer better reinforcement than whiskers due to their entangling effect [185, 186]. However, it is easier to predict the mechanical properties from whiskers than it is from nanofibers due to the more defined dimensions of the former.

Table 2.6 tabulates some of the nanocomposites that have been prepared so far using chitin nanofibers or whiskers as its reinforcement. Addition of chitin nanofibers or whiskers usually improves the mechanical properties of the neat matrix in term of stiffness and strength, but often reduces the original strain to failure of the matrix. α-chitin from crab and shrimp is the most commonly used starting material due to its better stability and availability than β-chitin from squid pen. To the best of our knowledge, no nanocomposite study has been attempted using fungal based chitin nanofibers.

Table 2.6 Nanocomposite from chitin whisker and chitin nanofiber[a]

Chitin type	Chitin content (%)	Matrix	Composite type	Process	Ref.
		Crab shell			
	0–20	Latex	Film	Freeze dry → hot press	[33]
	0–20	Latex	Film	Casting/evaporation	[33]
	0–30	Soy protein isolate	Film	Freeze dry → hot press	[187]
	0–10	PLA	Film	Casting/evaporation	[188]
	20	PLA	Foam	Melt extrusion	[189]
	>50	PVA	Film	Casting/evaporation	[170]
	3–30	PVA	Fiber	Gel spinning	[190]
	0–5	WPU	Film	Casting/evaporation	[191]
Whisker	0–10	PVDF	Membrane	Casting/evaporation	[192]
	5–10	Chitosan	Film	Casting/evaporation	[193]
	0–30	Chitosan	Film	Casting/evaporation	[194]
	2.9–13.3	Chitosan	Gel	Casting/evaporation	[195]
	layer	Chitosan	Membrane	Layer-by-layer deposition	[196]
	layer	Xyloglucan	Film	Layer-by-layer deposition	[197]
	0–5	Maize starch	Film	Casting/evaporation	[198]
	50	Chitosan/PEO	Fiber mat	Electrospinning	[199]
	1–7	Sulfonated PES	Membrane	Casting/evaporation	[169]
	5–30	Hyaluronan/gelatin	Foam	Freeze drying	[200]
	5–20	PEO	Film	Casting/evaporation	[201]
	70	PMMA	Film	Resin impregnation	[202]
	0	Poly SSQ-UA	Film	Resin impregnation	[203]
	0–100	Chitosan	Film	Casting/evaporation	[142]
	3–10	Carrageenan	Film	Casting/evaporation	[204]
	40	Acrylic resin	Film	Resin impregnation	[130]
Nanofiber	14	Acrylic resin	Curvy film	Pickering emulsion	[205]
	40	(meth) acrylic resin	Film	Resin impregnation	[25]
	50	Hyaluronic acid	Tablet	Freeze drying → cold press	[206]
	18	Polyglutamic acid	Film	Solution grafting	[207]
	50–80	Carbon nanotube	Film & gel	Filtration/evaporation	[208]
	coat	Carboxymethyl cellulose	Film	Solution immersion	[209]
Platelet	0–5	Potato starch	Film	Casting /evaporation	[210]
		Lobster shell			
	5	PLA	Film	Film blowing extrusion	[211]
Whisker	5–20	Corn starch	Film	Casting/evaporation	[212]
	5–20	Corn starch	Mold	Extrusion/injection molding	[186]
	0–10	Cellulose nanofiber	Film	Hot pressing	[213]

[a]PLA = polylactic acid, PVA = poly(vinyl alcohol), WPU = waterbased polyurethane, PEO = polyethylene oxide PVDF = poly(vinylidenefluoride), PMMA = polymethyl methacrylate, SSQ-UA = silsesquioxane-urethaneacrylate.

Table 2.6 (continued) Nanocomposite from chitin whisker and chitin nanofiber[a]

Chitin type	Chitin content (%)	Matrix	Composite type	Process	Ref.
		Lobster shell			
	0–100	Chitosan	Film	Casting/evaporation	[214]
Nanofiber	5–20	Corn starch	Film	Casting/evaporation	[212]
	5–20	Corn starch	Mold	Extrusion /injection molding	[186]
		Shrimp shell			
	0–29.6	PVA	Film	Casting/evaporation	[171]
	0–29.6	PVA	Fiber mat	Electrospinning	[172]
	1–5	PHBV	Film	Casting/evaporation	[215]
	0.05–2	Alginate	Fiber yarn	Spinning extrusion	[216]
	0–29.6	Chitosan	Film	Casting/evaporation	[217]
Whisker	0–20	Polydioxanone	Fiber mat	Electrospinning	[218]
	0–30	Polyoctanediol-citrate	Film	Casting/evaporation	[219]
	0–50	Silk fibroin	Foam	Freeze drying	[220]
	10–50	Bacterial cellulose	Film	Filtration/Rapid-Köthen[b]	[221]
	10–50	Bacterial cellulose	Film	In-situ biosynthesis	[221]
	0–100	Cellulose/silk sericin	Sponge	Freeze drying	[222]
Nanofiber	40	Epoxy	Film	Resin impregnation	[40]
	25.2	Acrylic resin	Film	Resin impregnation	[149]
		α-chitin[c]			
	1	PP	Film	Extrusion → hot press	[223]
	1	PLA	Film	Extrusion → hot press	[224]
	2.5–10	PLA	Membrane	Electrospinning	[225]
	5–30	WPU	Film	Casting/evaporation	[226]
	0–55	Alginate	Hydrogel	Casting/evaporation	[227]
Whisker	0–10	Chitosan	Fiber	Wet spinning	[228]
	0–8	Cellulose	Film	Casting/coagulation	[229]
	5–15	Carrageenan	Film	Casting/evaporation	[230]
	0.25–2	Polyurethane	Film	Casting/evaporation	[231]
	0–6.07	Paper sheet	Paper	Colloidal immersion	[232]
	15–70	Graphene oxide	Foam	Freeze drying	[233]
	0.5	Recycled ABS	Film	Hot press	[234]
	0–20	Lithium perchlorate / PEO	Film	Hot press	[235]

[a]PVA = poly(vinyl alcohol), PHBV = poly(hydroxybutyrate-co-hyroxyvalerate), PP = polypropylene PLA = polylactic acid, WPU = waterbased polyurethane, ABS = acrylonitrile-butadiene styrene PEO = polyethylene oxide

[b]Semi-automatic sheet former.

[c]Commercial chitin, but the source was not stated. It can be either crab shell or shrimp shell.

Table 2.6 (continued) Nanocomposite from chitin whisker and chitin nanofiber

Chitin type	Chitin content (%)	Matrix	Composite type	Process	Ref.
		α-chitin[a]			
Nanofiber	0–0.15 (g)	Polyacrylamide	Hydrogel	Casting/evaporation	[236]
	5–30	Polycaprolactone	Film	Casting/evaporation	[237]
	5–30	Polycaprolactone	Fiber mat	Electrospinning	[237]
	3–10	Biobased epoxy	Mold	Compression molding	[41]
	97.5	Chitosan glycolate	Spray	Wet mixing	[238]
	91.1	Chitosan glycolate	Gel	Mixing	[238]
	10	Chitosan glycolate	Gauze	Wet spinning/freeze drying	[238]
		Squid pen			
Whisker	0–20	Latex	Film	Casting/evaporation	[5]
Nanofiber	0–75	Gelatin	Hydrogel	Casting/UV curing	[239]
	25–75	Silk fibroin	Film	Casting/evaporation	[240]
	layer	TEMPO[b] oxidized cellulose	Film	Layer-by-layer deposition	[241]
		***Riftia* tube**			
Whisker	0–10	Polycaprolactone	Film	Freeze drying / hot pressing Casting / evaporation	[32]

[a]Commercial chitin, but the source was not stated. It can be either crab shell or shrimp shell.
[b]TEMPO = 2,2,6,6-tetramethylpiperidine-1-oxyl.

The most common type of chitin nanocomposite is a film and the most common method to prepare the film is by casting a chitin-matrix solution in a petri dish via evaporation. This method usually can produce stronger films than the hot pressing technique as a continuous percolation network can be formed and protected via slow evaporation [34]. However, this method can induce nanofibers or whiskers aggregation if the matrix is hydrophobic in nature. Even if chitin is relatively more hydrophobic than cellulose [145], the presence of hydroxyl groups does confer some hydrophilicity. This hydrophilicity causes problems in terms of compatibility with the hydrophobic matrix such as aggregation and poor fiber/matrix interfacial adhesion in the resulting composite. Effective dispersion and good interfacial adhesion are crucial to realize the full potential of the reinforcing properties of chitin nanofibers or whiskers.

One way to mitigate the aggregation problem is by first dispersing the chitin nanofibers or whiskers in water and then filtering them to form a nanofiber or a whisker sheet. The sheets are then impregnated with a curable resin such as epoxy or acrylic resin, which will then fill the

pores between the fibers [25]. Although this method can prevents aggregation, it is not without problems. For instance, the prepared chitin sheet should possess pores that are big enough to allow resin impregnation. Filtration and a subsequent evaporation process remove water and cause fibers to adhere tightly with each other via hydrogen bonding. As a result, high porosity cannot be achieved. Henriksson et al. [18] has shown that the porosity of nanocellulose sheets can be increased (and controlled) by performing solvent exchange on the filtered sheet with ethanol or acetone before the drying process. This method was later adopted to prepare chitin sheets with varying porosity [140]. However, we were unable to find any studies that elucidate the effect of different sheet porosity on resin impregnation process.

The other problem associated with wet impregnation (and also with solvent casting) is that there is a limitation to the product shape. Inter-fiber bonding that occurs during sheet preparation makes it difficult to prepare complex 3D shapes, while molding via extrusion makes the nanoparticles susceptible to agglomeration. Recently, Shams and Yano reported a preparation of doubly curved chitin nanofiber-reinforced composites via Pickering emulsification method [205]. Briefly, the acrylic resin droplets that are trapped in the chitin nanofiber network prevent the strong inter-fiber bonding to be formed extensively between adjacent chitin fibers. The resin-nanofiber sheet obtained after the filtration process is soft and can be molded into a curvy shape before the whole specimen is cured.

2.7 On The Use of Fungi as a Potential Source for Chitin

Recent estimates in 2011 suggest that as many as 5.1 million fungal species exist, but less than 100 000 have been described so far [242]. Different species have different ratios of chitin to glucan in their cell walls. Existence of glucan, on one hand will complicate the characterization process, but on the other hand offers material scientists with limitless possibilities of different types of natural and renewable reinforcing nanomaterials. While chitin is rigid, branched glucan is not. This native nanocomposite architecture, when extracted, can give both strong and tough fibers with optimized proportions of chitin and glucan. This proportion can be regulated by controlling the nutritional and environmental parameter during the fungal growth. This possibility does not exist for animal chitin.

Fungi grow by hyphae branching, creating a vast network of web-like mycelium. Each individual mycelia is about 2–3 μm thick. This mycelium in itself has many prospects to be used

as an alternative bio-restoration medium, for example, as water filtration media for pathogens [243]. An interested reader can gain more insight about the potential of using mushroom mycelium for bioremediation by reading 'Mycelium running' [244] written by a prominent mycologist, Paul Stamets.

Table 2.7 shows the advantages and disadvantages between animal-based chitin and fungal-based chitin. Fungal mycelium is a living cell, thus its growth is largely dictated by changes in nutritional environment. If we can align this mycelium through a directed growth, we can end up with an anisotropic fungal structural element – a highly oriented macrofiber that contains chitin-glucan nanofibers. This is a very promising concept that can be used in fabricating aligned natural fiber reinforced composites. The possibility of realigning the fibers via directed solid state growth does not exist for animal chitin. When compared to bacterial cellulose, in which bacteria *A. xylinum* secretes nanofibers during fermentation, the cellulose nanofiber cannot be oriented easily as the bacterial fermentation needs to be carried out in liquid. Fungi on the other hand can be grown in both liquid submerged fermentation and solid state fermentation. The company Ecovative[9] has used fungal mycelium as a bio-based composite binder. Instead of preparing composite from isolated units, they 'grow' their material by fermenting their fungi in the presence of waste material such as rice straw. The idea of using fungal mycelium as a binder is not new. In Asian countries like Indonesia, their traditional food, tempeh, were made by fermenting mucor fungus *Rhizopus oligosporus* with cooked soybeans. Upon solid state fermentation, the mycelium binds the soybeans together.

Fungal chitin is also free from the crustacean allergenic protein, tropomyosin [245], which further extends its potential usability. For example, KitoZyme[10] has extracted a chitin-glucan complex from a black mold *Aspergillus niger*, and further market it as a food supplement [120]. The scientific committee of European Food Safety has regarded their chitin-glucan supplement as safe to use [246], and US Federal Drug Agency had also approved their GRAS[11] status. In UK, Quorn[12] products utilize mycoprotein extracted from fungus *Fusarium venetatum* as a meat substitute for vegetarians.

[9] www.ecovativedesign.com
[10] www.kitozyme.com
[11] Generally Recognized as Safe
[12] www.quorn.co.uk

Table 2.7 Advantages and disadvantages between crustacean-based and fungal-based chitin[a]

Chitin source	Advantages and disadvantages
Crustacean	**Advantages** • High chitin content per dry mass • Almost pure chitin → easy to characterize • Well established extraction method and nanofibers preparation • Already commercialized and can be bought easily • Extensive research and literature accounts **Disadvantages** • Limited supply → seasonal and regional • Sea pollution (e.g. heavy metal, radioactive) can affect chitin quality • Problem with crustacean allergenic protein 'tropomyosin' • Deacetylation process for chitosan production involve concentrated sodium hydroxide → cost and environmental concern
Fungi	**Advantages** • Renewable, non-allergenic • Not dependent on seasonal fluctuation and the effect of sea pollution • Fungi - Does not need sunlight; can be grown anywhere, anytime - Fast growth (mushroom) → typically 2–3 weeks - Can be grown by staking (vertical growth) → minimal land required - Limitless supply, can provide chitin all year round - Growth can be controlled easily → more consistent chitin quality - Inexpensive raw material waste can be used as a growth substrate - Zygomycetes → direct chitosan extraction, no deacetylation process required • Readily available fungal biomass '*A. niger*' from industrial citric acid production • Readily available mushroom waste (irregular shape and stalk) from mushroom industry • Bypass dimineralisation step - Reduce overall production cost - No chain depolymerization due to acid • High level of acetylation on chitin → can offer hydrophobicity • Possibility of aligned chitin fiber via directed mycelium growth • May possess bioactive function, as a result of β-glucan • Can utilize nature nanocomposite architecture : chitin-glucan **Disadvantages** • Low chitin content • Not a pure chitin, association with glucan → complicate characterization • Extraction process not yet being scaled up to industrial level • Limited literature on extraction for nanofiber production

[a]Input were gathered from ref. [247] , other literatures, and author's own observation/reading.

However, fungal chitin is not without problem. First, the chitin yield from fungi is low compared to the animal-based counterpart. Although this problem can be compensated with rapid fungal growth rate, the major obstacle that discourages chitin researchers from working with fungal chitin is the presence of glucans. We believe that this is not an unequivocal disadvantage, however, as mentioned previously: the glucans complicate the characterization, but they also offer new possibilities.

CHAPTER THREE
MATERIALS & METHODS

3.1 Introduction

Chemicals, raw materials, and instruments used throughout this study will be described in this chapter. The methods used, starting with extraction process of chitin-based materials, preparation of films/composites and the relevant characterization methods will be discussed. Figure 3.1 gives an overview of the entire study flow. There are 6 themes in this study: comparative study, grammage study, optimization study, film composite study, laminate study, and binder study.

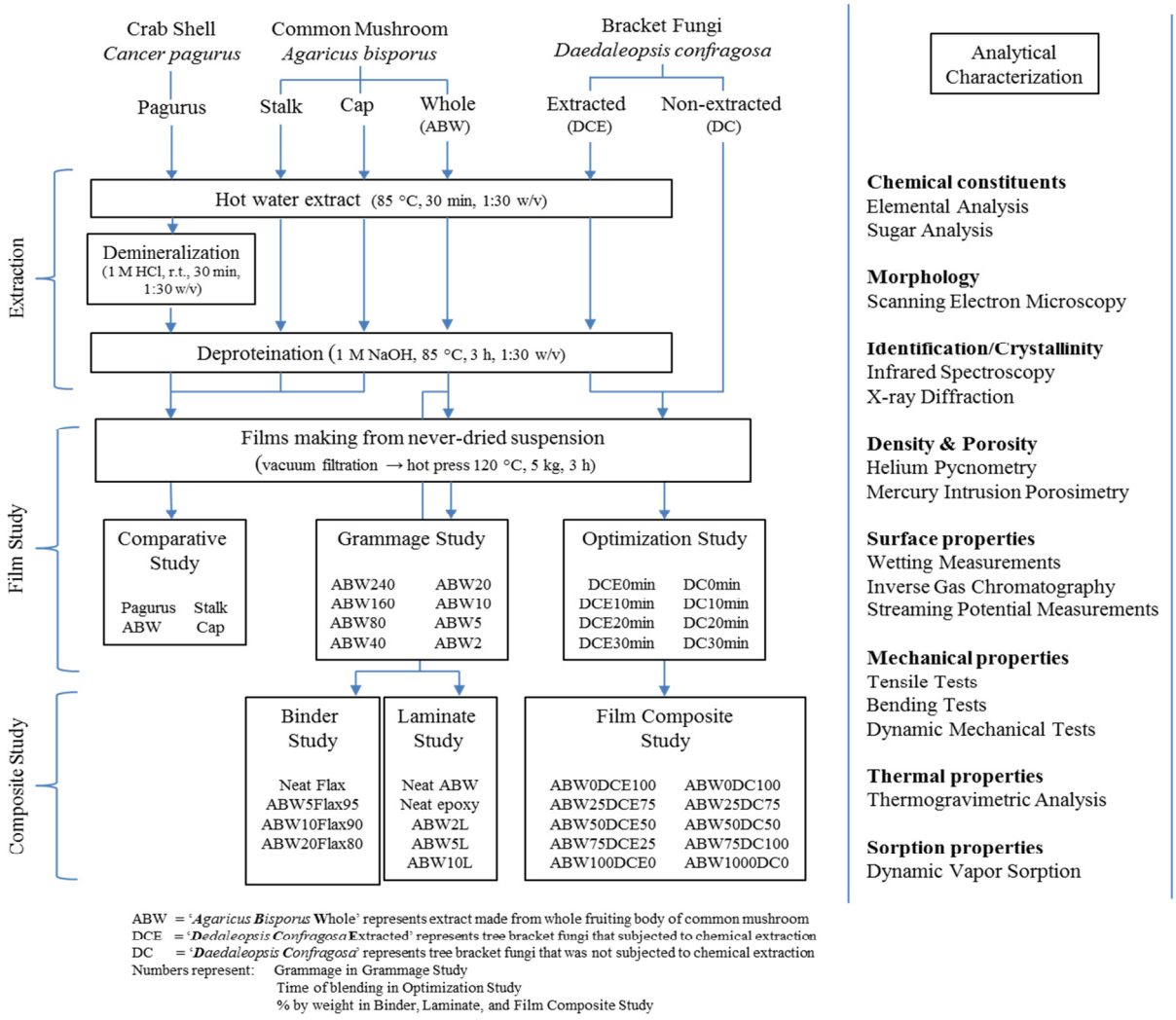

Figure 3.1 Flowchart of experimental procedures and analytical methods used throughout the study.

3.2 Materials

3.2.1 Chemicals

Chitin flakes from shrimp shells were purchased from Sigma-Aldrich (C9213, practical grade) and were finely ground in a ball mill prior to use. Sodium hydroxide (Sigma Aldrich, pellets), hydrochloric acid (Sigma-Aldrich, 37% w/w), and sulfuric acid (Merck, 72% w/w) were used during chitin extraction and sugar hydrolysis. Sugar Recovery Standards (SRS) for carbohydrate analysis were prepared from D-(+)-glucose (BDH Prolabo), D-(+)-xylose (Merck), D-(+)-galactose (Merck), D-(+)-arabinose (Chalbiochem), D-(+)-rhamnose (BDH Prolabo), D-(+)-mannose (Merck), and D-(+)-glucosamine hydrochloride (Sigma-Aldrich). For wetting measurements, the following test liquids were used: *n*-heptane (Sigma-Aldrich, purity ≥ 99%), *n*-dodecane (Sigma Aldrich, purity ≥ 90%), benzylalcohol (Sigma-Aldrich, purity ≥ 99%), formamide (Sigma-Aldrich, purity ≥ 99.5%), decalin (Riedel-de Haën, purity ≥ 98%), and ethyleneglycol (Arcos Organic, purity ≥ 99.9%). All test liquids for inverse gas chromatography were HPLC grade and purchased from Sigma-Aldrich: *n*-hexane, *n*-heptane, *n*-octane, *n*-nonane, *n*-decane, dichloromethane, ethyl acetate, acetone, and acetonitrile. For the composite study, Araldite LY556 resin and Araldite XB3473 hardener (MouldLife, UK) were used as epoxy matrix system. Ultrapure water (CENTRA-R 200 or PURELAB Classic, 18.2 MΩ cm^{-1} resistivity, <10 ppb inorganic impurities) was used for all experiments, when needed.

3.2.2 Raw Materials

Common white mushrooms, *Agaricus bisporus,* having an average cap diameter of 5–7 cm were purchased from a local store. Whole fruiting body, stalk-only, or cap-only were weighed and kept frozen to prevent water loss and enzymatic degradation. Tree bracket fungi, *Daedaleopsis confragosa,* a polypore fungus commonly found on decaying willow trees were collected from Wormwood scrubs (Google Earth location : 51° 31' 13.57" N, 0° 14' 00.10" W) during autumn. The bracket is characteristically tough with a leathery texture, brownish in color and had a width of approximately 10–12 cm. Untreated carapaces of brown edible crab, *Cancer pagurus*, with a width of approximately 12–16 cm were purchased from C-Quest Ltd (Dorset, UK). The shells were oven dried at 60 °C, crushed into smaller pieces, and ground for 5 min in a ball mill giving average particle size of 150–300 μm. Figure 3.2 shows the photograph of raw materials used in this study.

Figure 3.2 Raw materials for chitin/chitin-glucan extraction: (a) *A. bisporus* common mushroom, (b) *D. confragosa* tree bracket fungi, (c) *C. pagurus* crab carapace.

For the preparation of the flax nonwovens, short, loose flax fibers of approximately 25 mm in length were kindly supplied by S.A.R.L. Novalin France (Millam, France). The fibers were used as it is without any chemical pretreatment. The following abbreviations will be used hereafter: ABW (*A. Bisporus* whole mushroom extract), Pagurus (*C. Pagurus* crab shell chitin extract), DCE (*D. Confragosa* extract), DC (*D. confragosa* as it is, non-extracted), stalk (stalk extract from *A. bisporus* mushroom), cap (cap extract from *A. bisporus* mushroom), and flax (flax fibers).

3.3 Extraction Process and Film/Composite Preparation

3.3.1 Chitin-Glucan Extraction from Common Mushrooms

Prior to extraction, 500 g frozen mushrooms were thawed in 1 L distilled water for 5 min and rinsed to remove any observable impurities. The procedure was repeated three times followed by 5 min initial blending in kitchen blender (Breville VBL065 Pro 800W, Oldham, UK). The extraction process started with a hot water treatment to remove any water soluble components followed by a deproteination step in alkaline solution to remove proteins, lipids, and alkali-soluble glucan. Briefly, water was added to the blended slurry until its final volume reached 1.5 L and the suspension was stirred at 85 °C for 30 min. The excess water together with the soluble components was then removed by centrifugation at 7000 rpm for 15 min (ThermoScientific, Sorvall Legend RT+). The precipitate (cake) obtained after centrifugation was then soaked in alkaline solution (1 M NaOH) until its final volume reached 1.5 L. The suspension was heated to 65 °C for 3 h while stirring before it was neutralized by successively re-centrifuged

in excess water. The neutralized cake was then resuspended in water (0.8% w/v) and dispersed by final blending for another 1 min. The suspension was stored at 4 °C until further use.

Apart from using never dried suspension, the extracts also freeze dried (ThermoScientific, Heto PowerDry LL1500 Freeze Dryer). Freeze dried sample will be used for elemental and sugar analysis, density measurement, powder X-ray diffraction, thermogravimetric analysis, and surface energy determination by inverse gas chromatography.

3.3.2 Chitin-Glucan Extraction from Tree Bracket Fungi

The brackets were soaked in distilled water overnight before being diced into pieces with average dimensions of 5 mm x 5 mm x 5 mm, followed 10 min initial blending to yield a fibrous slurry. Half of the slurry was subjected to the extraction process similar to the procedure described for common mushrooms in Section 3.3.1. The other half of the slurry was not extracted. Neutralized sample, both extracted and non-extracted were resuspended in water (1.0% w/v) and dispersed by final blending for different times (0, 10, 20, 30 min). The suspension was stored at 4 °C until further use. Apart from using never dried suspension, the extracts also freeze dried.

3.3.3 Chitin Extraction from Crab Shells

The extraction procedure is similar to common mushrooms described in Section 3.3.1 except that a demineralization step was included between the hot water extraction and deproteination step. Briefly, 1 M HCl was added to centrifugation cake from hot water extract until its final volume reached 1.5 L and the suspension was stirred for 30 min at room temperature. After demineralization, the insoluble residue was neutralized before being subjected to alkali treatment for deproteination. Finally, the neutralized alkali insoluble cake was resuspended in water (0.8% w/v) and dispersed by final blending for another 10 min. The suspension was stored at 4 °C until further use. Apart from using never dried suspension, the extracts also freeze dried.

3.3.4 Preparation of Chitin/Chitin-Glucan Film from Crab Shells Nanofibers, Common Mushroom Nanofibers, and Bracket Fungi Microfibers

For comparison between fungal chitin film and animal chitin film (comparative study), 0.8% (w/v) suspension from mushroom (stalk, cap, whole) and crab extracts were weighed corresponding to final film specification (grammage: 80 g/m^2, diameter: 90 mm) followed by vacuum filtration through cellulose filter paper (VWR 413, 5–13 µm retention value) supported in Büchner funnel. The resulting filter cake was then wet pressed between blotting paper (3MM CHR blotting paper, VWR) to remove excess water before being pressed one final time in an oven held at 120 °C for 3 h under 5 kg weight. Once completed, the sample was left overnight under a weight at room temperature to prevent film shrinkage. All films were 80 g/m^2 and the following abbreviations were used: pagurus film, stalk film, cap film, and ABW film. Figure 3.3 shows the photograph of common mushroom suspension, filtration method, and filtration cake.

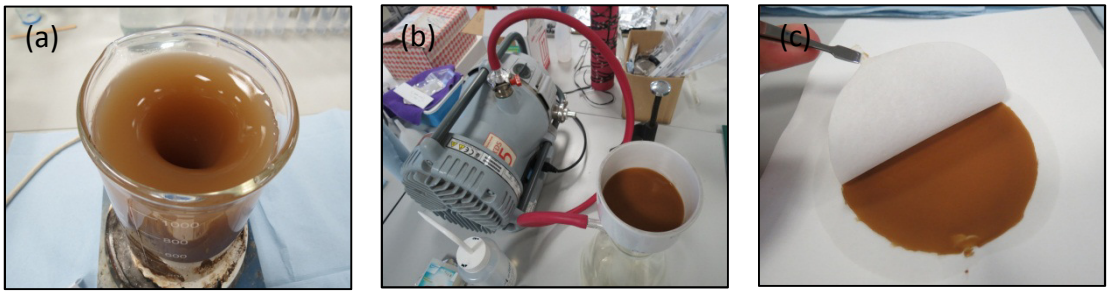

Figure 3.3 Film preparation from fungal chitin-glucan extract: (a) never dried 0.8% w/v suspension, (b) vacuum filtration of the suspension, (c) film obtained after the filtration.

To evaluate the effect of different film grammage (grammage study), only suspension from whole mushroom was used. Films ranging from 10 g/m^2 to 240 g/m^2 were prepared. For 2 g/m^2 films, solvent casting method is used, in which a pre-weighed 0.8% whole mushroom suspension was gently poured into a plastic petri dish and left to dry overnight. All other films were prepared using vacuum filtration followed by hot pressing method as described previously. Following abbreviations were used: ABW2, ABW10, ABW20, ABW40, ABW80, ABW160, and ABW240, in which the numbers represent grammage in g/m^2.

To evaluate the effect of blending time (optimization study), suspension of bracket fungi which were blended for various times (0, 10, 20, 30 min) were used. The blending time that

produced the strongest films was used to prepare the raw materials for subsequent film composite study, in which the bracket fungi suspension will be mixed with common mushroom suspension. Films were prepared similar to the filtration and hot pressing procedure described above, except that PTFE cloth was added on top of filter paper during filtration. The PTFE filter was used since the filter cake from bracket fungi tends to adhere strongly to filter paper, and addition of porous PTFE facilitates the detachment of filter cake from the filtration membrane. All films were 80 g/m^2 and the following abbreviations will be used: DCE0min, DCE10min, DCE20min, DCE30min, DC0min, DC10min, DC20min, and DC30min, where numbers represent blending time in minutes.

3.3.5 Preparation of Common Mushroom Nanofibers – Bracket Fungi Microfibers Composite Film

Composite films were made by combining whole mushroom extract (ABW, 0.8% w/v) with either bracket fungi extract (DCE, 1.0% w/v) or non-extracted bracket fungi (DC, 1.0% w/v) at varying weight ratio of 25/75, 50/50, and 75/25. The stock solution was diluted by adding 100 ml distilled water to the mixture prior to vigorous mixing by hand for few seconds followed by preparation of film using a bracket fungi's film preparation procedure (see Section 3.3.4). All composite films were 80 g/m^2 and the following abbreviations were used: ABW25DCE75, ABW50DCE50, ABW75DC25, ABW25DC75, ABW50DC50, and ABW75DC25, where numbers represent weight content (%) of preceding word.

3.3.6 Preparation of Common Mushroom Nanofibers – Epoxy Resin Laminated Composite

Mixture of resin and hardener was first heated in vacuum (60 °C, 20 min) to reduce its viscosity and to remove any bubble generated during mixing. Two gram of the resulting epoxy was then spread onto one side of ABW film (80 g/m^2) and sandwiched with another layer of ABW film (80 g/m^2) to proceed with laminated composites. Sandwiched layers were passed through a gap adjustable printing proofer (K Printing Proofer, RK PrintCoat Instruments Ltd.) to ensure homogenous and thin epoxy distribution. This process was repeated when multiple layers of laminated composites are desired. Resulting two, five, or ten layers composites were then sandwiched between non-perforated release film before placed into pre-coated aluminum mold (coating agent: Frekote 700-NC, Henkel). The procedure is depicted in Figure 3.4.

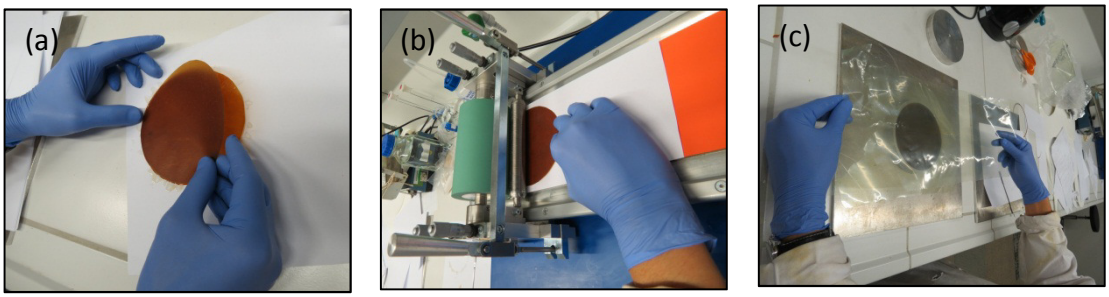

Figure 3.4 Preparation of 2 layers laminate: (a) uncured epoxy resin is sandwiched between two 80 g/m^2 ABW film, (b) resin was spread uniformly using gap adjustable printing proofer, (c) laminate in mold is covered with release film prior to hot pressing.

The composites were then cured by initial heating at 120 °C for 2 h, followed by 180 °C for 2 h, and finally 120 °C for another 2 h in a 1 ton hydraulic hot press (Carver Inc., Wabash, USA). The following abbreviations were used: ABW2L (2 layers laminate), ABW5L (5 layers laminate), and ABW10L (10 layers laminate).

The reinforcement weight fraction, $w_{f,\ ABW}$ was calculated using the following equation:

$$(w_{initial,\ ABW} / w_{final,\ composite}) \times 100 \qquad \text{(Equation 3.1)}$$

where $w_{initial,\ ABW}$ represents the weight of total ABW film used during composite preparation and $w_{final,\ composite}$ represents the weight of respective composite after being cured.

Meanwhile, the reinforcement volume fraction, $v_{f,\ ABW,}$ was determined by dividing the total film volume by the composite volume:

$$[\ (m_{ABW\ film}/\rho_{ABW\ film}) / (m_{composite}/\rho_{composite})\ ] \times 100 \qquad \text{(Equation 3.2)}$$

where m and ρ represent the weight and density of corresponding constituents, respectively.

In order to predict the composite theoretical performance in term of modulus and strength, rule of mixture (ROM) was used:

$$\text{ROM for modulus : } [(v_{f,\ ABW})(E_{ABW})] + [(v_{f,\ epoxy})(E_{epoxy})] \qquad \text{(Equation 3.3)}$$

$$\text{ROM for strength : } [(v_{f,\ ABW})(\sigma_{ABW})] + [(v_{f,\ epoxy})(\sigma_{epoxy})] \qquad \text{(Equation 3.4)}$$

where $\nu_{f,\ ABW}$, $\nu_{f,\ epoxy}$, E_{ABW}, E_{epoxy}, σ_{ABW}, and σ_{epoxy} represent reinforcement volume fraction, matrix volume fraction, modulus of ABW film, modulus of epoxy, strength of ABW film, and strength of epoxy, respectively.

3.3.7 Preparation of Nonwoven Flax Preform using Common Mushroom Nanofibers as a Binder

Both flax fibers and common mushroom extract suspension (ABW) were pre-weighed to adjust the slurry consistency to desired final composite specification (1000 g/m^2, 110 cm in diameter, weight ratio ABW/Flax: 0/100, 5/95, 10/90, or 20/80). Flax fibers were first 'fluffed' by dry blending in a kitchen blender for few seconds to increase its surface area before being mixed with ABW extracts suspension. Composite preforms were manufactured using layer-by-layer filtration using the method described by Fortea-Verdejo et al. [248]. Briefly, the ABW/Flax or flax only mixture were dispersed in 1 L water, further divided into 4 equal volumes having the same consistency, and left soaked overnight. Thereafter, the first suspension was poured into a Büchner funnel, manually dispersed by hand and then vacuum filtered. The second suspension then poured directly onto previous wet filter cake, dispersed, and filtered as before. The procedure was repeated with third and fourth suspension to build up wet filter cake layer-by-layer. The wet filter cake was then wet pressed between blotting papers, placed in aluminum mold, and hot pressed at 120 °C for 2 h under 1 ton pressure using hydraulic hot press (Carver Inc., Wabash, USA). Figure 3.5 depicts some photographs during preform preparation.

Figure 3.5 Preparation of ABW/Flax preform: (a) flax fiber soaked in ABW suspension overnight, (b) filtration of ABW/Flax mixture, (c) ABW/Flax preform in mold before hot press.

All composite had an aerial weight of 1000 g/m^2 and the following abbreviations were used: ABW0Flax100, ABW5Flax95, ABW10Flax90, and ABW20Flax80, where numbers represent weight content (%) of preceding word.

3.4 Characterization Process for Freeze Dried, Film, and Composite Samples

3.4.1 Chemical Constituents Determination

Carbon, hydrogen, nitrogen, sulfur, and oxygen content in the respective freeze dried extract were determined by elemental analyzer (EA 1108 CHNS-O, Carlo Erba Instruments). Carbohydrate analysis was carried out by high performance anion exchange chromatography (HPEAC). Briefly, 300 mg freeze dried sample was mixed with 3 mL of 72% sulfuric acid at 30 °C for 60 min. The acid was then diluted with water to a consistency of 4% concentration and the mixture was placed in an autoclave at 121 °C for 60 min. The HPEAC was performed to the previously diluted acid hydrolyze with a Dionex ICS3000 chromatograph equipped with a CarboPac PA20 column (Dionex, Sunnyvale, CA, USA). Sugar Recovery Standards (SRS) were prepared and pre-treated in identical hydrolysis conditions prior to HPAEC analysis in order to analyze their recovery throughout the procedure.

3.4.2 Scanning Electron Microscopy (SEM) for Morphological Investigation

Morphology of extracted material was studied using a high-resolution field emission gun scanning electron microscope (LEO Gemini 1525 FEG-SEM, Oberkochen, Germany). The accelerating voltage used was 5 kV. Prior to SEM, 3 µL suspension of extracted samples (0.01% w/v) was dropped onto a 400 mesh TEM copper grid attached on carbon tabs, air dried and chromium coated (K550 sputter coater, Emitech Ltd., Ashford, Kent, UK) for 30 s at 80 mA. Thin film samples were also investigated.

Morphology of laminated composites and flax nonwovens were studied using a bench top SEM (JCM-6000, JEOL GmbH, Eching, Germany) operating at an accelerating voltage of 15 kV. Prior to SEM, fractured composites were fixed onto SEM stubs using carbon tabs and gold coated for 1 min at 30 mA using a sputter coater (JFC-1200, JEOL GmbH, Eching, Germany).

3.4.3 Density and Porosity Measurement

Helium pycnometry (AccuPyc II 1340, Micromeritics, Aachen, Germany) was used to determine the true density of freeze dried sample and films. The measurement was carried out at 23 ± 1 °C and averages of 10 measurement cycles were reported. Mercury intrusion porosimetry (AutoPore IV 9500, Micromeritics) was used to measure the porosity of films and composites. The envelope density (ρ_e) of the sample was measured at 0.002 MPa where pores larger than 150 µm were filled by mercury while the skeletal density (ρ_s) was measured at maximum pressure of 227 MPa. Given the limit of mercury penetration into pores for this instrument is 6 nm at maximum pressure, the true porosity of the sample was calculated as follows:

$$\text{Porosity (\%)} = \left(1 - \frac{\rho_e}{\rho_{true}}\right) \times 100 \qquad \text{(Equation 3.5)}$$

where ρ_e is a film or composite envelope density obtained from MIP, while ρ_{true} is film or composite density obtained from Helium pycnometry.

3.4.4 X-Ray Diffraction (XRD) for Crystallinity Index (CI%) Determination

The XRD pattern of freeze dried powders and films sample was measured using an X-ray diffractometer (PANanalytical X'pert Pro, PANanalytical Ltd., Cambridge, UK) equipped with 1.54 Å Cu Kα X-ray source. The diffraction pattern of film samples were measured by irradiating 1 cm x 1 cm sample film on zero background silicon plate. All measurements were taken within the range of $5° \leq 2\theta \leq 40°$ using a step size and scan speed of 0.02° and 30 s, respectively. To avoid possible orientation effects, both powder and film sample were rotated at 16 revolutions per minute. Crystallinity index (CI %) was determined by deconvolution method according to Goodrich and Winter (2007) [173]. Briefly, the baseline corrected diffraction data was smoothed by applying a Savitsky-Golay filter using a second-order polynomial function with 10 points and deconvoluted using Gaussian function, followed by dividing the total area under crystalline diffraction peaks by the total area under the curve within the range of $5° \leq 2\theta \leq 30°$. Scherrer's equation [249]

$$L_{020} = \frac{0.93 \times \lambda}{\beta \times \cos\theta} \qquad \text{(Equation 3.6)}$$

where θ, β, and λ are the Bragg's angle (in degree), full width at half maximum of the 020 reflection (in radian) and wavelength of the X-ray source (in Ångstrom), respectively, was used to determine chitin crystallite size.

3.4.5 Attenuated Total Reflection Infrared Spectroscopy (ATR-IR) for Infrared Absorbance Analysis and Degree of Acetylation (DA) Determination

ATR-IR spectra of films were recorded using a Spectrum One FTIR-spectrometer (Perkin Elmer, Massachusetts, USA). Films were pressed onto diamond crystal using pressure arm and the spectra were collected at a resolution of 2 cm^{-1}, within range of 600 cm^{-1} and 4000 cm^{-1}. A total of 16 scans was measured and averaged to produce each spectrum. To measure the degree of acetylation (DA), the absorbance spectra were first submitted to ATR correction to correct the variation in the depth of penetration using built-in software. DA was then calculated based on absorbance ratio of 1560 cm^{-1} to 1025 cm^{-1} ($A_{1560/1025}$)using the baseline suggested by Duarte et al. (2002) [250]. For fungal chitin, rough estimate of chitin DA value is calculated by dividing the $A_{1560/1025}$ with the chitin ratio in chitin-glucan complex.

3.4.6 Mechanical Testing for the Film and Composite Sample

For film samples, tensile tests were conducted using a TST350 tensile tester (Linkam Scientific Instruments, Surrey, UK). Specimens were cut into dog bone shape using a Zwick cutter, giving an overall length of 35 mm and the narrowest part of 2 mm, with 10 mm gauge length. Prior to the test, the specimens were secured onto testing cards using a two-part cold curing epoxy resin (Araldite 2011, Huntsman Advanced Materials, Cambridge, U.K.). This was to prevent the clamp of the tensile testing equipment from damaging the test specimens while spreading the stress concentrations in order to avoid premature failure initiation sites. Prior to mechanical testing, all specimens were conditioned at 27 ± 2 % relative humidity (RH)[13] by storing them in a desiccator for at least 24 h. The crosshead speed used was 1 mm/min. A 200 N load cell was used to test films with grammage of 80 g/m^2 and above, while a 20 N load cell was used for films having a grammage of 40 g/m^2 and below. The machine compliance was determined using ASTM C1557-14, and it was found to be 6.38 x 10^{-3} mm/N and 1.33 x 10^{-2}

[13] During film tensile testing, the room humidity and temperature were observed to be 41 ± 2 % RH and 20.3 ± 2 °C, respectively.

mm/N for 200 N and 20 N load cell, respectively. The tensile test was conducted in accordance to ASTM D638-14. The film thickness was determined using a handheld microscope on a polished epoxy embedded samples, calibrated using 100 x 0.01 mm microscope graticule (Graticules Ltd., Tonbridge, Kent, UK). A total of 5 specimens were tested for each type of samples.

For laminated composite and flax nonwovens, both tensile and flexural test were performed using an Instron 5969 Universal Tester (Instron GmbH, Buckinghamshire, UK). The tensile test was conducted in accordance to ASTM D3039M-14 using crosshead speed of 1 mm/min and 1 kN load cell. Laminated composites were cut using bench saw into test specimens having rectangular dimensions of 50 mm x 5 mm with 20 mm gauge length, and flax nonwovens were cut into test specimens having rectangular dimensions of 80 mm x 15 mm with 50 mm gauge length. Specimens were end-tabbed with woven glass fiber reinforced polyester using a two-part cold curing epoxy resin (Araldite 2011, Huntsman Advanced Materials, Cambridge, UK). The actual strain during testing was measured using a video extensometer equipped with Imetrum video gauge software (Imetrum Ltd., UK). Flexural tests in three-point bending mode were performed on un-tabbed composite specimens having similar dimensions as the tensile test specimen described previously, in accordance to ASTM D7264M-15 using a crosshead speed of 1 mm/min and 1 kN load cell. A span-to-thickness ratio of 40:1 and 32:1 were used for laminated composites and flax nonwovens, respectively. The sample thickness of all composites sample was determined using digital micrometer (705-1229, RS components, Corby, UK). All laminated composite and flax nonwovens were preconditioned and tested at 40 ± 1 % RH and 21 ± 1 ºC. A total of 5 specimens were tested for each type of samples.

3.4.7 Dynamic Mechanical Thermal Analysis (DMTA) to Investigate Modulus Evolution as a Function of Temperature

Dynamic mechanical analysis was conducted in tensile and flexural mode using a RSA-G2 equipment (TA Instruments). Temperature scans were run from 25 °C to 250 °C at a heating rate of 3 °C/min and 1 Hz frequency. Sample dimensions were approximately 15 mm (length), 5 mm (width) and 0.07 – 0.7 mm (thickness). The gauge length used was 10 mm.

3.4.8 Wicking Test for Critical Surface Energy Measurements

The critical surface energy (γ_c) of the films was determined using a wicking method [251]. Rectangular strips (5 mm x 20 mm) were cut and mounted at one end onto the K100 Tensiometer (Krüss, Hamburg, Germany) microbalance using the sample clip. The reservoir containing test liquids was moved upward toward the free end of the strip, and immediately upon contact, the movement of the reservoir was stopped. This ensures that the mass gain is only a result of the penetration of the test liquid into the strip by capillary action. The mass gain of the strip was recorded as a function of time and a total of 6 strips were tested for each test liquid. The γ_c of the samples was then evaluated using a modified Washburn equation:

$$\gamma\cos\theta = \left[\frac{2}{A^2 r}\right]\left[\frac{\eta}{\rho^2}\right]\left[\frac{m^2}{t}\right] \qquad \text{(Equation 3.7)}$$

where γ, η, ρ, are the surface tension, viscosity, and density of the test liquid, respectively. m, A, r, θ, and t are the mass gain due to capillarity action (wicking), the cross-sectional area of capillary, radius of the capillary, contact angle, and time, respectively. However, in this study, the capillary geometry of the tested sample is not known. By assuming the capillary geometry is constant for all films prepared using the same method, the factor $[2/A^2 r]$ can be grouped into a constant factor [1/C], which leads to:

$$C\gamma\cos\theta = \left[\frac{\eta}{\rho^2}\right]\left[\frac{m^2}{t}\right] \qquad \text{(Equation 3.8)}$$

The critical surface energy of a solid in analogy to a Zisman plot [251], which corresponds to the maximum of the function $[m^2/t][\eta/\rho^2] = f(\gamma)$ can be determined by performing wicking measurements using a series of different test liquids with known surface tensions. The summaries of test liquid used in this experiment are shown in Table 3.1.

Table 3.1 Properties of the test liquids used for wetting measurements[a]

Test liquid	γ (mN/m)	η (mPa.s)	ρ (g/cm^3)
n-heptane	20.4	0.409	0.684
dodecane	25.4	1.350	0.749
decalin	30.6	3.596	0.895
benzylalcohol	39.0	7.052	1.042
ethyleneglycol	48.3	21.810	1.109
glycol/water (80:20)	52.2	8.133	1.109
formamide	59.0	3.607	1.133
glycol/water (20:80)	64.8	1.331	1.109
water	72.8	1.002	0.998

[a] γ, η, and ρ are the liquid surface tension, viscosity, and density, respectively.

3.4.9 Contact Angle Measurements

The contact angle of 10 µL water droplets on the film surfaces was measured after 1 min after placing a droplet onto the film surface using the static sessile drop method (DSA 10 MK2, Krüss, Hamburg, Germany). The experiment was conducted at room temperature and at least five measurements were taken for each sample.

3.4.10 Inverse Gas Chromatography (IGC) for Surface Energy Analysis

Brunauer-Emmett-Teller (BET) specific surface area and surface energy heterogeneity of the sample were determined by means of inverse gas chromatography using surface energy analyzer (SEA, Surface Measurement Systems, UK). Approximately, 100 mg sample powder or 500–700 mg film was packed in pre-silanized IGC columns (Surface Measurement Systems Ltd., London, UK) and pre-conditioned for 1 h at 30 °C and 0% RH. Helium at a flow rate of 10 sccm was used as a carrier gas and methane was used to determine the dead volume correction factor. BET surface area was measured using octane as a probe and the dispersive surface energy component (γ^d) was measured by injecting a series of n-alkane probes (hexane, heptane, octane, nonane, and decane) at a range of 0.1% to 30% target surface coverage (n/nm). The polar probes (dichloromethane and ethyl acetate) were injected at the same concentrations to determine specific (acid-base) interaction (γ^{ab}). All chromatogram peaks were defined using first statistical moment at peak's center of mass (Peak COM) and the net retention volumes were calculated based on Schultz method [252].

3.4.11 Streaming Potential Measurements for Film's Electrokinetic Behavior Analysis

The electrokinetic behavior of films was evaluated using ζ-potential measurements (SurPASS Electrokinetic Analyzer, Anton Paar) based on streaming potential method using Adjustable Gap Cell (AGC). For each measurement, a pair of films with the same top layer was fixed on the rectangular sample holders having dimension of 20 mm x 10 mm using double-sided adhesive tape. The sample holders were inserted in AGC such that the surfaces of the samples were facing each other with approximately 100 μm gap size. The pH-dependence of streaming ζ-potential was measured by pumping 1 mM KCl electrolyte solution through the gap with the pH value gradually being varied in a range of 2 to 10 by adding 0.1 M HCl or 0.1 M KOH using automatic dual syringe pump system.

3.4.12 Thermogravimetric Analysis (TGA) for Thermal Stability Evaluation

Thermogravimetric analyzer (Discovery TGA) was used to measure thermal stability of freeze dried sample and films. Temperature scans run from 40 °C to 600 °C at a heating rate of 10 °C/min in nitrogen and air atmosphere. Onset degradation temperature was taken when the sample mass was reduced to 90% of its original weight and DTG curve were plotted by taking first derivative of percentage mass loss over temperature range.

3.4.13 Dynamic Vapor Sorption (DVS) for Moisture Adsorption Behavior Analysis

Moisture sorption/desorption behavior for films and composites was investigated using dynamic vapor sorption (DVS Intrinsic, Surface Measurement System, London, UK). The sample was loaded into small pan and attached to an ultramicrobalance, which is located inside a thermostatically controlled chamber. The humidity inside the chamber was then controlled following the sequence of: 0% →50%→0%→90%→0%, with 12 or 24 h time interval between each step to allow the samples to equilibrate. All measurements were run at 25 °C and the change in mass as a result of moisture sorption/desorption was measured as a function of time.

CHAPTER FOUR
CHITIN-GLUCAN NANOFIBERS FROM COMMON MUSHROOM: A COMPARATIVE & GRAMMAGE STUDY

4.1 Introduction

In Section 3.1, six major themes for entire study were presented: comparative study, grammage study, optimization study, film composite study, laminate study and flax study. This chapter attempts to discuss the first two of them in light of the following questions: (1) what is the difference between fungal and animal chitin and how will it affect the bulk properties of resulting film? and, (2) what is the effect of grammage on fungal film properties?

4.2 Extraction Process and Chemical Constituents of the Extract

Mild extraction process was adopted in this study in order to preserve the native quality of chitin-based fibers. Prolonged acid treatment during demineralisation step are known to degrade chitin chain while longer deproteination reduces its acetyl content [123]. Lower levels of inorganic materials in mushroom suggest a demineralisation step is not necessary during the extraction process. Peroxide or chlorinated bleaching on the other hand, was not carried out due to their known depolymerization effect on biopolymer chain [253]. In case of cellulose or animal based chitin, this effect might be minimal. However, chitin in fungi are linked chemically to the branched glucan polymer [4]. It is this branched part that is more susceptible to chemical attack during bleaching treatment. As we want to maintain chitin-glucan composite structure, we decided to not include any decolorization process throughout our study.

Although both mushroom's stalk and cap were originated from identical mycelium, we decided to investigate them separately. Deformation on a stalk revealed it is five time stiffer longitudinally than a cap, which is ascribed to its elongated cell structure and denser vertical packing [254]. At low magnification, stalk mycelium was observed to be longer than cap mycelium (see Figure 4.1). We were interested to see whether this anisotropic macroscopic structure leads to longer structural fibers in stalk wall. If this is true and if the fibers were not severely damaged during extraction process, we might see distinct difference in mechanical properties of the respective films.

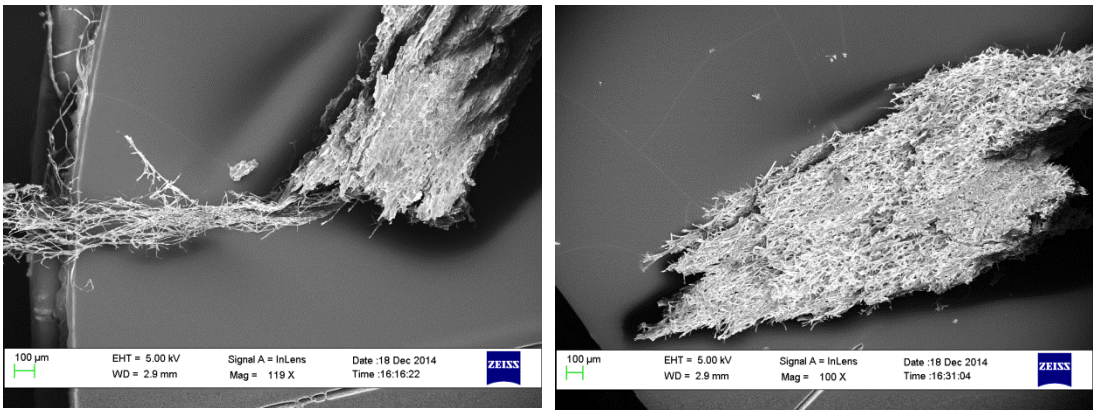

Figure 4.1 Scanning electron micrograph of (a) *A. bisporus* stalk mycelium, (b) *A. bisporus* cap mycelium.

Figure 4.2 depicts an extract at 3% w/v consistency obtained from 3 kg fresh whole mushroom. It is a viscous paste (see Figure 4.2a) and easily resuspended in water with minimal agitation. Enzymatic browning during mushroom postharvest [255] and bruising during pre-blending treatment explains the brownish color of the extract. Extracts from both mushroom and crab shell were stored in never-dried condition to prevent fiber hornification. Hornification causes irreversible loss of fiber swelling as a result of pore closure in the fiber wall during drying [256], which in turn reduces fiber dispersive stability in suspension. Figure 4.2c shows stability of whole mushroom extract suspension (0.8% w/v, 1 min post-blending time) after one week. Never-dried extract resulted in a stable colloidal suspension indicating particulate fiber size, whereas freeze dried suspension tended to settle at the bottom, indicating aggregation of fibers. Extract that is subjected to slow freezing (via freezer, 0 °C) prior to freeze drying is more susceptible to hornification compared to extract that is subjected to fast freezing (via liquid N_2). Slow ice formation during slow freezing provided more time for fibers to reorient themselves into bigger aggregates. Only never-dried extracts were used in our film preparation.

One kilogram of fresh whole mushroom yielded 14.0 g of fiber while one kilogram of fresh stalk and one kilogram of fresh cap yields 15.4 g and 11.2 g fiber mass respectively. For crab, one kilogram of dried shell yields 97.2 g fiber. A lower amount of fiber was expected from the mushroom source as water made up around 94% of their fresh body mass. Table 4.1 compares the yield of respective extracts per dry weight along with their elemental constituents. While the N content in crab is in accordance to the N content of commercial chitin, a lower N

value was observed for mushroom source. This is due to the existence of glucan as suggested by the higher oxygen content responsible for more hydroxyl groups in mushroom source. Chitin and glucan contents can be determined based on their monomer precursor, glucosamine and glucose, respectively (see Table 4.2).

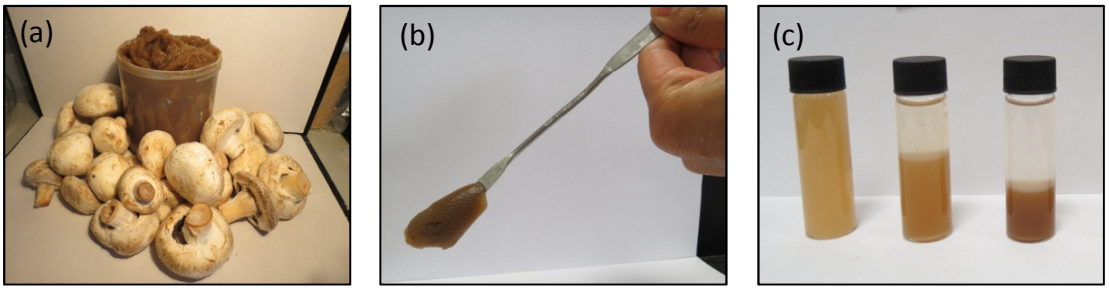

Figure 4.2 (a) chitin-glucan extract from 3 kg fresh mushroom, (b) 3% w/v extract consistency, (c) 0.8% w/v suspension after 7 days: left = never dried suspension, middle = resuspension of freeze dried sample (fast freezing), right = resuspension of freeze dried sample (slow freezing).

Table 4.1 Elemental analysis of extracted samples

Sample	C (%)	O (%)	H (%)	N (%)	S (%)	Yield (%)
Commercial chitin	44.64	39.61	7.29	6.49	< 0.02	NA
Pagurus	43.83	39.73	7.22	6.39	< 0.02	9.72
Stalk	42.22	44.45	7.24	2.95	< 0.02	25.44
Cap	42.87	43.36	7.20	3.28	< 0.02	15.04

Table 4.2 Contents of sugar monomers in the extracted samples[a]

Sample	Galactose (%)	Glucose (%)	Xylose (%)	Mannose (%)	Glucosamine (%)	Total sugar (%)
Commercial chitin	0.0	0.0	0.0	10.8	65.7	76.5
Pagurus	0.0	0.0	0.0	10.7	58.3	69.0
Stalk	0.2	46.8	1.0	5.8	29.8	83.6
Cap	0.4	39.6	0.9	6.5	32.3	79.7

[a]Arabinose and rhamnose were not detected in any of the samples.

Extract from crab consist mainly chitin while the rest is mannose sugar (see Table 4.2). The origin of the sizable content of mannose in our crab extracts is unclear, and a similar proportion can also be found in commercial grade chitin. Higher calcification in *C. pagurus*

exoskeleton [257, 258] tends to contribute lower chitin yield (9.7%) per shell dry mass when compared with other crab species (10–33% chitin yield) [145, 259, 260]. As for mushroom extract, the main polysaccharides are chitin and glucan. Stalk comprises of 36% chitin and 56% glucan, while cap comprises of 41% chitin and 50% glucan (per total sugar). Denser mycelium packing in *A. bisporus* stalk correlates with the higher yield of total fiber mass but chitin content tends to be higher in the cap. These observation also shared by other researchers [84]. Small amounts of mannose, xylan, and galactose might be originate from the water soluble polysaccharide fraction [261, 262] that was entrapped during extraction process or from residual hemicellulose-like material that cannot be removed during the extraction process.

4.3 Fiber Morphology and Film Preparation

Shams et al. obtained chitin nanofibers with a variable width of 30–110 nm when using high speed blender under neutral pH [145]. Blending under acidic condition fibrillates the fibers further to 20–30 nm due to cationic repulsion of protonated amine group [146]. In accordance with the mild extraction process, we only use a domestic kitchen blender at neutral pH to facilitate nano-fibrillation of our never-dried extract. This approach has also been tried on never-dried cellulose, yielding a uniform nanofibers (15–20 nm width) after 30 min high speed blender treatment and able to produce less fiber damages compared to grinder or homogenizer treatments [263].

In our case, uniform nanofibers with 10–20 nm diameter and several micrometer in length can be obtained directly after chemical extraction of the whole mushroom (see Figure 4.3a,c). Further nanofibrillation is unnecessary as the size of the fiber is already similar to the one attained by grinder treatment [60]. Nevertheless, 1 min post blending is carried out to facilitate the formation of a homogenous suspension. On the other hand, aggregate of fibrous features are more prevalent in crab shell extract (see Figure 4.3b). After the chemical extraction, 10 min post-blending of crab extract breaks the aggregate into nanofibers with an average diameter of 80–120 nm (see Figure 4.2d) – up to six times bigger than the size typically obtained from grinder or homogenizer treatment [21, 22, 57]. Longer blending time of up to 20 min did not change an overall fiber size, indicating an insufficient shear force of kitchen blender. With regards to the fiber dimensions originated from different part of mushroom, both stalk and cap possess uniform fibers with similar widths (10–20 nm), but the former can be seen to be more oriented and longer

(see Figure 4.3e,f). We are unable to discern the true length of individual fiber due to the high aspect ratio of chitin nanofibers, making it impossible to fit the whole fibers in the micrograph without losing the resolution – a common problem also with cellulose nanofibers [264].

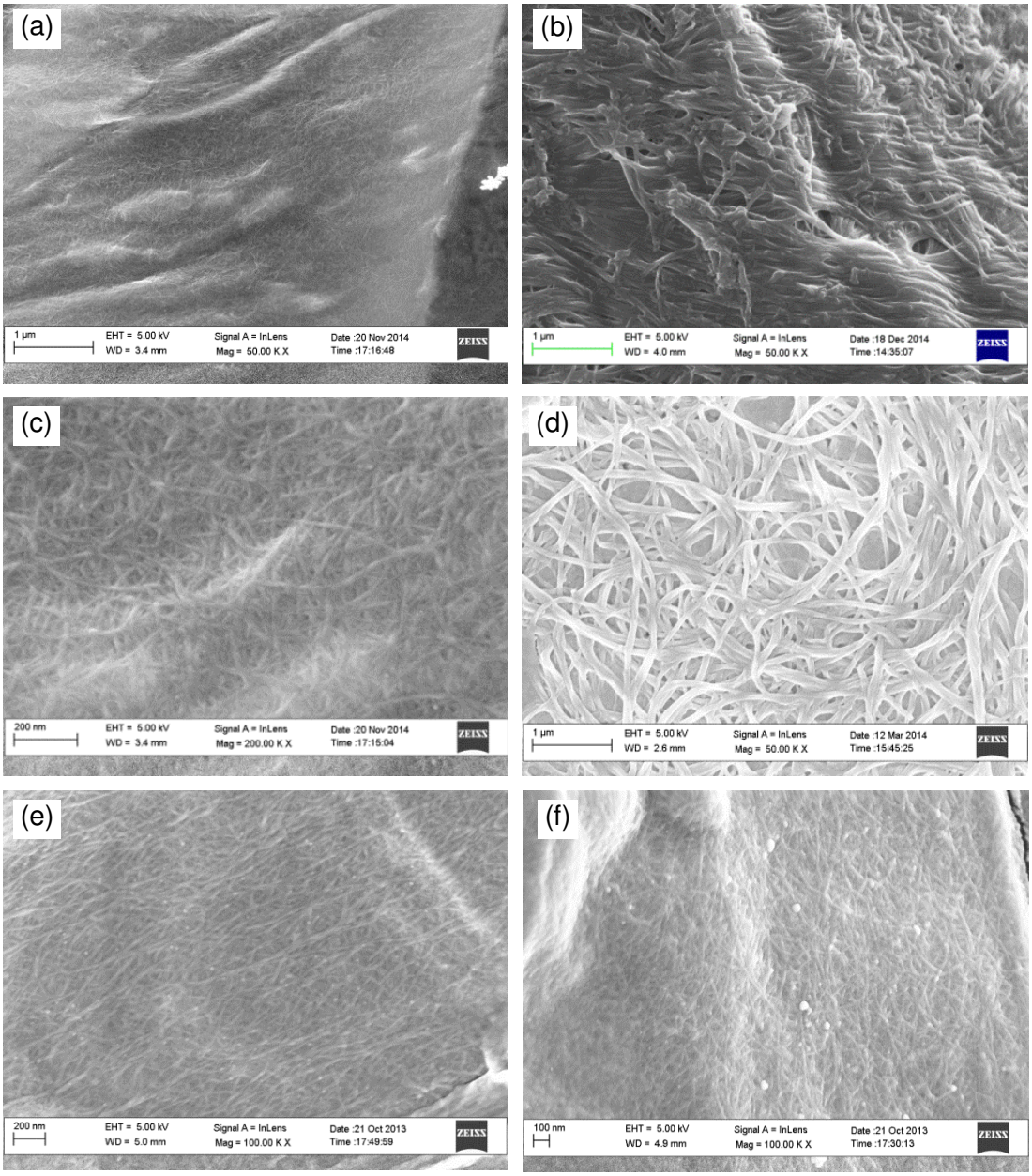

Figure 4.3 (a) unblended whole mushroom extract, (b) unblended pagurus extract, (c) unblended whole mushroom extract at higher magnification, (d) pagurus extract after 10 min post-blending, (e) stalk extract after 1 min post blending, (f) cap extract after 1 min post-blending.

As far as energy consumption is concerned, being nanosized without undergoing any harsh post-mechanical nanofibrillation signifies a clear advantage of using mushrooms over crustaceans for chitin based product. This might be attributed to the high water content in the mushroom fruiting body (>90%), which renders the structural fibers in mycelium cell wall to be always in water-swollen state, thus suppressing the hornification effect.

At lower magnification, a dilute suspension of fungal based extract exhibits a good film forming capability in contrast to the more disintegrated nature observed in animal based extract (see Figure 4.4a,b). This can be ascribed to the presence of amorphous glucan that can act as glue, which bind fibers together in a dense network. Similar film forming capacity was also observed in the freeze dried sample (see Figure 4.4c,d).

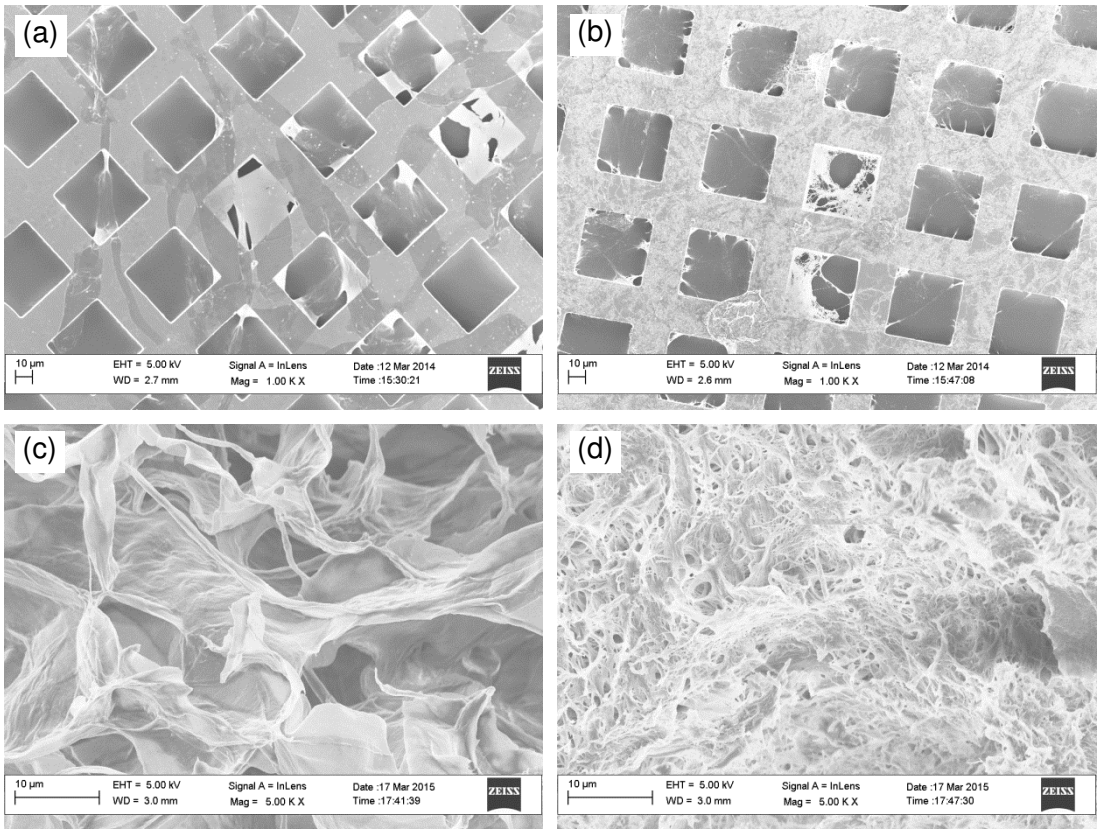

Figure 4.4 (a) 0.01% w/v blended whole mushroom chitin-glucan extract, (b) 0.01% w/v blended pagurus chitin extract, (c) freeze-dried whole mushroom chitin-glucan extract, (d) freeze-dried pagurus chitin extract.

During film preparation, significant differences in filtration time were observed for each extract. When a 100 mL water suspension containing 0.5% crab extracts was vacuum filtered to produce a wet thin film of 90 mm in diameter, the duration was only 10 min. This fast filtration time, approximately 9 times faster over cellulose nanofiber has been reported earlier [145]. On the other hand, whole mushroom extracts took 60 min to be filtered under the same conditions demonstrating fungal chitin has higher water affinity than animal chitin. This can be ascribed to the amorphous structure of glucan in contrast to the semi-crystalline structure of chitin. Water swells the glucan matrix completely while it is only accessible to the surface of the chitin nanofiber. Presence of an additional hydroxyl group from glucan and denser packing due to smaller nanofibers can also explain long filtration time. It is interesting to note that fibers from different parts of the mushroom show totally different filtration behavior. For example, under the similar conditions mentioned previously, filtration time for the cap extract took almost 120 min compared to only 20 min for the stalk extract. Difference in water affinity as a function of glucan content failed to explain this stark disparity as more glucan were found in stalk than in cap. It might be the case that fiber morphology plays a more dominant role on dewatering resistance during the filtration process. Shorter and less oriented nanofibers observed in cap – this is only tentative as we are not sure whether it is really shorter or really less oriented, we can only assume from SEM image – are more easily conformed to each other when packed under gravity filtration yielding less porous network. In addition, the presence of complex melanin pigment originated from the mushroom cap gill might also confer an additional resistance to the overall filtration flow rate.

Figure 4.5a shows films that were prepared from never-dried suspension of the respective extract. Amorphous glucan acts as the cementing material between the fibrils, making the surface of fungal chitin-glucan film smoother than crab chitin film. This smoothing effect is analogous to the way lignin is being softened during hot pressing, acting as binder to cellulose nanofibrils [265].

Optically, all films (100% fiber content, 60–80 µm thickness) are translucent even though no decoloration process took place during the extraction process (see Figure 4.5b). Fungal based films were observed to be more translucent than the crab based film as a result of smaller nanofibers and less light scattering due to a smoother surface. The cap film is slightly darker than the stalk film as a result of additional dark pigment originated from the gill (spore bearing

structure underneath mushroom cap). In addition, the pagurus film is less brittle than the fungal based film, and can be folded like a standard filter paper. Nevertheless, the fungal-based films possessed some flexibility on their own (see Figure 4.5c).

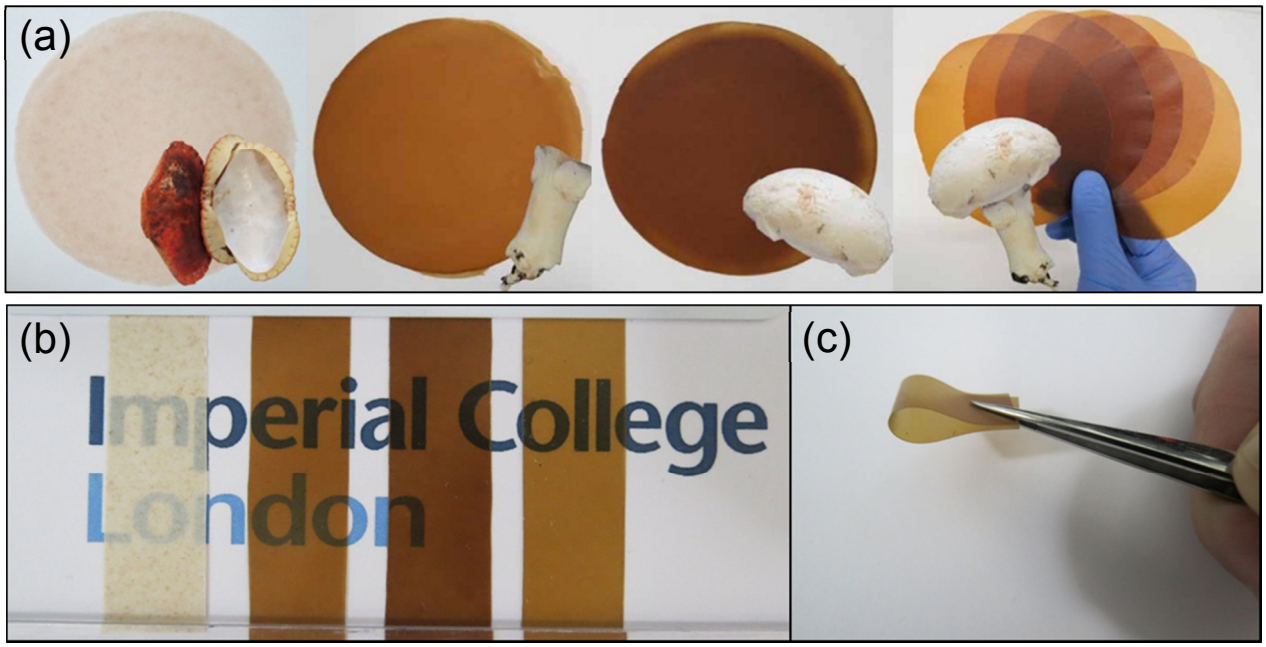

Figure 4.5 (a) films made from the nanofibers extract with their respective source materials, (b) optical appearance of the 80 g/m^2 films with a thickness between 60 to 80 µm, (c) flexibility of 80 g/m^2 fungal based film.

4.4 Crystallinity and Degree of Acetylation

The XRD pattern of the freeze dried sample and its respective films are shown in Figure 4.6. Powder diffraction patterns for crab extract exhibited typical diffraction peaks of α-chitin at 9°, 12°, 19°, 20°, 23°, and 26° which correspond to the diffraction plane of 020, 021, 110, 120, 101, and 130, respectively [10, 63]. Similar patterns were observed for commercial chitin sourced from a shrimp shell. On the other hand, fungal extract exhibited only two broad peaks at 9° and 19° demonstrating poor crystallinity and a presence of a considerable quantity of amorphous material. The amorphous content in fungal extract can be ascribed to glucans that masks the crystalline peaks of the chitin. Acid treatment during extraction process has been shown to

sharpen fungal diffraction patterns considerably whereby all α-chitin peaks can be observed [88]. However, this comes at the expense of further N-deacetylation and chain depolymerization.

The crystallinity index (CI%) of all samples was calculated based on the area under the curve of the diffraction pattern, instead of the more common peak height method [266, 267]. The peak height method is derived from Segal's empirical equation [268] for native cellulose devoid of any impurities and therefore, inaccurate when used to calculate amorphous-laden samples such as wood cellulose [269] or in this case, chitin-glucan sample from a fungal source. Sample crystallinity values and chitin crystallite sizes at 020 plane of the freeze dried samples and films are tabulated in Table 4.3.

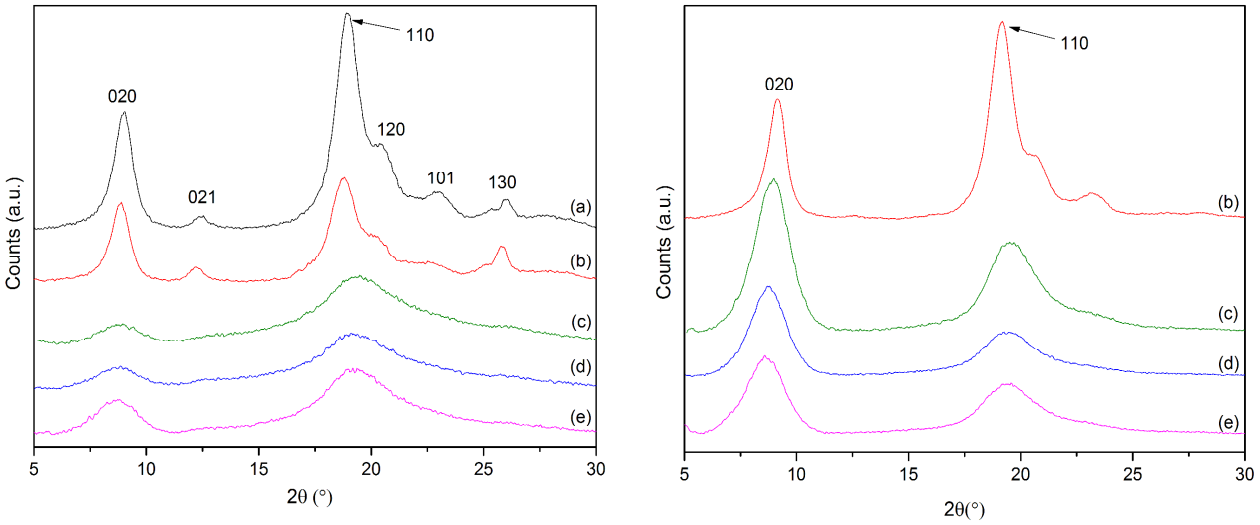

Figure 4.6 X-ray diffraction patterns. Left: freeze dried powder sample, right: film sample. (a), (b), (c), (d), (e), and (f) represent commercial chitin, pagurus, stalk, cap, and ABW respectively.

Table 4.3 Sample crystallinity index, chitin crystallite size, and degree of acetylation (DA)

Sample	Crystallinity Index (%)		Crystallite size, $L_{(020)}$ (Å)		DA (%)
	powder	film	powder	film	film
Commercial chitin	76.4	N/A	66.9	N/A	88.1
Pagurus	82.2	85.7	65.4	63.8	91.8
Stalk	44.3	63.9	34.5	40.2	114.5
Cap	56.4	65.3	35.3	37.8	112.6
ABW	50.9	65.8	37.1	40.6	123.0

Crystallite size for fungal chitin is smaller than animal chitin and due to amorphous glucan, overall sample crystallinity index (CI%) of fungal chitin is lower than animal based chitin. It is interesting to note that significant change in CI% occurred when fungal extract is converted into film with pronounced increase in diffraction intensity at 020 reflections (see Figure 4.6, right). An increase in CI% up to 44% was observed for stalk film, while 29% and 16% increase was observed for the whole mushroom film and the cap film, respectively. Increase in CI% at the cross-sectional plane of the film is expected as a result of a layered structure formed during filtration process [18]. However, our diffractogram was taken perpendicular to the film surface where random fiber orientation dominates. Without external stimuli such as cold drawing [19] or wet stretching [270], there should be no or minimal CI% change expected as occurred in our crab film sample. We speculate that the significant increase in CI% for fungal film was due to the reorientation of amorphous glucan as a result of heat treatment during hot pressing, which in turn allows some reorganization of chitin chain.

Figure 4.7 shows an IR absorbance of film sample under ATR reflection mode. Both commercial chitin and crab chitin show identical spectra with a split amide I band at 1620–1670 cm^{-1} (C=O stretching) characteristic of α-chitin polymorph [68] .

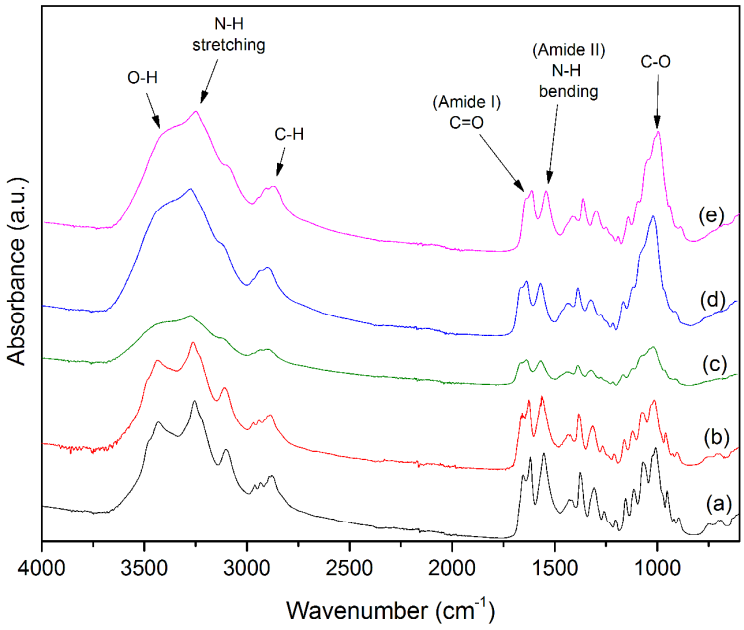

Figure 4.7 ATR-FTIR absorbance of film sample. (a), (b), (c), (d), (e), and (f) represent commercial chitin, pagurus, stalk, cap, and ABW respectively.

This doublet feature can also be seen in fungal spectra but in a convoluted form due to low sample crystallinity. Deacetylation of chitin into chitosan converts the acetamide group into a primary amine group, which will weaken amide I band considerably. O-H stretching region at 3450–3480 cm^{-1} is broader in fungal sample than in animal chitin source as a result of an additional hydroxyl group originated from glucan chain. We should note that the region of OH stretch is also heavily influenced by absorbed water which is difficult to eliminate in IR measurements. It might be the case that apart from introducing more hydroxyl group, amorphous glucan also allows more water to be absorbed, hence a broader OH band. Similar band broadening was also reported for other mushroom species [60, 92], while well resolved peak was observed in higher crystalline chitin source found in marine algae [63].

Preservation of the acetyl group via mild extraction process renders the chitin film more hydrophobic, stronger, and less prone to enzymatic degradation [126]. All our samples exhibited a high degree of acetylation (DA) (see Table 4.3). For fungal sample, the true nature of linkage between chitin and glucan were not elucidated, hence its DA value is only relative rather than absolute. Given its DA value > 100%, there is strong tendency that the chitin chain in our fungal source are fully acetylated. This observation was also shared by other researchers when the extraction process only consisted of NaOH treatment [105]. Even with the inclusion of an acid during the extraction process, high DA values ranging between 80% to 95% can still be maintained in fungal source [60, 86].

4.5 Physical and Mechanical Properties of the Films

Table 4.4 shows the density, porosity, and specific surface area of the respective films. The fungal films have higher densities than the pagurus film. The density of the pagurus film (1.40 g/cm^3) is lower than theoretical chitin density (1.46 g/cm^3) [271] because of the deacetylation effect that occurs during the extraction process and the development of interstitial spacing during film preparation. The pagurus film is more porous than the fungal film as a result of larger nanofiber size. Capillary action during water evaporation leads to the collapse of fibers and therefore all films exhibit very low surface areas. The fungal film has approximately 10–17 times lower surface area than the pagurus film. This can be ascribed to the presence of amorphous glucan that masks the crystalline chitin fiber surface – a feature that can be beneficial for barrier properties. We should also acknowledge that the presence of mannose in crab-based

sample can also contribute to amorphous character. Nevertheless its proportion is certainly lower than that of glucan in the fungal-based sample, and thus not really affects the interpretation.

Table 4.4 Physical and mechanical properties of the films[a]

Sample	ρ (g/cm^3)	P (%)	SSA (m^2/g)	Tensile strength (MPa)	Young modulus (GPa)	Elongation at break (%)	Tensile toughness (MJ/m^3)
Pagurus	1.40	67.30	1.75	69.5 ± 4.6	2.7 ± 0.5	6.2 ± 0.7	2.7 ± 0.4
Stalk	1.50	64.99	0.11	191.9 ± 10.6	5.0 ± 0.3	9.2 ± 1.3	10.1 ± 1.6
Cap	1.47	62.29	0.17	192.9 ± 12.0	5.2 ± 0.5	7.4 ± 1.5	8.0 ± 1.6
ABW	1.47	58.95	0.22	204.4 ± 4.0	6.9 ± 1.2	5.3 ± 0.4	5.3 ± 0.5

[a] ρ, P, and SSA represent film density, porosity, and specific surface area, respectively.

Figure 4.8a illustrates stress-strain behavior of films under uniaxial tension with their respective data summarized in Table 4.4.

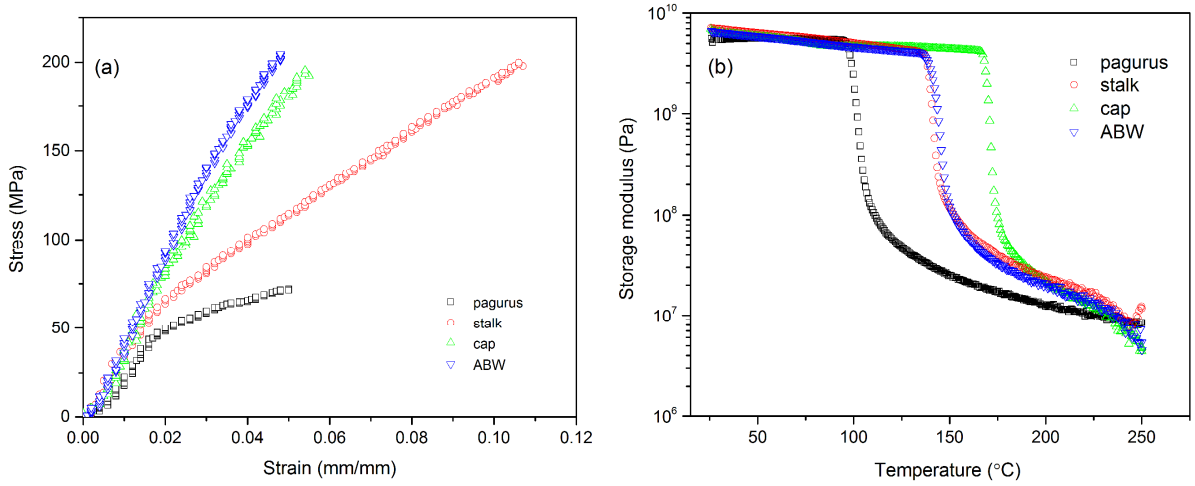

Figure 4.8 (a) stress-strain curve from uniaxial tensile test, (b) evolution of storage modulus from DMTA tests.

All fungal film possesses higher modulus and strength than pagurus film (see Table 4.4). With tensile strength approximately 200 MPa, film made from common mushroom chitin-glucan extract is three times stronger than the film made from crab shell chitin. To our knowledge, this is the highest value ever reported in chitin literature. Our pagurus film still exhibits superior film strength and comparable modulus when compared with other crustacean chitin films made from

10–20 nm width fiber [25]. Another researcher working with 20–30 nm width chitin nanofiber isolated from crab also shared a similar film strength (77 MPa) as our pagurus film. However, they reported a higher modulus value of 8.2 GPa. This is probably caused by a higher consolidation pressure applied during film preparation that leads to a less porous film [140]. When milder extraction is used, Berglund's group found the strength of the chitin film can be improved up to 153 MPa but saw no improvement in film modulus [26]. This illustrates that extraction process, especially the one that promotes minimal fiber damage, has a more dominant role towards improving film strength than the size of nanofiber while the modulus is largely governed by film porosity. It might explain why our stalk, cap and ABW films exhibits much higher strength than the pagurus film since their fiber extraction is devoid of any acid treatment. The other reason might be attributed to amorphous glucan, which may act as plasticizer that mitigate the brittleness factor of chitin. With more glucan content and presumably longer fibers, the stalk film has higher strain to failure and tensile toughness than the cap film.

The evolution of film's storage modulus in tensile mode across the full temperature range is depicted in Figure 4.8b. At room temperature, all samples possess approximately similar storage modulus that fluctuates between 4 to 6 GPa. The trend continues until about 100 °C, when a drop of two orders of magnitude is observed for the pagurus film. Similar drop of magnitude was also observed with the fungal based film but it occurs at higher temperature: around 140 °C for stalk and ABW film, and 165 °C for cap film. Chitin supposedly makes a film stiffer due to its semi-crystalline structure. Higher chitin content in cap might explain why it can retain the modulus at higher temperature than the ABW or stalk films. The pagurus film consist mostly chitin, but acid treatment during the extraction process leads to fiber damage and deacetylation that can compromise the inherent properties of the resulting film.

4.6 Surface Characteristic Analysis

The hydrophobicity of a material can be assessed by the contact angle of a water droplet deposited onto its surface. Stalk, cap, and ABW films exhibit relatively hydrophobic character with water contact angles three times higher than that of the pagurus film (see Figure 4.9a). Even after 1 h, fungal based film still retains the shape of a droplet while a collapse is apparent on the pagurus film (see Figure 4.9b).

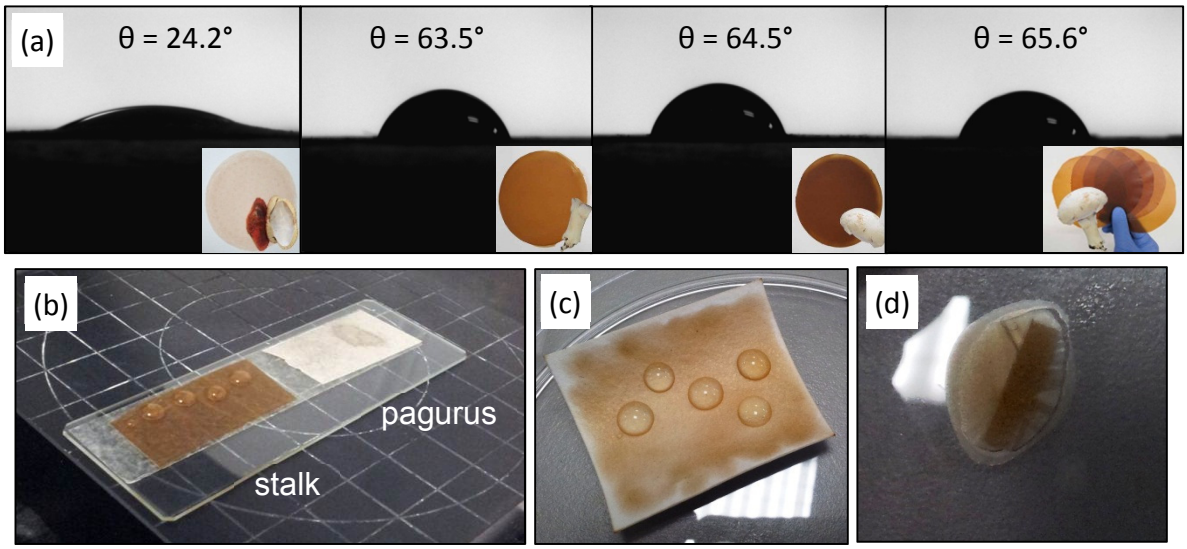

Figure 4.9 (a) water contact angle after 60 s on the films from depicted source materials, (b) water contact angle after 1 h, (c) water drop on ABW coated blotted paper, (d) ABW coated filter paper.

Because all films possess approximately similar porosity, the contact angle results can be said to be comparable. Nevertheless, the pagurus film surface is rougher than the fungal based film surface and this factor can induce water hysteresis, which subsequently lowers its contact angle. By pelleting crab chitin whiskers at high pressure, Nair et al. [35] obtained a contact angle as high as 50°. A similar value of 55° was observed with animal chitin film consisting of 10–20 nm width nanofibers [145]. We suspect the contact angle of our pagurus film will fall around these values if higher pressure was applied during film preparation – though the value is still lower than the contact angle of our present fungal based films.

Higher relative hydrophobicity for the fungal film can be attributed to the better acetylated chitin polymer. Although additional glucan supposedly increase film hydrophilicity by adding numerous more accessible hydroxyl groups and by absorbing water, the polar contribution in the pagurus film was found to be more significant than in the fungal based film (will be discussed later in inverse gas chromatography section). The effect of hydrophobin, a unique fungal protein that imparts hydrophobicity to the fungal mycelium [272] can be ruled out because of the denaturing effect of alkaline towards proteins during the extraction process. The hydrophobic nature of fungal chitin can be exploited, for example, as a coating agent on an

otherwise highly hydrophilic material. Figure 4.9c shows how a thin coating using 0.8% w/v fungal extract prevents water from being absorbed through a blotting paper. The coatings are not only smooth, but it also adheres strongly to the surface. When a suspension of fungal extract dropped on a small piece of filter paper, formation of a thin film is visible around the outer edge (see Figure 4.9d).

During a wicking test, the fungal based film absorbs a smaller amount of solvent than the animal based film. Typical wicking curves for formamide are shown in Figure 4.10a. The initial slope is a result of the capillary effect imbibing the wetting liquid while the plateau is caused by the balance between capillarity and gravity. By evaluating the initial slopes of the wetting curves, a plot of normalized wetting rate (right hand side of Equation 3.8) against the surface tension of the test liquids can be produced (see Figure 4.10b). The data points for each sample are averaged from five repeated measurements and fitted using a Gaussian curve. The plot maximum which corresponds to Zisman's critical solid-vapor surface tension is used to define the critical surface energy (γ_c) of the respective film [273]. The liquids with surface tension to the left of the maximum fully wetted the test film while partial wetting was observed for liquids having surface tensions to the right of the maximum.

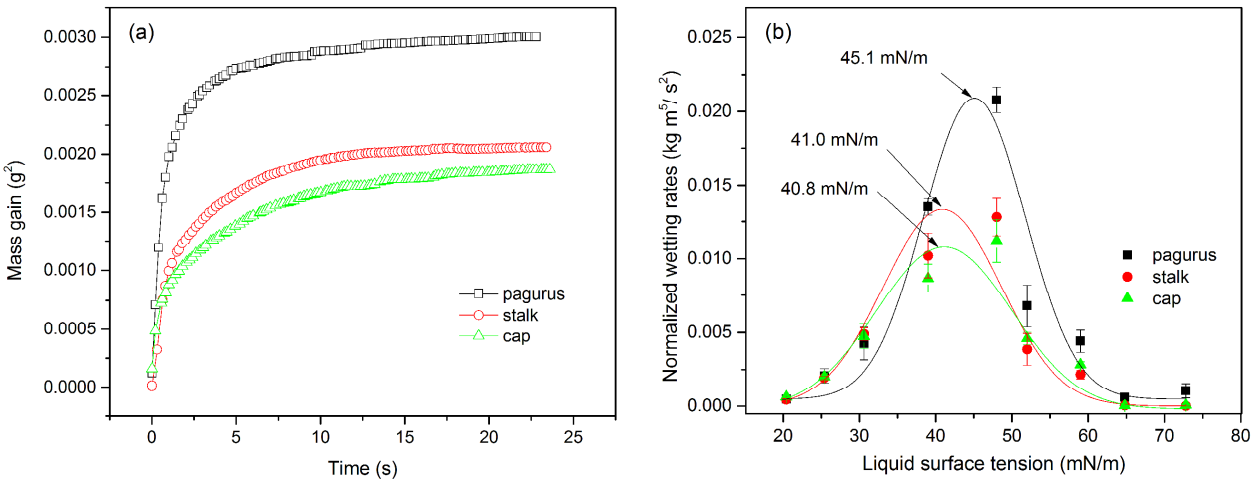

Figure 4.10 (a) typical wetting curve of the sample films by formamide, (b) normalized wetting rates as a function of the surface tension of the test liquids.

The stalk and the cap films have approximately similar γ_c of 41.0 mN/m and 40.8 mN/m respectively, while a higher value of 45.1 mN/m is observed for the pagurus film. The high γ_c

value of the pagurus film can be ascribed to its higher crystallinity and purity. By contrast, the fungal based films are composite material consisting of semi-crystalline chitin and amorphous glucan.

Figure 4.11a,b illustrates the surface energy profiles for both the freeze dried samples and the thin films measured by inverse gas chromatography (IGC). Their values for dispersive surface energy (γ^d), acid-base surface energy (γ^{ab}), and total surface energy (γ^t) at infinite dilution (n/n_m = 0.01) were summarized in Table 4.5. Surface energy characterization by inverse gas chromatography (IGC) is traditionally carried out at 'infinite' dilution or near zero surface coverage where only the most active site is considered. However a genuine solid surface is often heterogeneous as a result of (1) unevenly distributed disparate functional groups, (2) the presence of impurities, and/or (3) irregular surface topography. A single value at 'infinite' dilution will only account for an upper limit estimate, which is not necessarily representative of the whole surface. Injecting a higher amount of probing molecule (finite concentration) allows more interaction to occur at lower energy sites of the sample, hence allowing surface heterogeneity profile to be plotted [274].

The decreasing trend of surface energy with increasing surface coverage is due to interaction with less energetic sites and the upper value of $n/n_m = 0.3$ is chosen to rule out vapor-vapor interaction that occurs at higher surface coverage.

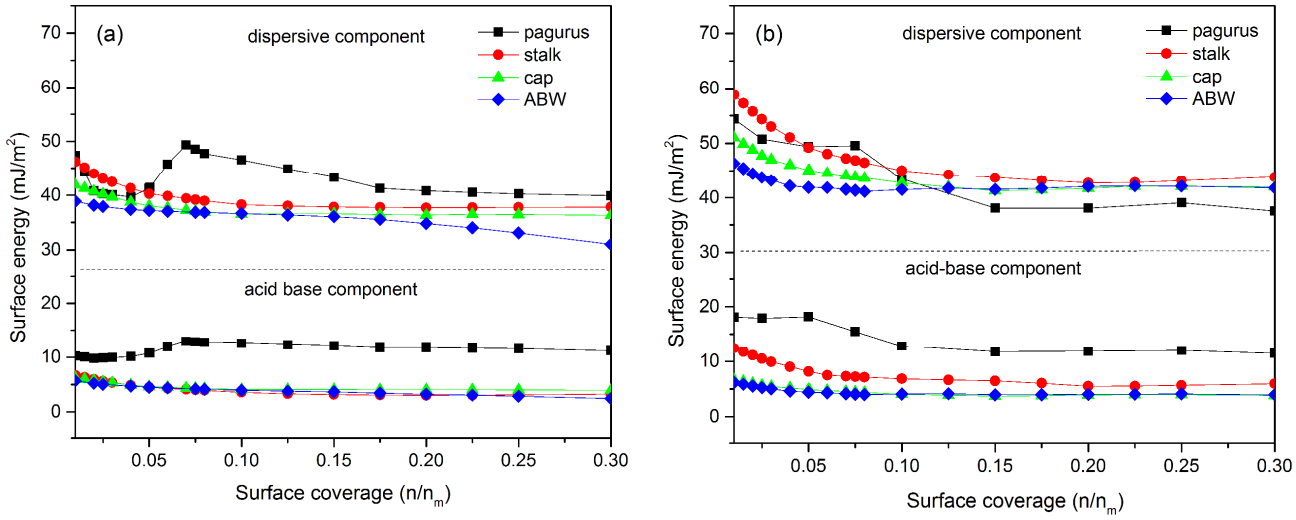

Figure 4.11 Surface energy profile measured by inverse gas chromatography for (a) freeze dried powder sample, (b) film sample.

Table 4.5 Dispersive (γ^d), acid-base (γ^{ab}), and total (γ^t) surface energy at $n/n_m = 0.01$ as measured from inverse gas chromatography

	γ^d (mJ/m^2)		γ^{ab} (mJ/m^2)		γ^t (mJ/m^2)	
	powder	film	powder	film	powder	film
Pagurus	47.3	54.4	10.2	18.1	57.5	72.5
Stalk	46.2	58.8	6.7	12.4	52.9	71.2
Cap	41.8	51.0	6.2	6.7	48.0	57.7
ABW	38.8	46.3	5.7	6.2	44.5	52.5

Our freeze dried sample was first powdered using non-cryogenic milling in order to facilitate their insertion into the IGC column. Intense milling activity generally increases γ^d due to the formation of a higher energy amorphous surface [275], but a decrease in γ^d is also possible if a lower energy crystal surface can be exposed during the process [276]. Less intense milling adopted in this study (3 min, 1 cycle) should not markedly alter the surface energy of the powdered sample. Yet, our γ^d = 47.3 mJ/m^2 for the pagurus powder is higher than what has been reported in literature for crustacean chitin: γ^d = 37–41 mJ/m^2 [277-279]. The disparity can be explained by the different processing and drying techniques used. All IGC result reported for chitin so far used commercial chitin that has been heat-dried compared to the freeze-dried sample in our study, thus the difference in the surface energy is expected. Severe fiber collapse during the heat treatment reduces the overall surface area, hence, obstructing potential exposure from the more active sites on the sample. In addition, our measurement at 0% RH reduces the occupation of water molecules at higher energy adsorption sites, thus producing a higher total surface energy value.

In the current study, all powder samples exhibit lower γ^d than the films due to their lower crystallinity. Stalk, which possesses the largest difference in crystallinity between its powder and its film, displayed the highest γ^d difference of 12.6 mJ/m^2. Pagurus, on the other hand, exhibited the smallest γ^d difference (7.1 mJ/m) between the powder and the film sample, which reflects its modest crystallinity difference between the two forms.

The films surface was also found to be more heterogeneous in surface energy than the powder surface. Among the fungal based films, the stalk film has the most heterogeneous surface profile with a difference between the highest energy site (γ^d_{max}) and the lowest energy site (γ^d_{min}) to be as large as 16.1 mJ/m^2. In comparison, cap and ABW films possess a difference of only 8.8 mJ/m^2 and 4.1 mJ/m^2, respectively. Similar trend in heterogeneity ($\gamma^d_{max} - \gamma^d_{min}$: stalk > cap >

ABW) was also observed for the fungal powder. A higher fiber anisotropy in stalk, presumably longer and more oriented, could be the reason for its more heterogeneous γ^d profile.

The pagurus sample was more polar than the fungal sample. The relatively high value of γ^{ab} in the pagurus sample can be attributed to a greater percentage of polar amide groups, which, in the case of fungal sample, will be lower due to the presence of glucan. The hydroxyl groups on glucan are less polar than the amide groups on chitin. Higher surface polarity not only causes pagurus film to be more hydrophilic (which evidenced by contact angle measurement), but also increase its total surface energy. As a result, the pagurus sample has a higher γ^t than the fungal based sample. It is worth noting that the polar nature is much more complex and there are many factors that influence the polarity other than just the amount of hydroxyl and amides. How the amides and hydroxyls are exposed in the chitin crystal is crucial, for example.

ζ-potential provides information on the surface chemistry of a solid material when it is in contact with an aqueous electrolyte solution. Dissociation behaviour of surface functional groups across a pH range can give an indication of surface basicity or acidity of the test material [280]. Figure 4.12 shows the streaming ζ-potential of pagurus, stalk, cap, and ABW film as a function of pH.

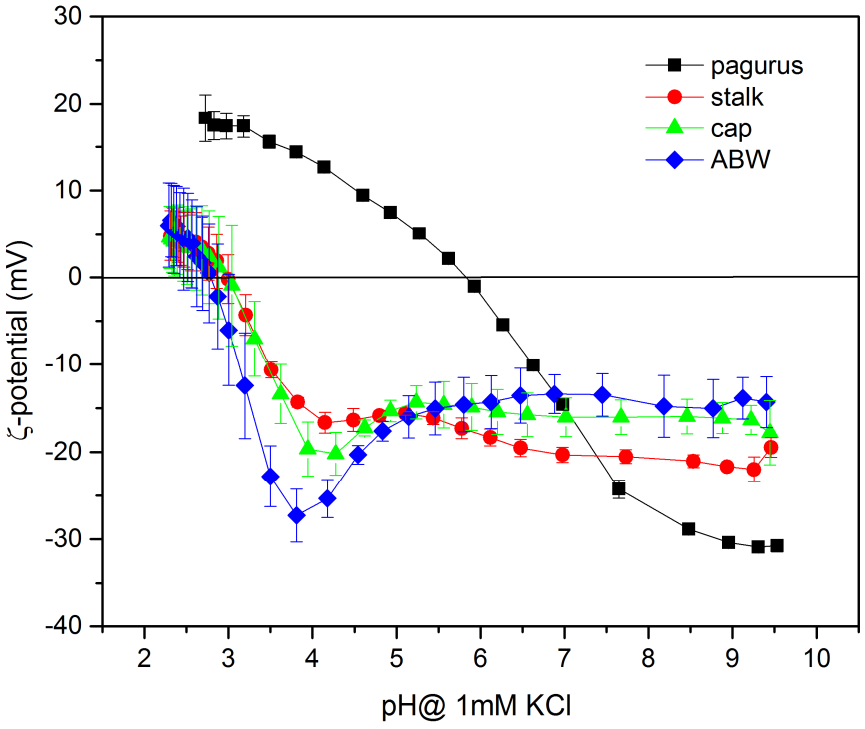

Figure 4.12 Streaming ζ-potential of the films as a function of pH.

All fungal based films exhibited a plateau at high pH, indicating that the surface is acidic as all dissociable functional groups are fully deprotonated. The acidic character is due to hydroxyl and carboxyl groups originated from glucan chain. Identical isoelectric points (iep) at pH 3 for the different fungal based films indicate similar charged surface groups between stalk, cap, and ABW. Lower plateau region observed in stalk ($\zeta_{plateau}$ = -20 mV) compared to cap or ABW ($\zeta_{plateau}$ = -14 to -15 mV) can be ascribed to a lower amount of impurities in the form of additional pigmentation compound that exist in cap gill. The absence of gill pigment consequently improves the accessibility of anionic dissociable groups in the stalk film.

On the other hand, the pagurus film exhibits a sigmoidal $\zeta = f(\text{pH})$ curve which indicates an amphoteric surface character. The protonation of the free amino group in chitin imparts a positive surface charge on the pagurus film surface, exemplified by the positive value of ζ-potential in the broad acidic region. By contrast, in the fungal-based film the percentage of free amino groups is minimal due to the higher acetylation degree: positive ζ-potential at very low pH occurred not because of amino group protonation but rather because of adsorption of protons (H_3O^+) on the film surface. Without additional glucan, the basic amino groups in the pagurus film were also more in balance with the acidic hydroxyl groups in the chitin chain, therefore, causing iep to be shifted to near-neutral pH (iep = pH 5.8). The more negative plateau region observed for the pagurus film ($\zeta_{plateau}$ = -30 mV) compared to the fungal based film ($\zeta_{plateau}$ = -14 to -20 mV) at higher pH can be attributed to the higher crystallinity of animal chitin film. Presence of amorphous glucan in fungal-based film promotes swelling in water. This swelling causes the transfer of the plane of shear into the electrolyte which exclude the diffusive part of the electric double layer from mechanical and electrical interaction [281], which consequently reduce the ζ-potential (going towards 0 mV).

4.7 Thermal and Moisture Sorption Properties

Thermal degradation behavior of the freeze dried sample under N_2 and air atmosphere is shown in Figure 4.13a,b. Commercial chitin (heat dried) was included for comparison.

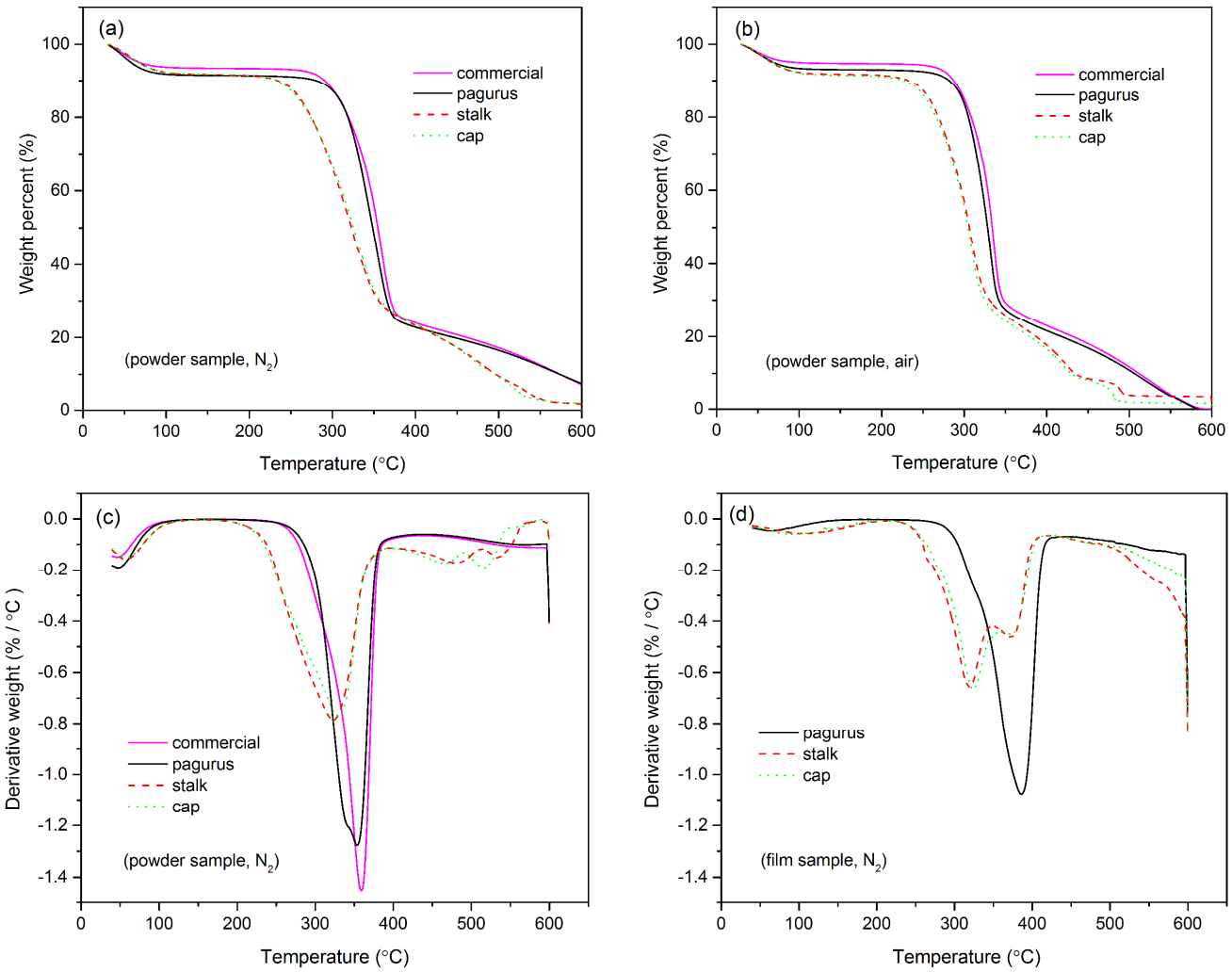

Figure 4.13 (a) TGA curve for powder sample in N_2, (b) TGA curve for powder sample in air, (c) DTG curve for powder sample in N_2, (d) DTG curve for film sample in N_2.

The initial weight loss between 60–100 °C in all investigated samples is mainly due to the removal of moisture. Onset temperature at 10% weight loss ($T_{d,10\%}$) is higher for the pagurus and the commercial sample ($T_{d,10\%}$ = 280–290 °C) than for the stalk and the cap samples ($T_{d,10\%}$ = 230–240 °C) (see Table 4.6). Better thermal stability of the animal based chitin is ascribed to its

bigger chitin crystallite size [282]. An increase in $T_{d,10\%}$ for all investigated samples up to 40 °C can be gained by a conversion into a film. The thermograms of the pagurus and commercial samples in both heating environments shows a single-step degradation, with the DTG curve indicating a maximum weight loss at 350–360 °C (see Figure 4.13c). This thermal event is primarily due to depolymerization of chitin with the formation of low molecular products and the formation of char [283].

Table 4.6 Onset degradation temperature at 10% weight loss ($T_{d,\ 10\%}$) by TGA analysis and moisture uptake for the film at 50% and 90% RH as determined by dynamic vapor sorption

Sample	$T_{d,10\%}$ (°C), powder		$T_{d,\ 10\%}$ (°C), film		moisture uptake (%), film	
	air	N_2	air	N_2	50% RH	90% RH
commercial chitin	287	291	–	–	–	–
pagurus	280	280	315	329	8.0	20.7
stalk	233	234	273	275	7.7	32.7
cap	227	233	272	277	8.0	30.0
ABW	237	234	246	251	7.9	32.7

Although the cap and the stalk samples seem to result in similar single-step thermograms as the commercial chitin, they possess wider DTG peaks in the temperature range of 239 °C to 407 °C. Given that the proportion of chitin and glucan in our fungal sample is almost similar, we suspect that this wider DTG peak is a product of two thermal events. An increase in chitin crystallinity and a decrease in glucan amorphous content during film preparation create two distinguishable phases that possess distinct decomposition temperatures. Thus, when DTG thermogram is plotted for the fungal film, a split into two thermal events is apparent (see Figure 4.13d). The first DTG peak at 319 °C can be ascribed to the decomposition of less crystalline glucan while the second DTG peak at 372 °C can be ascribed to the decomposition of more crystalline chitin. The temperature at which the second DTG peak occurs in the fungal film also coincides with the DTG peak of the pagurus film.

Moisture uptake profiles for the investigated films at 50% RH and 90% RH are shown in Figure 4.14 and the subsequent mass gains are summarized in Table 4.6. Originally, our fungal based film contains 1.5 times more moisture than the pagurus film. This can be clearly seen at t=0 min, where moisture accounts for 4.4% and 2.9% of the total mass of the fungal and the

pagurus films, respectively. A similar magnitude of moisture loss can also be seen during the thermogravimetric analysis.

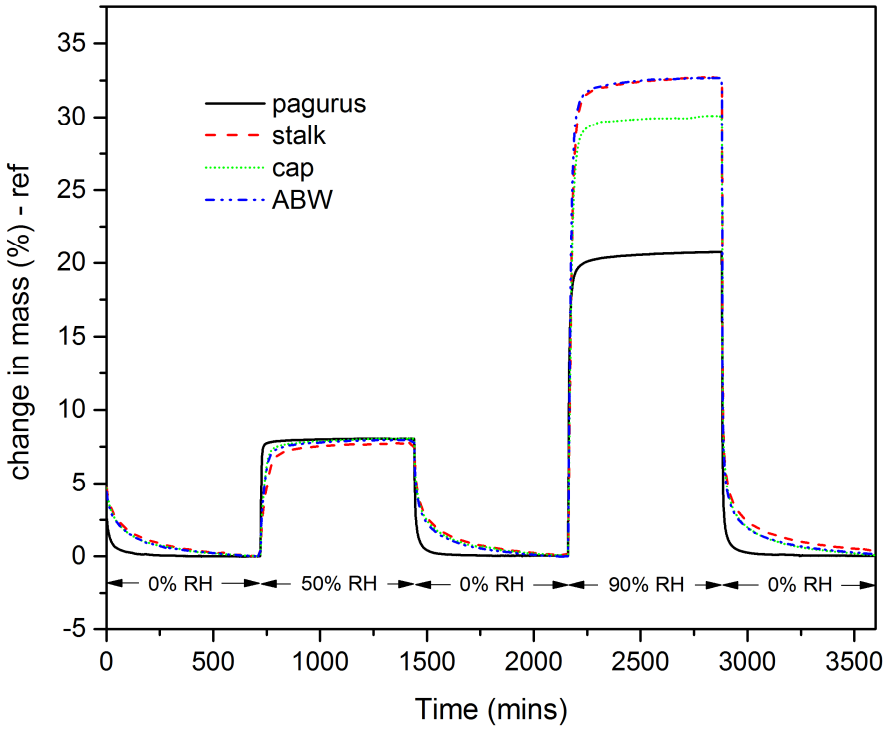

Figure 4.14 Film's moisture uptake profile at 50% RH and 90% RH.

During the first step, the moisture inside the films is slowly being removed by purging N_2 at 25 °C and 0% RH. The removal of moisture occurs much slower in the fungal films than in the pagurus film as evidenced by the gradual decrease in weight loss. Upon reintroduction of moisture at 50% RH, the pagurus film regained its mass and reached an equilibrium state almost immediately. In contrast, it takes approximately 500 min for the fungal film to reach the equilibrium state. Interestingly, the total amount of moisture uptake was identical for all samples (~8%) after 12 h except for the high humidity at 90% RH, where fungal film adsorbs 1.5 times more moisture than the pagurus film. The higher moisture uptake at 90% RH can be ascribed to the more swollen state of amorphous regions at higher humidity, which allows easier penetration of water vapor into the disordered molecular lattice. Throughout the measurement, moisture desorption rate is always slower in the fungal films than in the pagurus film, suggesting better vapor retention properties.

4.8 The Case of Different Grammage

We decide to investigate the effect of grammage on mechanical properties of the fungal based films. The aim for this work was twofold: (1) to find the optimal film grammage in terms of mechanical properties, a result which will be beneficial during laminated composite fabrication, and (2) to find the lowest film grammage that can still practically maneuvered. Only the whole mushroom extract (ABW) was used in this study.

Figure 4.15a shows the appearance of ABW films at different grammage values. Optically, all films between 2 g/m^2 to 160 g/m^2 exhibits good transparency against the background. Even our thickest film with the thickness of ~200 µm was found to be translucent (see Table 4.7 for other grammage thickness). These good optical properties at 100% fiber content can be ascribed to the small size of our nanofibers and the smooth surface of the resulting films which reduces the effect of light scattering. The residual golden color of the film is a byproduct of a pigment compound that was not removed during the extraction process.

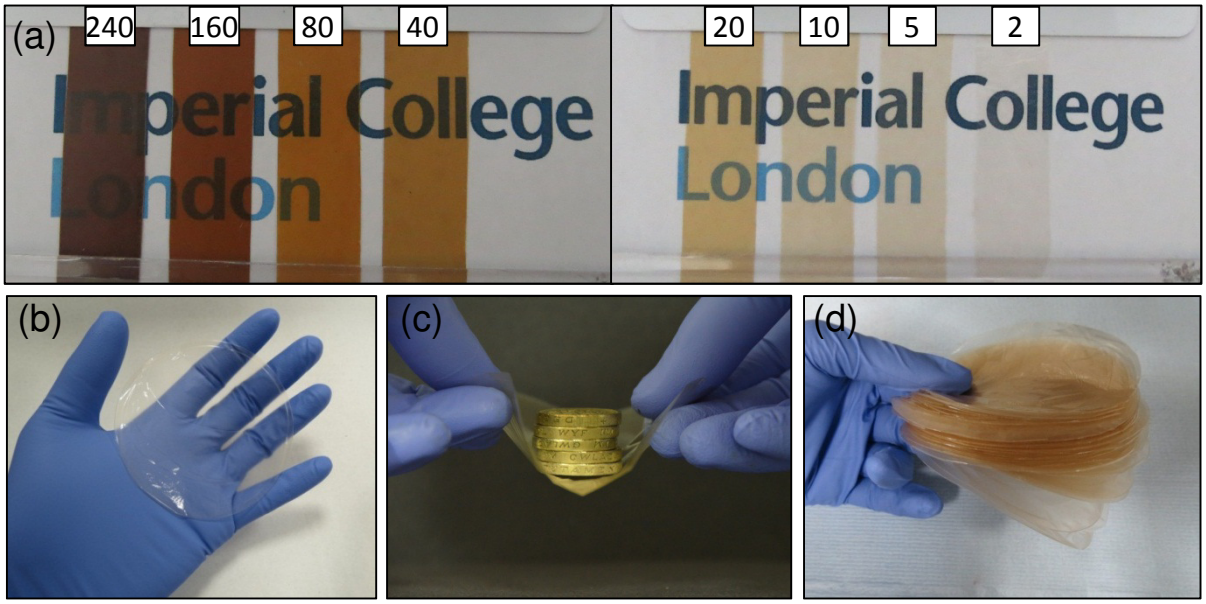

Figure 4.15 (a) appearance of ABW film against background; the numbers represent the grammage (b) 2 g/m^2 film with a thickness of 2 µm, (c) 50 g weight sustained by one 2 g/m^2 film, (d) Sixty 2 g/m^2 film with a total weight of 1 g.

We especially would like to address our thinnest free-standing 2 g/m^2 film. Contrary to the other films that were prepared via vacuum filtration technique, this film was prepared by casting-evaporation method on a polycarbonate petri dish due to its very thin nature. The film forming ability of the fungal extract allows the formation of a strong and smooth film upon evaporation. The resulting film can be peeled from the petri dish without noticeable surface defects (see Figure 4.15b). It can also sustain many times its weight despite having a thickness of only 2 µm, as illustrated in Figure 4.15c. In addition, the simple evaporation process allows more films to be produced simultaneously in less time. Figure 4.15d shows sixty 2 g/m^2 film with a total weight of 1 g that had been prepared in just one day.

SEM images revealed that our film surface consists of dense nanofiber network (10–20 nm fiber width) with no preferred orientation (see Figure 4.16a,b). This dense network leads to the formation of a very smooth surface at a macroscopic level.

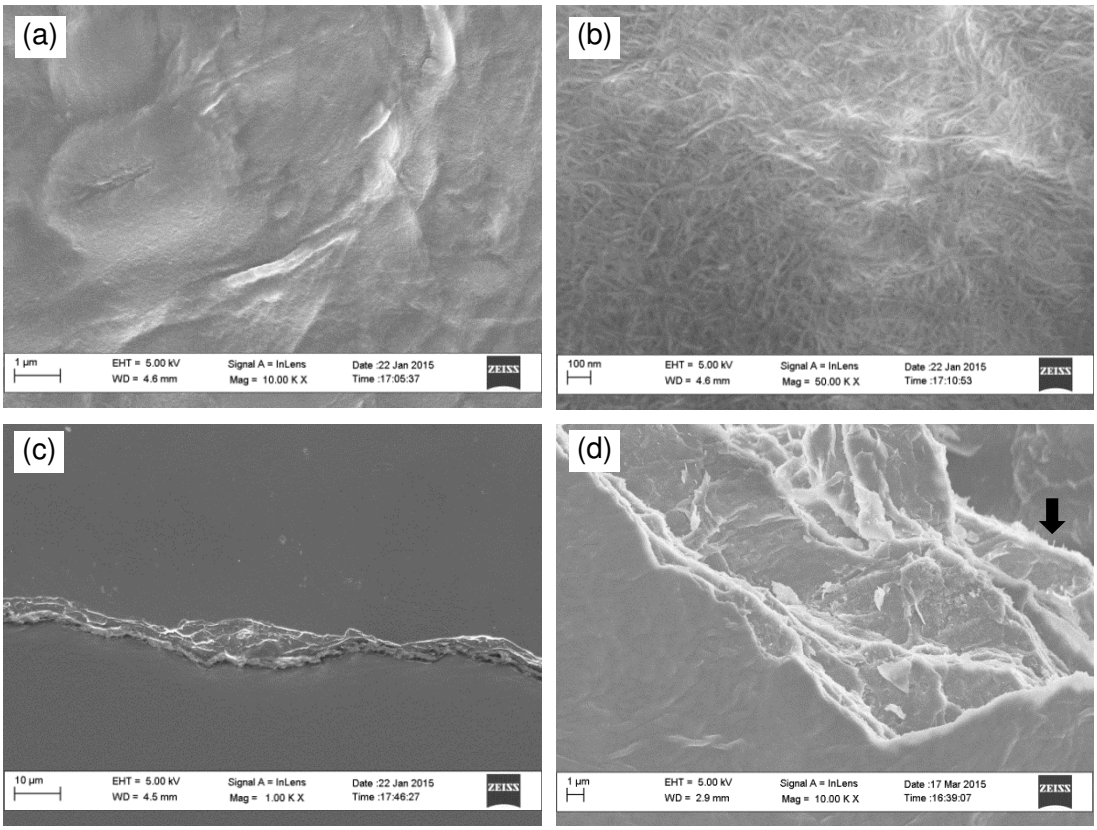

Figure 4.16 Scanning electron microscopy of (a) 80 g/m^2 film surface, (b) magnified image of 80 g/m^2 film surface, (c) 2 g/m^2 film fracture surface, (d) magnified image of 240 g/m^2 film at fracture point.

Due to slow evaporation, the surface of 2 g/m^2 film is smoother than the rest of other films (see Figure 4.16c). A layered structure was observed irrespective of film grammage. At the fracture point, the majority of nanofibers seems to be glued together rather than exhibiting a fibrous free edge profile as in animal chitin [140] or cellulose nanopaper [18]. Only few fibers can be seen protruding from the masses (see arrow in Figure 4.16d) largely because of the brittle characteristics of the film, evidenced by its catastrophic failure during tensile tests.

Stress strain curve and the evolution of film's specific properties over grammage are depicted in Figure 4.17a,b. The corresponding data were tabulated in Table 4.7.

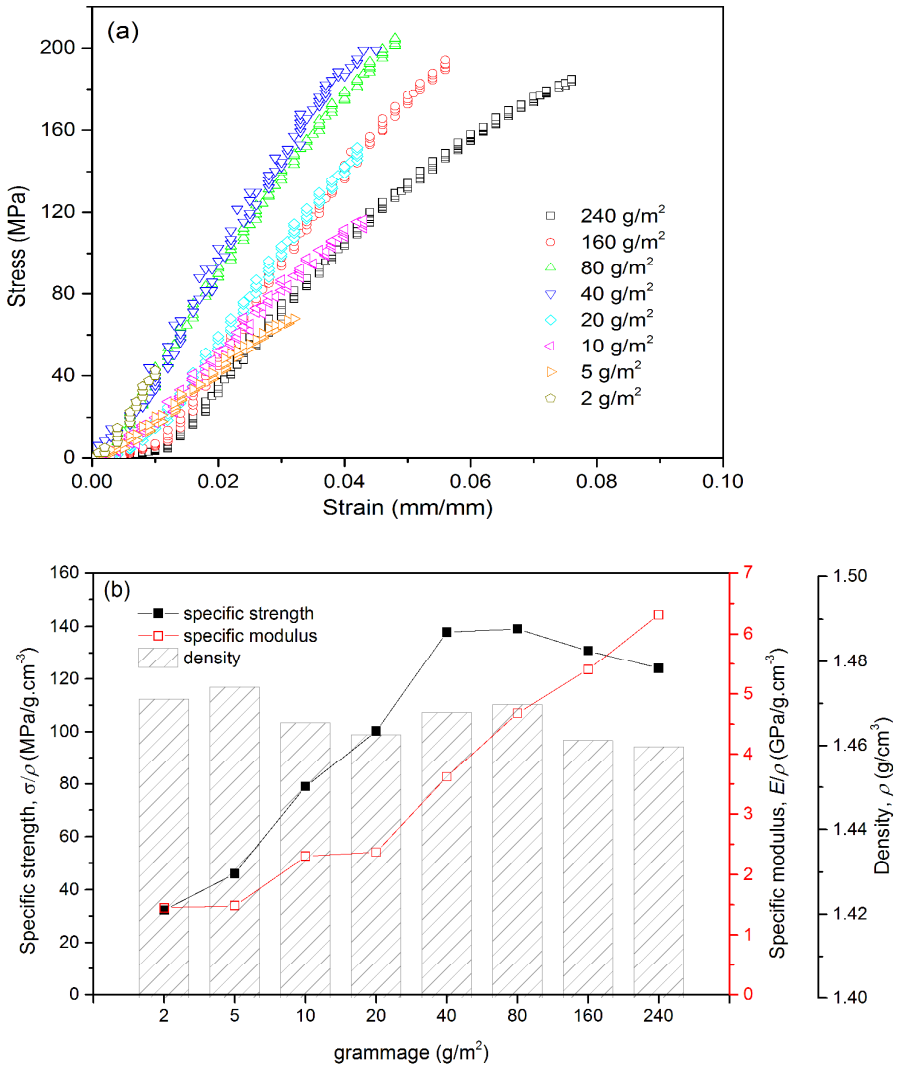

Figure 4.17 (a) stress-strain curve of ABW film at different grammage, (b) evolution of specific strength, specific modulus, and film density as a function of grammage.

Table 4.7 Physical and mechanical properties of ABW film at different grammage[a]

Sample (g/m^2)	*t* (µm)	P (%)	SSA (m^2/g)	Tensile strength (MPa)	Young modulus (GPa)	Elongation at break (%)	Tensile toughness (MJ/m^3)
240	207.1	28.58	0.16	181.1 ± 7.4	9.2 ± 1.1	7.1 ± 0.6	6.5 ± 0.8
160	109.4	34.47	0.11	191.2 ± 11.1	7.9 ± 1.1	5.5 ± 0.3	4.9 ± 0.4
80	59.3	58.95	0.22	204.4 ± 4.0	6.9 ± 1.2	5.3 ± 0.4	5.3 ± 0.5
40	28.3	63.99	0.25	202.4 ± 17.2	5.3 ± 0.7	4.8 ± 0.7	5.1 ± 1.3
20	14.8	76.80	0.36	146.6 ± 10.8	3.5 ± 0.3	4.4 ± 0.4	3.0 ± 0.5
10	10.1	83.90	0.33	115.7 ± 13.3	3.4 ± 0.4	4.0 ± 0.7	2.2 ± 0.7
5	6.6	89.95	0.42	68.0 ± 6.4	2.2 ± 0.4	3.3 ± 0.2	1.2 ± 0.1
2	2.0	88.02	0.71	47.5 ± 9.5	2.1 ± 0.4	1.3 ± 0.4	0.3 ± 0.1

[a] *t*, P, and SSA represent film thickness, film porosity, and film specific surface area, respectively.

The film density at different grammage values shows little variation, fluctuating between 1.46 g/cm^3 to 1.47 g/cm^3. However, the porosity of the sample gradually decreases with increasing thickness, which can be related to the difference in filtration time. It took 7 to 8 hours to filter a 200 mL fungal extract suspension in order to make the 240 g/m^2 film with 90 mm diameter. This is much slower than ~1 h needed to prepare 80 g/m^2 film, or ~10 min for 10 g/m^2 film under the same condition. A slower filtration rate causes a slower wet cake build up and promotes better filling of cavities at the film's surface (higher envelope density), which subsequently leads to lower porosity. A decrease in porosity allows more contact between fibers as demonstrated by a gradual decrease in film's surface area. This consequently will create better three dimensional percolation networks which can transfer the stress more efficiently throughout the sample, causing an increase in film modulus along with the increase in grammage. Increasing the grammage also reduces the film brittleness. This is indicated by a higher strain to failure and improved toughness.

The evolution of tensile strength over grammage is not straightforward. At low grammage (2 g/m^2 to 40 g/m^2), all specific tensile properties increased with increasing grammage, reached a maximum between 40 g/m^2 and 80 g/m^2 before gradually declining at 160 g/m^2 and 240 g/m^2. Because tensile strength is measured at the sample fracture point, slight defects during sample preparation will cause premature rupture. A probability for inducing defect like microcracks is

greater when cutting a thicker sample. A similar trend was also reported by I'Anson et al. [284, 285] and he attributes the decline to an increased probability of weak points in the fiber network with an increasing sample volume.

From inverse gas chromatography measurement, higher grammage films (80 g/m^2 to 240 g/m^2) gave higher dispersive surface energy (γ^d) than lower grammage films (see Figure 4.18a,b). This is true for surface coverage of $n/n_m > 0.1$ while no simple correlation can be made at lower surface coverage. With γ^d = 40 mJ/m^2, 2 g/m^2 film has the lowest surface active site on its surface. It is also energetically less heterogeneous compared with the other films – a byproduct of a smoother surface generated by a slow casting-evaporation process. Little variation in acid-base component was observed (2 mJ/m^2) between grammage value beyond $n/n_m > 0.1$, indicating similar functional group in all films, which is expected.

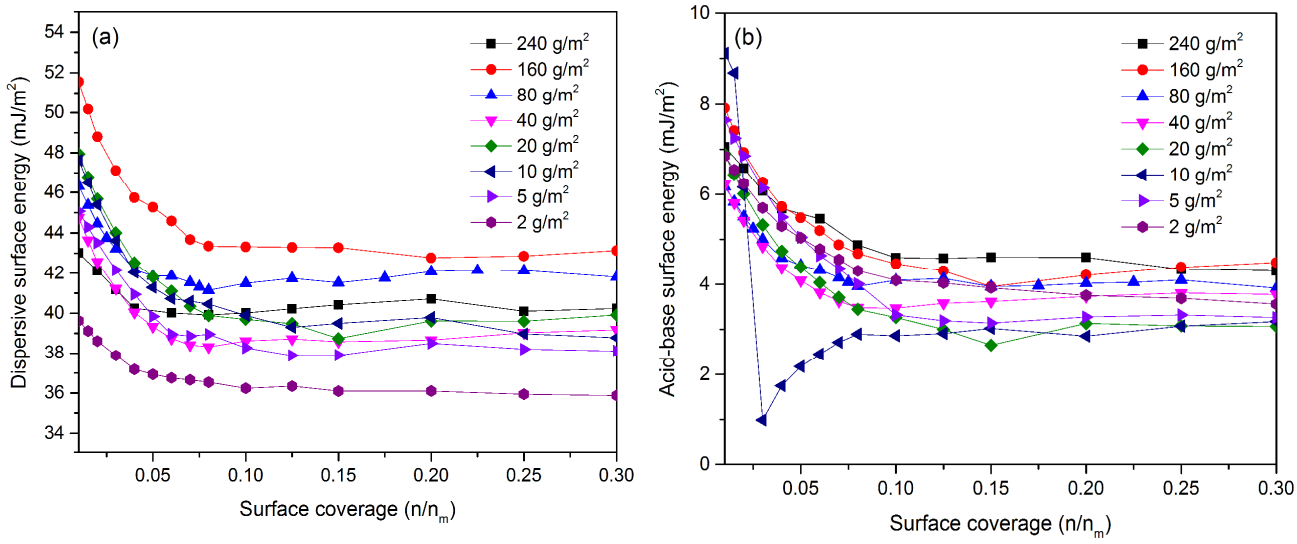

Figure 4.18 (a) dispersive surface energy profile at different grammage, (b) acid-base surface energy profile at different grammage; measurement is by inverse gas chromatography.

CHAPTER FIVE
GLUCAN RICH MICROFIBERS FROM TREE BRACKET FUNGI: OPTIMIZATION & FILM COMPOSITE STUDY

5.1 Introduction

In this chapter, we will extend our knowledge on fungal based chitin by looking on bracket fungi. How much chitin do they have? Can we still get nanofibers from bracket fungi as easily as from a common mushroom? What happens if we mix those two together? These are some of the questions that we would like to answer in this chapter. Two themes presented in Section 3.1 will be covered: an optimization study and a film composite study.

5.2 Extract and the Film: Its Morphology and Chemical Constituents

Bracket fungi come in various textures and colors. Their fibrous nature has led to a creation of non-cellulosic fungal-based paper[14] which possesses intriguing properties not found in conventional paper [286]. Our selected tree bracket fungus, *D. confragosa,* has a rubbery texture with a dense upper part and an elongated porous structure at the bottom (see Figure 5.1a). The bracket hardens when dried at high temperature and cannot revert to its original rubbery texture. Hardly any defined fiber can be seen at low magnification (see Figure 5.2a,b). The mycelium and few young spores are held together in an amorphous matrix causing the structure to remain intact when diced into smaller pieces. Figure 5.1b shows fibrous brown slurry obtained after blending a diced sample in a kitchen blender for 10 min. In order to investigate the effect of alkaline extraction on the resulting film properties, we studied both non-extracted sample (DC) and an extracted sample (DCE). DC sample yields a pulp-like structure, while DCE produces a more disintegrated structure (see Figure 5.1c,d). To prevent fiber hornification, we used never dried DC and DCE suspensions (1% w/v) during film preparation.

Upon blending, our diced sample disintegrates into uniform microfibers with 1–2 μm diameter and several hundreds of micrometers in length (see Figure 5.2c). Each of them is a collection of nanofibers aligned in the direction of the microfiber length (see Figure 5.2d).

[14] The term ‘paper’ commonly refers to cellulosic-based material. We will restrict ourselves with the term ‘film’ even though our bracket fungi extract gave a film with a paper-like appearance.

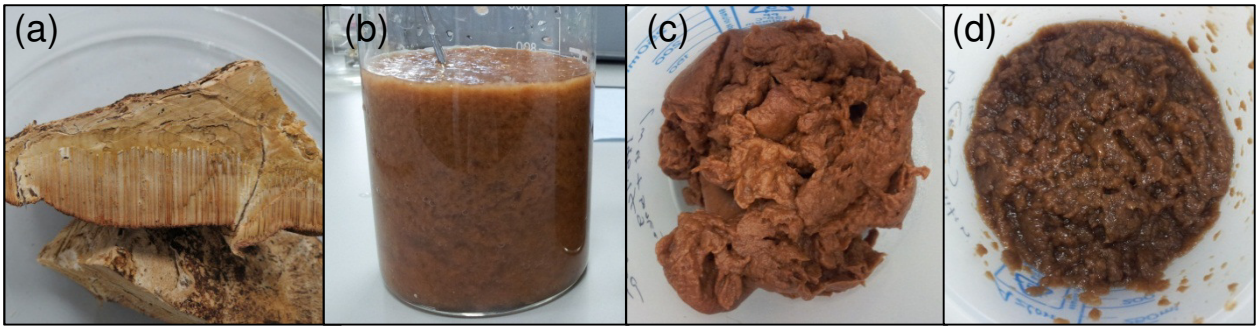

Figure 5.1 (a) texture of sliced *D. confragosa* bracket fungi, (b) fibrous slurry after 10 min blending of *D. confragosa*, (c) non-extracted sample, (d) hot water and alkali extracted sample.

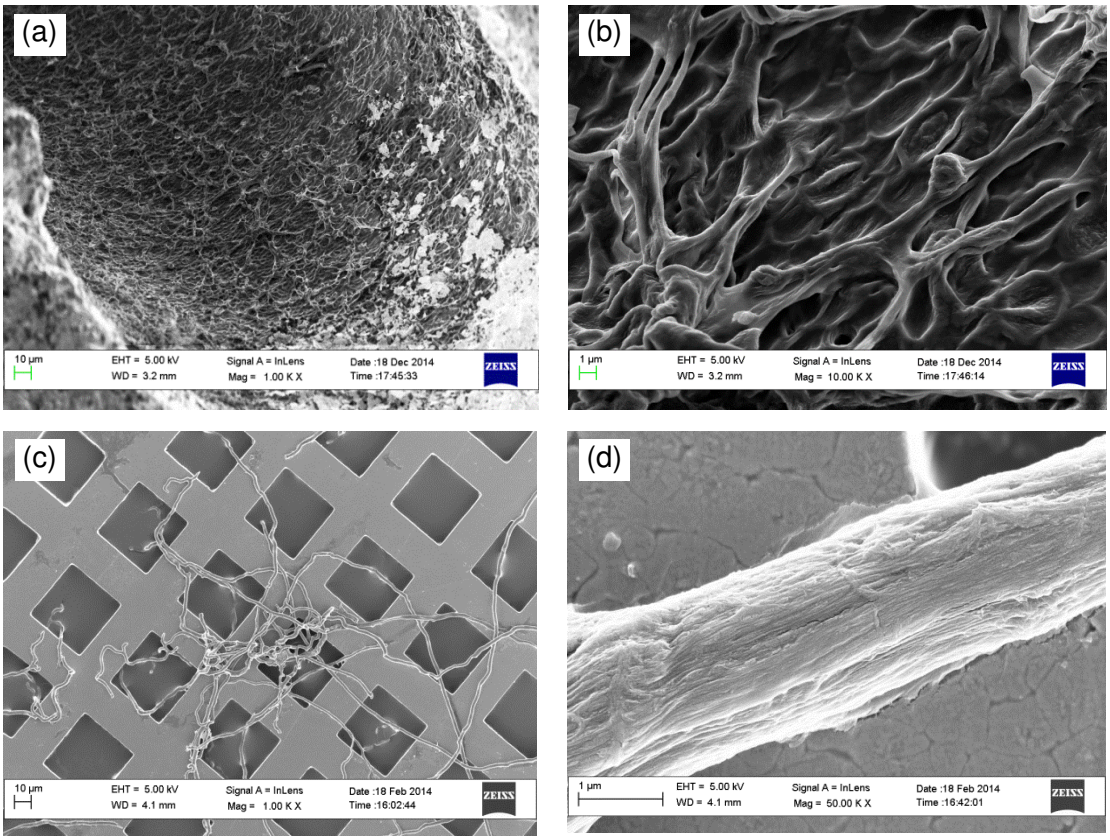

Figure 5.2 Scanning electron micrograph of: (a) inside the porous structure of *D. confragosa*, (b) magnified image of porous structure surface, (c) dilute fiber suspension from 10 min blended sample, (d) magnified image of an individual microfiber.

Forty minutes of blending using a kitchen blender even after chemical extraction was not sufficient to nanofibrillate the resulted microfiber. More powerful defibrillation methods such as

homogenization, microfluidization, cyrocrushing, ultrasonication, or grinding treatment are needed. Strong hydrogen bonding between nanofibers may be formed during bracket fungi life cycle, where they were exposed to repeated wet-dry environment resulting in possible fiber hornification. This is in obvious contrast with our previous study using common mushrooms where high humidity environment was always present throughout their growth.

Table 5.1 and Table 5.2 shows elemental and sugar analysis for the investigated sample. Up to 27% alkali soluble material was released during extraction process, indicated by the yield difference between DC and DCE. The nitrogen and glucosamine content for both sample is very low, suggesting the presence of chitin is almost negligible. In other words, both DC and DCE represent glucan-rich polysaccharides. Both elemental and sugar analysis in our sample bear resemblance to the results obtained from yeast cell wall polysaccharide, (1→3)/(1→6)-β-D-glucan [287].

Table 5.1 Elemental analysis of non-extracted (DC) and extracted (DCE) samples

Sample	C (%)	O (%)	H (%)	N (%)	S (%)	Yield (%)
DC	40.88	48.35	6.46	0.51	< 0.02	96.89
DCE	43.25	50.55	6.51	0.24	< 0.02	69.78

Table 5.2 Sugar analysis of non-extracted (DC) and extracted (DCE) samples[a]

Sample	Galactose (%)	Glucose (%)	Xylose (%)	Mannose (%)	Glucosamine (%)	Total sugar (%)
DC	0.1	92.2	0.5	0.8	1.1	94.7
DCE	0.0	96.8	0.0	0.0	1.1	97.9

[a]Arabinose and rhamnose were not detected in all samples

Figure 5.3a,b shows a fracture surface of 80 g/m^2 DC film. Filtration process during film preparation produces a layered structure. An extensive array of pull out fibers can be seen at the fracture point, indicating a non-brittle mechanism which led to paper-like rupture during tensile test. The surface morphology of both films is defined by a network of uniform width microfibers with 1–2 µm fiber diameter (see Figure 5.3c,d). Under similar grammage, the DC film was found to be 50% thicker and 18% more porous than the DCE film. Higher porosity can be ascribed to a rough fiber surface and intercalating impurities that exist between individual fibers (see Figure 5.3e). Alkali extraction not only removes most of the impurities, but also causes the fiber to

swell (see Figure 5.3f). A somewhat similar swelling phenomena is also observed during mercerization of cellulose [288].

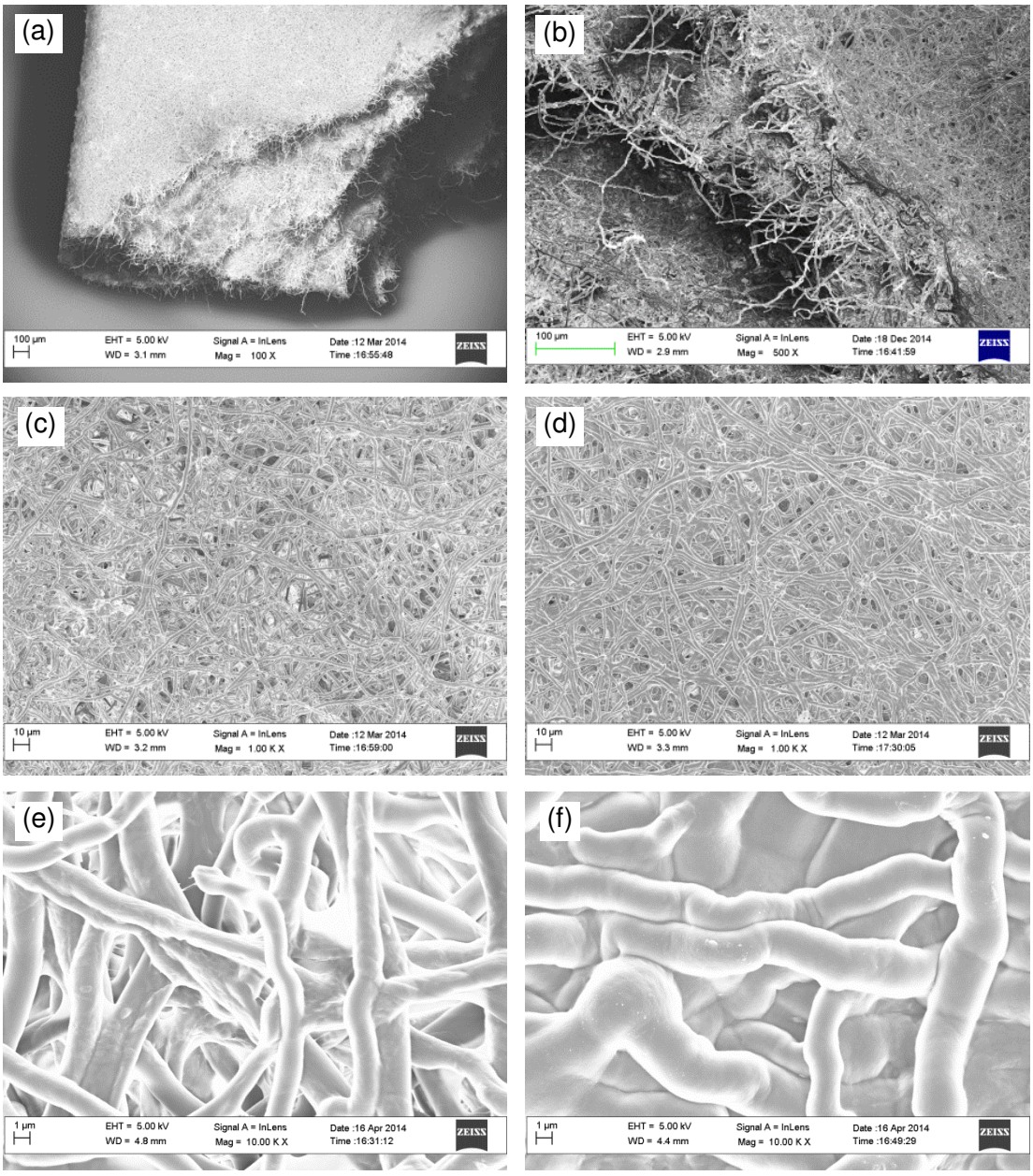

Figure 5.3 Scanning electron micrograph of: (a) bracket fungi film structure, (b) bracket fungi film fracture morphology, (c) surface morphology of DC film, (d) surface morphology of DCE film, (e) magnified image of DC film, (f) magnified image of DCE film.

The removal of impurities also improves the accessibility of hydroxyl surface groups and they are able to form more hydrogen bonds between neighboring fibers, leading to tight and less porous networks. It should also be noted that both DC and DCE fibers are finer and more uniform than other natural fibers originated from wood or other plants [289, 290]. This led to higher fiber numbers per volume, better energy dissipation upon fracture, and ultimately tougher and stronger film compared to conventional paper.

As previously stated, nanofibrillation of bracket fungi fibers cannot be achieved using a kitchen blender. However, some improvements in mechanical properties could be possible if the fiber can be dispersed optimally prior to film preparation. Therefore, the effect of different blending times on the mechanical properties of the film was investigated. All samples were initially pre-blended for 10 min and the numbers after the acronym (i.e. DC0min, DC10min, …) represents the post-blending rate (for details, refer Section 3.3.2 and Section 3.3.4). Photograph of the prepared films at different blending rates are shown in Figure 5.4a. In contrast to the more transparent common mushroom extract film, both the DC and the DCE films are opaque as a result of natural pigment, larger fibers and rougher surfaces (see Figure 5.4b). The color of the DC film is more homogenous because any fiber imperfection is covered by thick pigmentation. Hot water and alkaline treatments help to remove any soluble pigment and impurities, causing the surface inhomogeneity or imperfection on DCE film to be more exposed.

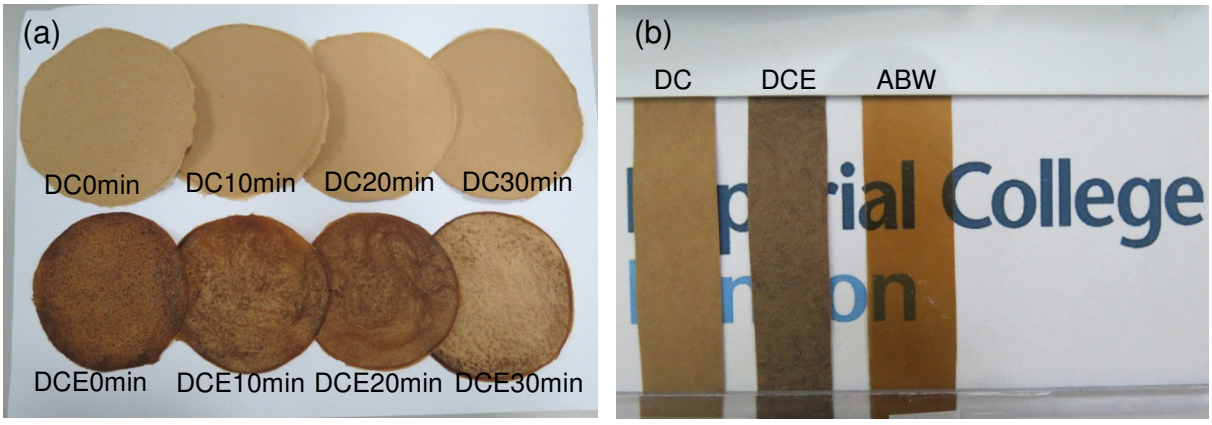

Figure 5.4 (a) appearance of the films made from different blending rate, (b) optical appearance of the 80 g/m^2 films. DC, DCE, and ABW represent non-extracted bracket fungi, extracted bracket fungi, and whole common mushroom, respectively.

5.3 IR Absorbance and Crystallinity Analysis

Figure 5.5a shows ATR-FTIR spectra for the DC and the DCE films. The absorbance spectrum of a cellulose filter paper was added for comparison. The broad band between 3000–3600 cm^{-1} indicates different kind of –OH stretching mode including OH in adsorbed water, but most of it can be attributed to high percentage of glucan in DC and DCE film. The characteristic band for α-chitin, amide I doublet (1620 cm^{-1} and 1650 cm^{-1}), was not observed. They were possibly overlapped by absorbed water –OH and conjugated C=O band at 1640 cm^{-1}, a band that is common in cellulose (which is due to other material and oxidized structure along the cellulose chain) [291]. Although our DC and DCE spectra bear some resemblances with cellulose filter paper, they differ in chain conformation, possessing (1→3)-β-linkage in the backbone instead of (1→4)-β-linkage [110]. This difference can be elucidated qualitatively by comparing their respective XRD pattern.

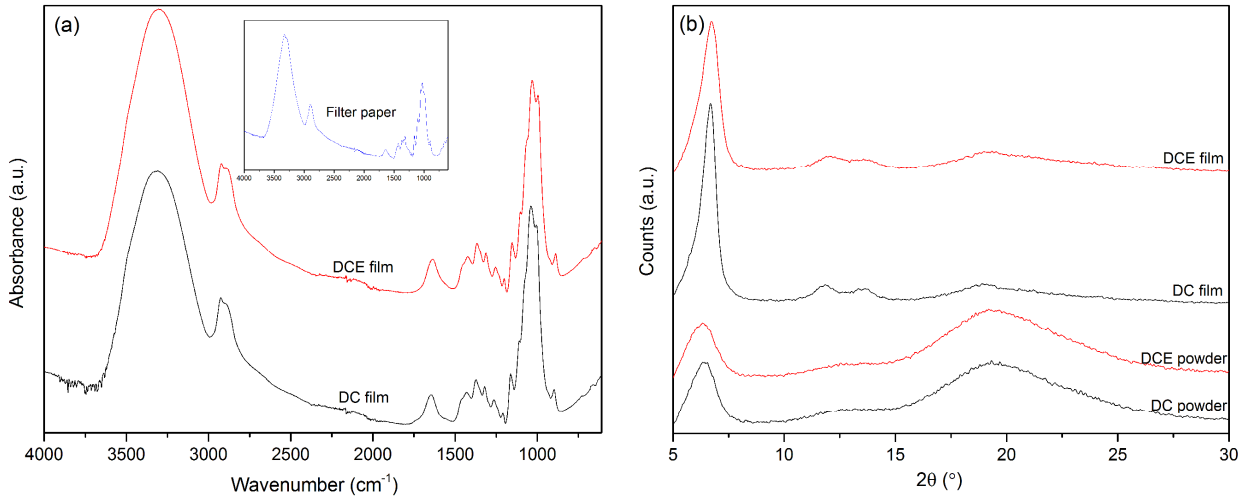

Figure 5.5 (a) ATR-FTIR absorbance of film sample, (b) XRD pattern for powder and film sample.

DCE has a higher crystallinity index (CI%) than DC due to a reduction in impurities. From powder to film, CI% for DC increases from 58.9% to 65.7% while for DCE the increase is from 66.5% to 70.0%. Because of the tough sample structure, a longer milling time (3 cycle, 3 min/cycle) was used and a reduction in crystallinity was expected in powdered sample [292]. During the XRD measurement, no characteristic cellulose peaks were observed in the DC or the

DCE samples (see Figure 5.5b). Native cellulose exhibits major peaks around 2θ = 15°, 17°, and 23°, while mercerized and regenerated cellulose exhibit major peaks around 2θ = 12°, 20°, and 22° [293]. Our powder sample gave a peak at 2θ = 6° with broad amorphous region centered at 2θ = 19°. In film, the 6° peak intensified, 19° region reduced, and additional peaks appeared at 12° and 14°. All these peaks indicates the presence of either linear (1→3)-β-glucans or branched (1→3)/(1→6)-β-glucans [287, 294-296]. Elucidation of the true chain conformations for our glucan is beyond the scope of this works.

5.4 Physical and Mechanical Properties of the Films

Table 5.3 shows the mechanical properties of DC and DCE films at different post-blending rates. Their respective stress-strain curves are shown in Figure 5.6a.

Table 5.3 Mechanical properties of the bracket fungi glucan rich films

Sample	Tensile strength (MPa)	Young modulus (GPa)	Elongation at break (%)	Tensile toughness (MJ/m^3)
DC0min	15.5 ± 0.8	0.3 ± 0.0	9.8 ± 0.4	1.0 ± 0.1
DC10min	22.6 ± 1.3	0.3 ± 0.0	13.4 ± 1.9	1.7 ± 0.3
DC20min	23.3 ± 2.6	0.4 ± 0.0	12.3 ± 1.5	1.8 ± 0.4
DC30min	23.2 ± 1.2	0.3 ± 0.0	12.7 ± 1.5	1.8 ± 0.3
DCE0min	37.5 ± 3.3	0.9 ± 0.2	5.7 ± 0.6	1.2 ± 0.2
DCE10min	54.5 ± 3.5	1.1 ± 0.0	11.0 ± 0.8	3.9 ± 0.6
DCE20min	65.3 ± 0.8	1.2 ± 0.1	13.2 ± 1.2	5.8 ± 0.5
DCE30min	51.6 ± 3.9	0.9 ± 0.1	13.4 ± 1.1	4.6 ± 0.8

At the optimum blending rate of 20 min, the DCE film is 2.8 times stronger, 3.3 times stiffer, and 3.1 times tougher than the DC film. The improvement in mechanical properties can be attributed to denser fiber packing in DCE (50.03% porosity) than in DC (72.87% porosity). Because a similar compressive force was used during paper making, the better fiber packing in DCE is mainly due to the removal of impurities on fiber surface and better fiber dispersion at optimal blending rate. This creates a better contact area between the fibers resulting in a more efficient stress transfer throughout the sample [297]. There is also no reduction in strain to failure for the DCE film, which suggests the fibers were not damaged during the extraction process.

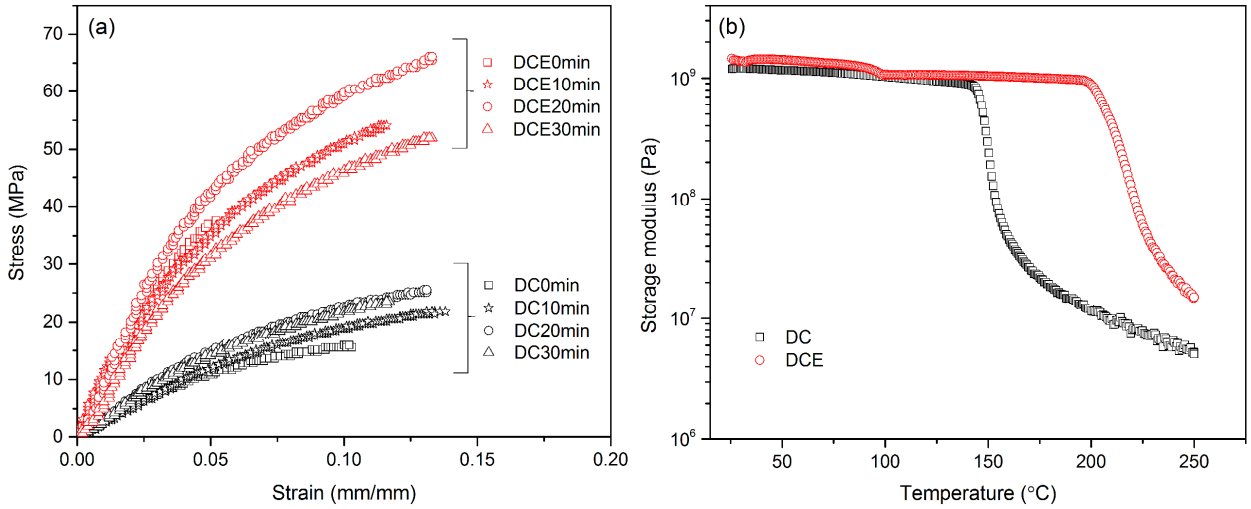

Figure 5.6 (a) stress-strain curves of DC and DCE films at different blending rates, (b) evolution of storage modulus of DC20min and DCE20min films across a temperature range of 25 °C to 250 °C.

The evolution of films' storage modulus in tensile mode across the temperature range is depicted in Figure 5.6b. The DCE film has a higher storage modulus than the DC film and it is capable of maintaining the modulus up to 200 °C. The removal of intercalating impurities in DCE prevents fiber slippage to occur prematurely. This creates a tight and stable fiber network that allows film stiffness to be retained over a wide range of temperatures. A drop in storage modulus of about two orders of magnitude was observed at a much earlier temperature (144 °C) for the DC film.

To the best of our knowledge, our DCE20min film has the highest mechanical properties compared to other bacterial-based glucan[15] films [298-300] , fungal-based glucan[16] films [287, 301-303] or euglenoid-based glucan[17] films [304, 305]. Cereal-based glucan[18] films can yield better tensile values [306, 307] but suffer from low melting points. They are also highly susceptible to humidity, and soluble in water. These factors prevent them to be used in paper or composite applications. Further improvements in mechanical properties are expected if our films

[15] Linear (1→3)-β-glucan, e.g. curdlan
[16] Mostly occur in branched form with (1→3)-β-glucan backbone and (1→6) side chain, e.g. schizophyllan, lentinan.
[17] Most crystalline form of linear (1→3)-β-glucan, e.g. paramylon
[18] Linear (1→3)(1→4)-β-glucan obtained from oat, barley, or wheat.

were made from nanofibrillated DCE fibers instead of microfibers [308]. Only films that were blended at the optimal rate (20 min) will be used henceforth.

5.5 Surface Characteristic Analysis

Figure 5.7a shows the evolution of water contact angle on DC and DCE film surfaces. For comparison purpose, we also include contact angle evolution for the film samples studied in Chapter 4. Due to higher porosity, water penetrates into the DC film faster than it does to the DCE film (see Figure 5.7b).

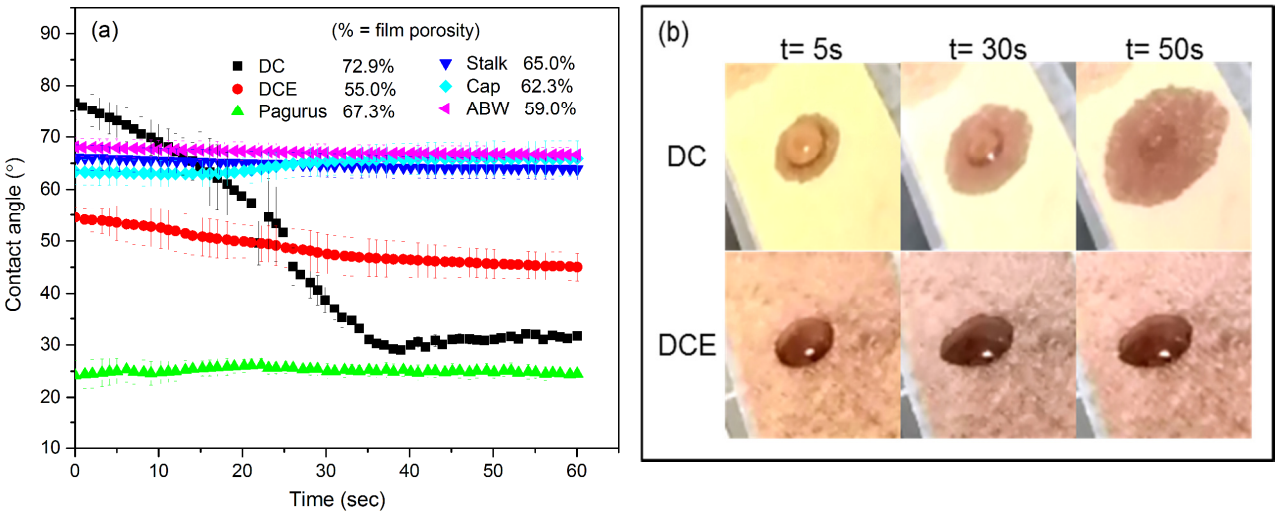

Figure 5.7 (a) evolution of water contact angle on investigated film surface, (b) pictograph of water droplet behavior on DC and DCE film.

Only the contact angle at t = 0 sec can be said to be representative of DC or DCE surface wetting character. This is in stark contrast with the other films discussed in Chapter 4, where all of them produced stable contact angles for at least 60 sec of measurement. The higher contact angle at t = 0 sec suggests DC (θ = 76.6°) to be relatively more hydrophobic than DCE (θ = 54.5°). This is expected as without alkaline extraction, residuals like lipids and waxy substances are more likely to adhere on the fiber surface and promote apparent hydrophobic effect. Even after these residuals have been removed, our DCE film still has a comparable contact angle to the film made by untreated cellulose (sisal nanofiber film, θ = 59.4°; sisal whisker film, θ = 44.6°) [309].

Influence of porosity on surface energy characterization can be circumvented by evaluating both samples using inverse gas chromatography. Figure 5.8 shows the surface energy profile for DC and DCE sample, both in powder and film form. The contribution of the dispersive component (γ^d) to the total surface free energy (γ^t) was larger than the contribution of the acid-base (polar) component (γ^{ab}). In powdered form, γ^d contribution accounts for 83.5% (DC) and 83.8% (DCE) of γ^t, while in film sample, γ^d accounts for 85.6% (DC) and 88.5% (DCE) of γ^t. The difference in acid-base contribution is minimal, suggesting there is not much difference in surface polarity between DC and DCE.

DCE surface was found to have a higher energy ($\gamma^t > 50$ mJ/m^2) than DC surface ($\gamma^t < 50$ mJ/m^2) (see Table 5.4). This supports our previous result where lower contact angle of water for the DCE film reflects its higher surface energy.

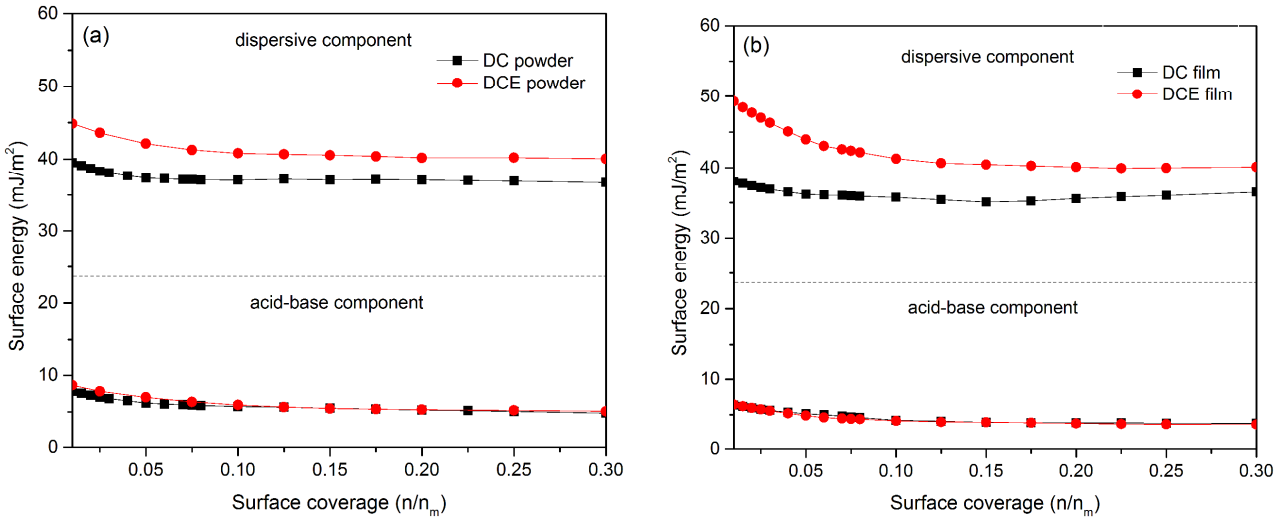

Figure 5.8 Surface energy profile for (a) freeze dried powder sample, (b) film sample; as determined by inverse gas chromatography

Table 5.4 Dispersive (γ^d), acid-base (γ^{ab}), and total (γ^t) surface energy at $n/n_m = 0.01$, as determined by inverse gas chromatography

Sample	γ^d (mJ/m^2)		γ^{ab} (mJ/m^2)		γ^t (mJ/m^2)	
	powder	film	powder	film	powder	film
DC	39.5	38.1	7.8	6.4	47.3	44.5
DCE	44.8	49.3	8.6	6.4	53.4	55.7

Adherence of lower energy foreign material, such as natural wax [310] will contribute to the decrease of γ^d in a non-extracted sample. A similar trend in γ^d reduction was also observed when lignin was added incrementally onto cellulose paper [265]. An increase in crystallinity in the film samples causes its γ^d value to be higher than in the powdered samples. This correlation between increased crystallinity and higher γ^d has been previously reported by Papirer et al. [311]. The DCE film surface was also found to be more heterogeneous energetically than that of the DC film. The difference between its largest γ^d and lowest γ^d is 9.3 mJ/m^2, compared to the difference of only 2.1 mJ/m^2 observed in the DC film. Removal of the extracted material is believed to expose more high energy sites that are otherwise inaccessible in the non-extracted sample.

Figure 5.9 shows the streaming ζ-potential values of the investigated films as a function of pH. A measurement for cellulose filter paper was added for comparison. Both DC and DCE films exhibited an acidic surface character indicated by their lower isoelectric point (iep; where ζ=0) [312]. The DCE surface is slightly more acidic (iep = pH 2.6) than the DC surface (iep = 2.9). This is expected as more surface hydroxyl groups are exposed after the removal of extractives. However, the difference is minimal. This coincides with our previous IGC results where there is almost no difference in acid-base component contribution between DC and DCE film. Both our films are more acidic than normal filter paper (iep = pH 3.5), indicating the presence of more surface free hydroxyl group.

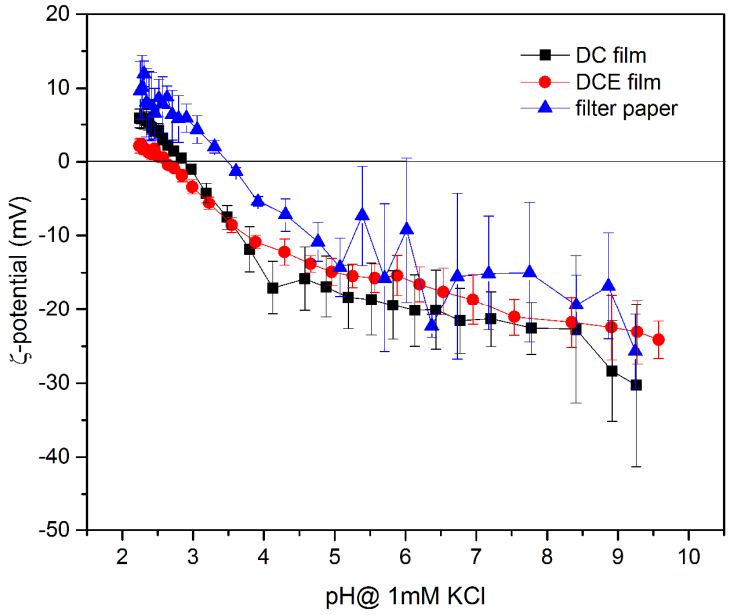

Figure 5.9 Streaming ζ-potential as a function of pH of the films.

Deprotonation of surface free hydroxyl group at higher pH produces a plateau ($\zeta_{plateau}$) in the basic region. Dewaxing and removal of impurities should causes an increase in $\zeta_{plateau}$ due to the increased accessibility of dissociable surface functional groups [313]. However, if the functional group is hydrophilic – like the hydroxyl group – swelling is likely to occur during passing the electrolyte solution. This will causes the shear plane to shift into the liquid phase and reduces the ζ-potential value [281]. This explains why our DCE film has a lower $\zeta_{plateau}$ (going to zero) than the DC film. Nevertheless, both of our films exhibit more negative plateaus (ζ_{plateu} = -20 to -30 mV) than the other –OH rich surface like natural fibers ($\zeta_{plateau}$ < -10 mV) [273, 313-316], indicating that our film has a lower tendency to swell in water.

5.6 Thermal and Moisture Sorption Properties

Thermal degradation behavior of freeze dried and film samples under N_2 and air atmospheres are shown in Figure 5.10. The initial weight loss between 60–100 °C in all investigated samples is mainly due to the removal of moisture. Between DC and DCE, there is not much difference between their onset temperatures at 10% weight loss ($T_{d,10\%}$) (see Table 5.5).

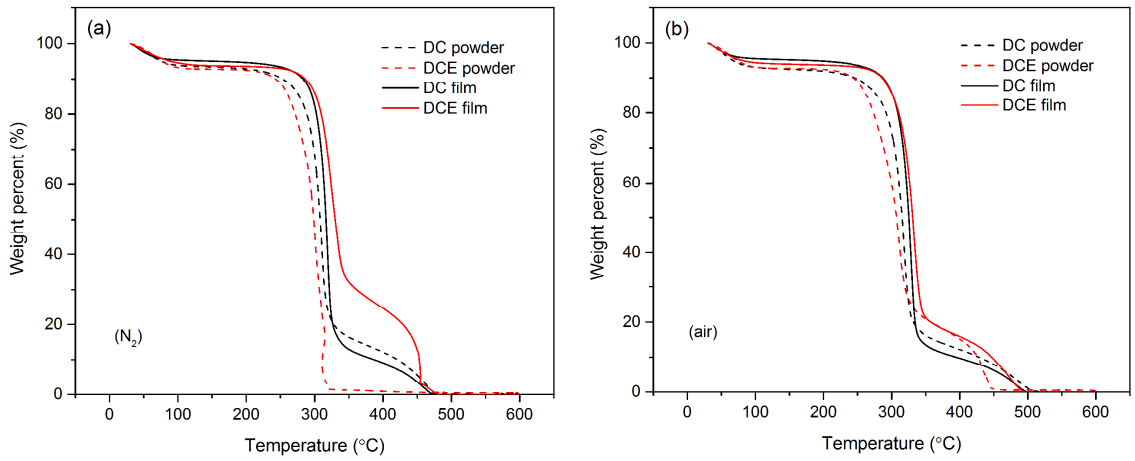

Figure 5.10 TGA curve for investigated samples in (a) N_2, (b) air.

Table 5.5 Onset degradation temperature at 10% weight loss ($T_{d,10\%}$) by TGA analysis and moisture uptake for the film at 50% and 90% RH as determined by dynamic vapor sorption

Sample	$T_{d,10\%}$ (°C), powder		$T_{d,10\%}$ (°C), film		moisture uptake (%), film	
	air	N_2	air	N_2	50% RH	90% RH
DC	245	253	287	283	9.9	28.3
DCE	243	243	286	286	11.4	31.1

The film samples start to degrade at 30–40 °C later than the freeze dried samples, as indicated by their higher $T_{d,10\%}$ value. When the first derivative weight loss is taken, both DC and DCE exhibit major weight loss (T_{peak}) at approximately a similar temperature. T_{peak} for the film sample occurs at a slightly higher temperature ($T_{peak,film}$ ~320 °C in N_2; ~330 °C in air) than for the freeze dried sample ($T_{peak,powder}$ ~305 °C in N_2; ~315 °C in air). Higher $T_{d,10\%}$ and T_{peak} for film can be attributed to their higher crystallinity. Our $T_{peak,powder}$ value is at the lower end of T_{peak} range exhibited by various cellulosic material, which lies between 300 °C to 350 °C [317], and much lower than T_{peak} of chitin which often occurs beyond 350 °C [73]. This suggests that our sample bears chemical similarity with cellulose and low chitin content (as detected by sugar analysis) unable to improve the thermal stability of the sample.

The moisture uptake profiles for the investigated films at 50% RH and 90% RH are shown in Figure 5.11 and the subsequent mass gains are summarized in Table 5.5. Initially, at t = 0 min, the DCE film contains 1.8 times more moisture than the DC film, and it continues to retain more moisture compared to the DC film at 50 % RH (1.5% more moisture by weight) and 90% RH (2.8% more moisture by weight). Removal of extractive materials in DCE during the alkaline treatment causes the amorphous glucan part to be more exposed, creating more space for moisture adsorption, hence a larger uptake by volume. Water molecules can also access surface hydroxyl groups more readily in the extracted fibers. Nevertheless, moisture in the DCE film can be released or reintroduced almost at the same rate with the DC film. This can be clearly seen at every RH% change interval (the slope) where moisture sorption and desorption rates are similar for both samples. It is worth noting that although DC and DCE films absorb more moisture than the common mushroom film (discussed in Chapter 4), the water desorbs much faster. This is indicated by the rapid weight loss when the environment changed from higher humidity (50% and 90% RH) to 0% RH.

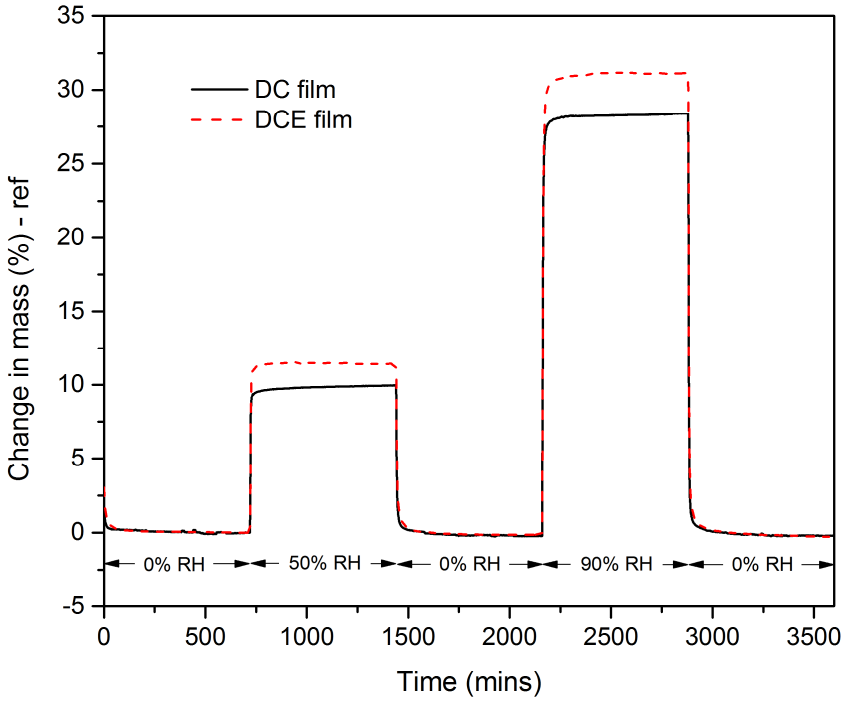

Figure 5.11 Films' moisture uptake profile at 50% RH and 90% RH.

5.7 The Case of Composite Film

We decided to investigate the effect of combining the microfibers from the bracket fungi (DC & DCE) and the nanofibers from common mushroom (ABW). The expectation is that some of the strength and stiffness from the ABW nanofibers can coexist with the ductility exhibited by the DC and DCE microfibers. The idea of using fibrous constituents at two very different scales had been previously reported for cellulose [318].

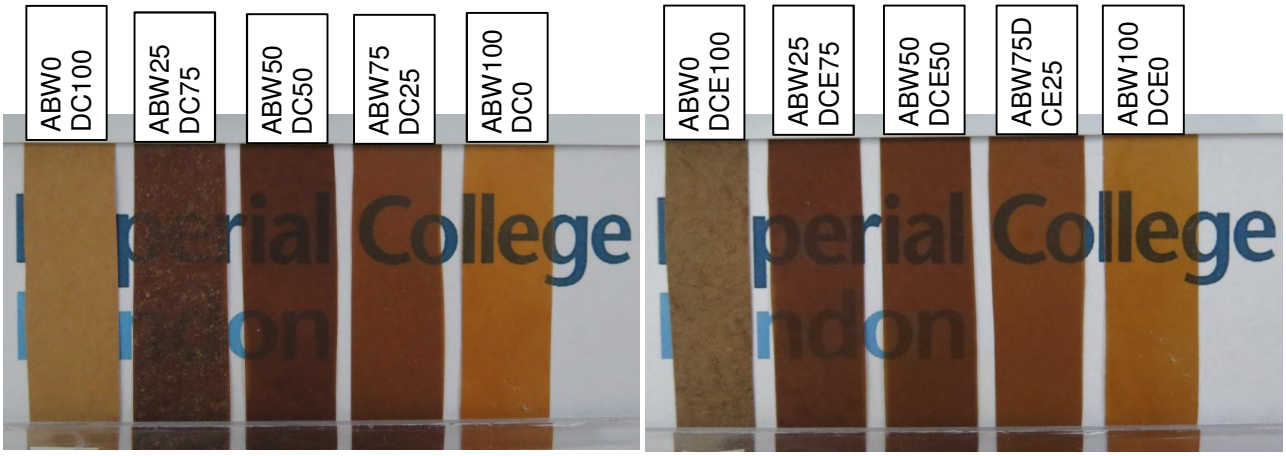

Figure 5.12 Appearance of ABW-DC and ABW-DCE composite film. Number represents the ratio by weight.

Figure 5.12 shows the appearance of ABW-DC and ABW-DCE composite films (80g/m^2) at different weight fractions. All films possess approximately similar thickness between 60 µm to 70 µm, except for ABW0DC100 with the thickness of about 110 µm. Upon mixing DC or DCE microfibers (see Figure 5.13a) with ABW nanofibers (see Figure 5.13b) at similar weight proportion (ABW50DC50 or ABW50DCE50), the resulting film was no longer opaque. For the DCE film, the introduction of 25% ABW nanofibers is already sufficient to make the film translucent.

The surface of the composite film was also found to be smoother than the neat DC or DCE film. This smoothening effect can be attributed to the ABW nanofibers that coat the surface of the microfibers. Figure 5.13c,d shows how the entire area of the DCE microfibers network was being 'coated' with ABW nanofibers at 50% DCE and 50% ABW weight ratio.

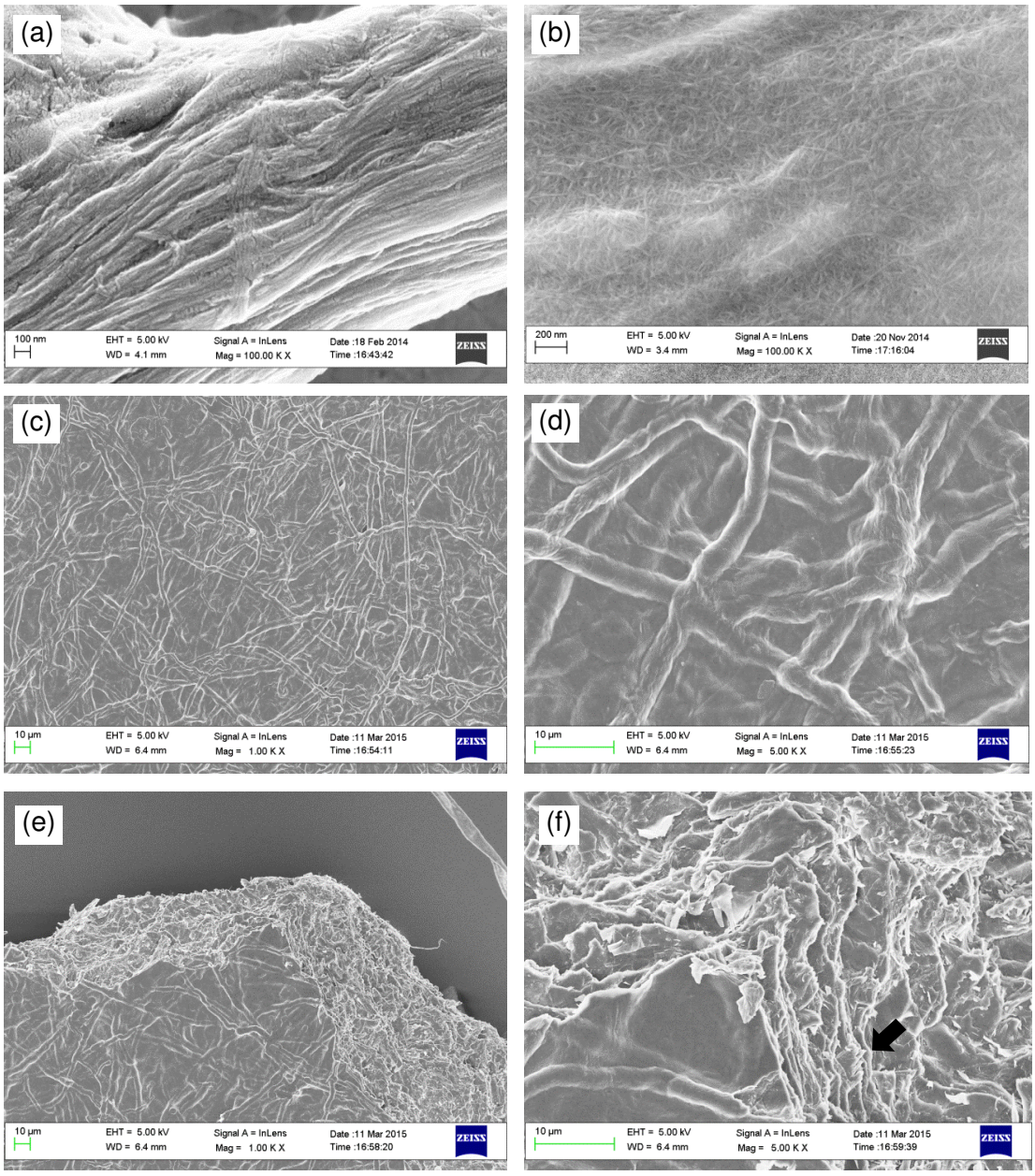

Figure 5.13 Scales difference at similar magnification between (a) single microfiber from DCE and (b) nanofibers from ABW. Scanning electron micrograph of ABW50DCE50 composite film: (c) surface morphology, (d) magnified image of the surface; notice how DCE macrofibers are coated with ABW nanofibers, (e) fracture image, (f) magnified fracture image, an arrow indicates DCE microfiber pullout.

At 25% and 75% ABW ratio, the coating also effectively covers the entire microfiber area. Similar coating effect was also demonstrated by the ABW-DC film. As a result of the mixing process and the slow filtration during film preparation, ABW nanofibers also went in-between the DCE or DC microfibers, simultaneously creating a layered network. Figure 5.13e shows the fracture surface of the DCE film with 50% of ABW nanofibers. Pull-out fibers that once dominated the fracture point became 'glued' together by the addition of film-forming ABW nanofibers (see Figure 5.13e). At higher magnification fractography, both the ductile characteristics of the microfibers and the brittle characteristics of the nanofiber can be seen (see Figure 5.13f).

Figure 5.14a,b shows the typical stress-strain curve exhibited by both ABW-DC and ABW-DCE composite films with their corresponding data tabulated in Table 5.6. The ultimate strength improved considerably by the addition of ABW, and the reason is most likely because of the inherent strength of the ABW nanofiber film rather than the improved fiber-fiber stress transfer. By itself, ABW is already strong and stiff, so much so, that when mixed with DC or DCE microfibers, its film forming nature becomes a liability. It will 'cement' the microfibers, restricts their movement and prematurely cause the microfibers to 'snap' during tensile test. Reduction in strain to failure as much as 50% is already apparent at 25% ABW addition.

Table 5.6 Physical and mechanical properties of ABW-DC and ABW-DCE film composite[a]

Sample (80 g/m^2)	ρ (g/cm^3)	P (%)	Tensile strength (MPa)	Young modulus (GPa)	Elongation at break (%)	Tensile toughness (MJ/m^3)
ABW0DC100	1.538	72.87	23.3 ± 2.6	0.4 ± 0.0	12.3 ± 1.5	1.8 ± 0.4
ABW25DC75	1.509	62.96	67.0 ± 2.0	1.8± 0.2	7.1 ± 1.2	2.8 ± 0.7
ABW50DC50	1.495	54.79	108.0 ± 1.1	3.1 ± 0.2	6.5 ± 0.5	3.9 ± 0.5
ABW75DC25	1.488	58.50	127.1 ± 11.6	4.0 ± 0.9	6.8 ± 1.0	4.9 ± 1.0
ABW100DC0	1.470	58.95	204.4 ± 4.0	6.9 ± 1.2	5.3 ± 0.4	5.3 ± 0.5
ABW0DCE100	1.539	55.03	65.3 ± 0.8	1.2 ± 0.1	13.2 ± 1.2	5.8 ± 0.5
ABW25DCE75	1.512	49.03	82.7 ± 4.2	2.1 ± 0.4	6.3 ± 0.5	3.0 ± 0.4
ABW50DCE50	1.492	48.56	114.8 ± 4.2	3.0 ± 0.5	5.7 ± 0.3	3.5 ± 0.3
ABW75DCE25	1.479	49.83	136.0 ± 6.0	3.7 ± 0.4	6.1 ± 0.2	4.5 ± 0.3
ABW100DCE0	1.470	58.95	204.4 ± 4.0	6.9 ± 1.2	5.3 ± 0.4	5.3 ± 0.5

[a]ρ and P represent film density and film porosity, respectively.

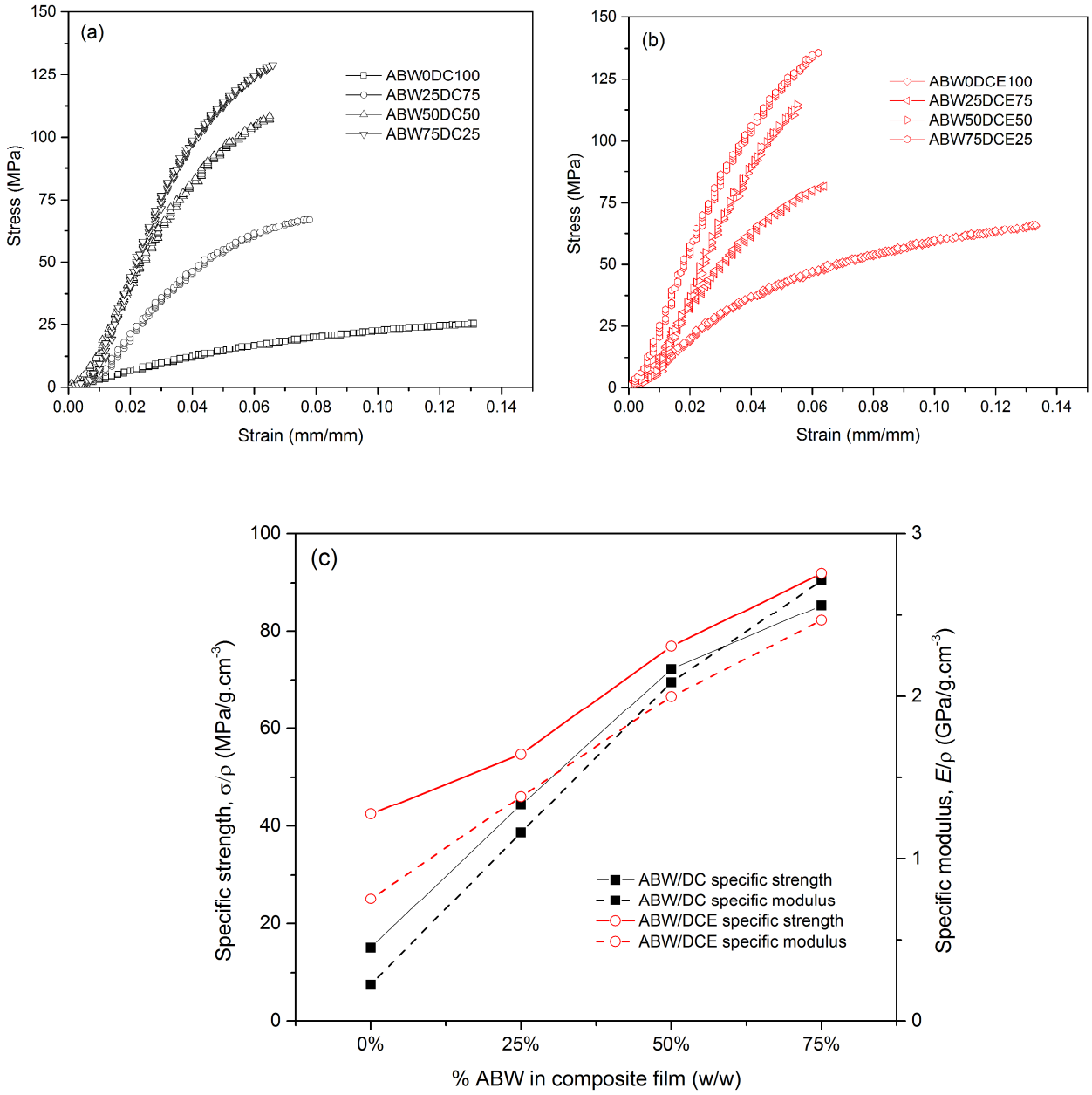

Figure 5.14 (a) stress-strain curves of ABW-DC composite, (b) stress-strain curves of ABW-DCE composite, (c) evolution of specific strength and specific modulus as a function of %ABW.

Nevertheless, from ABW point of view, slight improvements in ductility can be said to occur: strain to failure increases from 5.3% in the neat ABW film to 6–7% in composite film. Increasing %ABW in the composite film consequently reduces film density and porosity. These

causes an increase in the specific tensile strength and the specific modulus of the composite film (see Figure 5.14c).

At 50% RH, the neat ABW film experiences a low moisture uptake (7.9%) compared to the neat DC (9.9%) or the neat DCE (11.4%). By coating the surface of DC of DCE with dense ABW nanofiber, a reduction in moisture should be expected. This trend can be seen in Table 5.7.

Table 5.7 Moisture uptake for the composite film at 50% and 90% RH by dynamic vapor sorption, with onset degradation temperature at 10% weight loss ($T_{d,10\%}$) by TGA analysis

	moisture uptake, composite film				$T_{d,10\%}$ (°C), composite film			
	DC		DCE		DC		DCE	
	50% RH	90% RH	50% RH	90% RH	air	N_2	air	N_2
0% ABW	9.9	28.3	11.4	31.1	287	283	286	286
25% ABW	9.7	28.4	9.9	29.4	269	270	268	264
50% ABW	8.9	28.4	9.8	30.4	266	265	266	268
75% ABW	8.8	29.9	9.0	29.6	228	247	259	262

Reduction in moisture uptake upon the addition of ABW is more apparent for the DCE composite than for the DC composite due to higher water sorption of the neat DCE film. At 90% RH, the neat ABW film adsorbs more water (32.7%) than the neat DC (28.3%) or the neat DCE (31.1%). Thus, it was ABW that benefits from DC or DCE lower water uptake. Considering the mass gain between neat and composite films at either 50% RH or 90% RH, the difference is not significant. In fact, it is the desorption rate of DC (or DCE) that changed markedly upon the addition of ABW. When the environment moves from high to low humidity, the moisture took a much longer time to get released from the composite film than from the neat DC (or the neat DCE). The desorption behavior of the composite film follows the desorption behavior of the ABW film (see Figure 5.15).

With regards to the onset degradation temperature at 10% weight loss ($T_{d,10\%}$), the addition of ABW reduces an overall thermal stability of DC and DCE (see Table 5.7). This can be ascribed to inherently lower $T_{d,10\%}$ of the ABW film itself ($T_{d10\%,\ ABW\ film}$: air = 246 °C, N_2 = 251 °C).

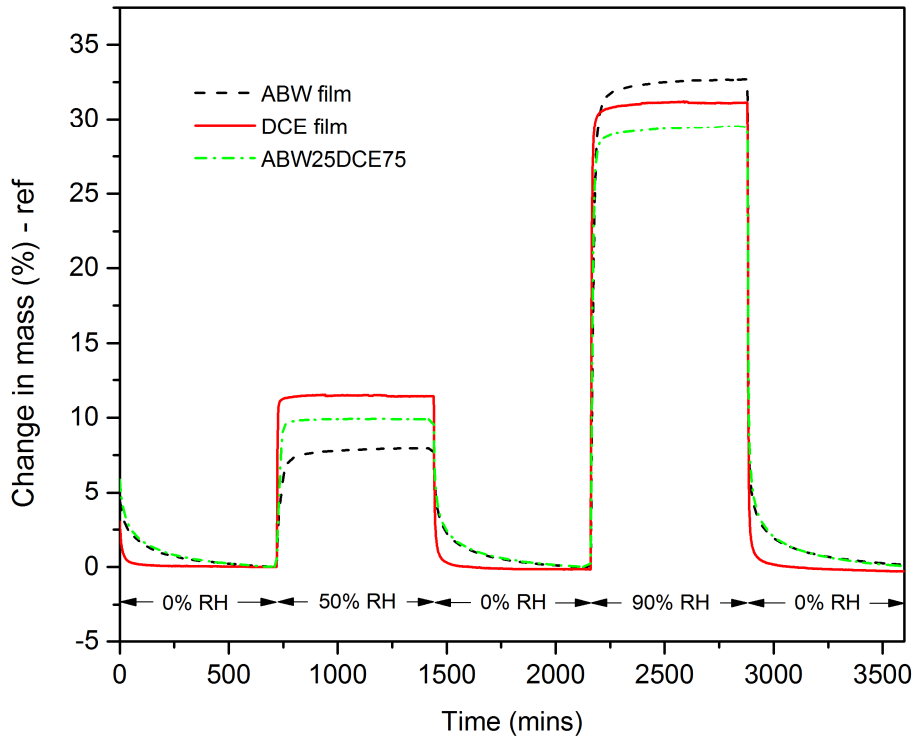

Figure 5.15 Moisture uptake profile for ABW25DCE75 composite film, ABW film, and DCE film.

In their composite form, both DC and DCE fiber surfaces are effectively being coated, and the resulting surface energy is supposedly to be governed by the coating material itself. The ABW film has a dispersive surface energy component (γ^d) of 46.3 mJ/m^2, hence ABW-DC or ABW-DCE should possess a surface energy around that value. However, this is not the case as ABW-DC possesses γ^d between 45 mJ/m^2 to 55 mJ/m^2 while ABW-DCE possesses γ^d between 55 mJ/m^2 to 59 mJ/m^2 (see Figure 5.16). The higher surface energy can be ascribed to the nature of the composite surface itself. Looking back at the SEM image (see Figure 5.13d), the presence of microfibers resulted in a rougher surface compared to the neat ABW film itself. The effect is substantial due to the significant different in scales between ABW nanofibers and DC/DCE microfibers. Rougher surface will hinder the movement of injected probe molecules and causes the retention time to be longer than on a flat surface [319]. Higher retention time corresponds to higher surface energy.

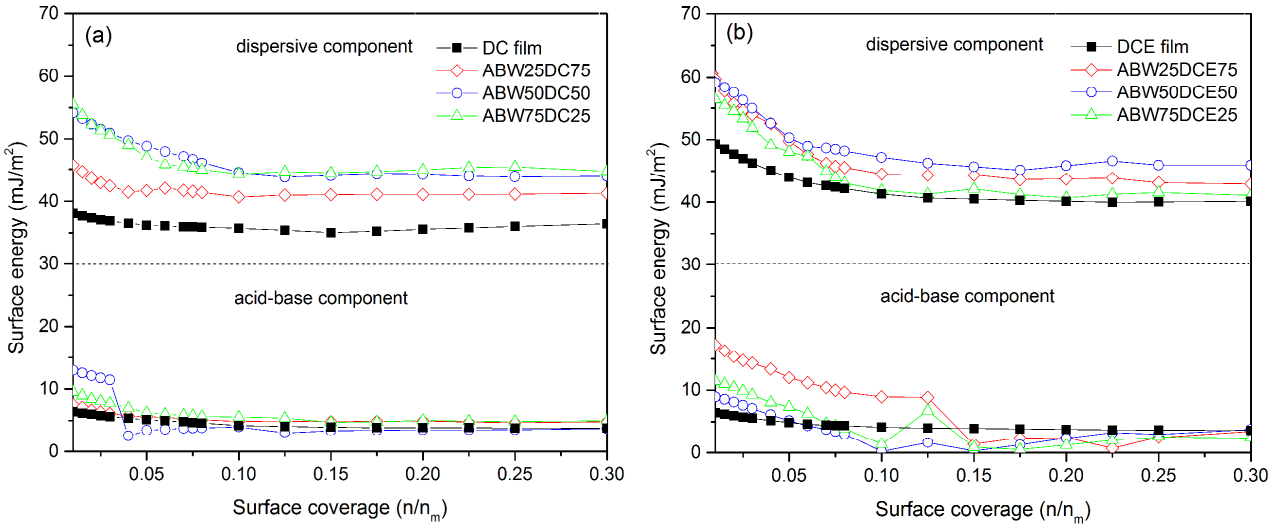

Figure 5.16 Surface energy profiles for ABW-DC and ABW-DCE composite film; as determined by inverse gas chromatography.

CHAPTER SIX
MUSHROOM CHITIN-GLUCAN NANOFIBERS AS A REINFORCEMENT FOR LAMINATED COMPOSITE & AS A BINDERS FOR FLAX NONWOVENS

6.1 Introduction

In Chapter 4 and Chapter 5, we focused on the development of thin films. However, for our fungal-based chitin to find any applications in engineering or structural materials, a greater material/film thickness is often required. This chapter describes the development of chitin based composites using fungal based chitin extracted from common mushrooms (ABW) as their reinforcing agent or binder for loose flax fibers for the production of flax nonwovens. Two themes presented in Section 3.1 will be covered: laminated composite and chitin binders.

6.2 Development of Mushroom Chitin-Glucan Paper Base Composite Laminate

6.2.1 Laminates: Preparation and Morphology

It is possible to produce specimen with considerable thickness from nanofibers suspension by filtration alone. Figure 6.1 shows specimen with a grammage of 1000 g/m^2 having a thickness about 0.7 mm fabricated by filtration of mushroom nanofibers suspension (ABW) with a consistency of 0.8% w/v.

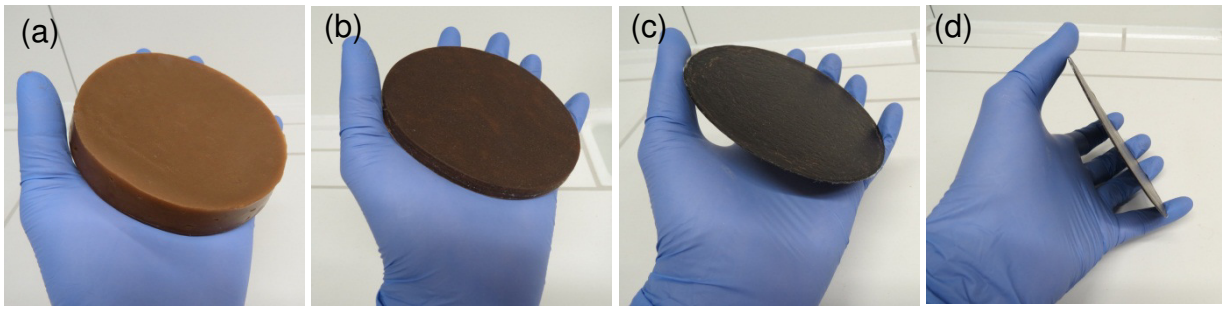

Figure 6.1 (a) ABW wet filtration cake with intended grammage of 1000 g/m^2 obtained by filtration of nanofibers suspension, (b) wet pressed ABW cake, (c & d) hot pressed ABW cake with a thickness ca. 0.7 mm.

The thickness of resulting wet filtration cake was carefully reduced by repeated press steps between blotting papers inside specially designed mold. The compressed cake is finally pressed and consolidated at elevated pressure and temperature to its final form.

However, the problem with this method is that it suffers from long filtration times (>12 h) and the wet filtration cake tends to collapse during compaction process. Inadequate wet compaction does entrap water, which upon drying will result in pore formation inside the finished product. In addition, there is a limit on how much suspension volume can be added into the filtration funnel before the pores of the filter become blocked.

Specimens with similar thickness can be prepared by stacking and laminating ten ABW films having individual film's grammage of 80 g/m^2. This lamination approach is scalable, quicker, and able to produce high volume fraction chitin composites; in this case the chitin films are used as reinforcement for the epoxy. Figure 6.2 shows schematically the layup of the laminate made from ABW films (ABW10L). Due to viscous nature of uncured epoxy, it bleeds from the laminates during the initial pressing step. The excess flush is visible between release films after the curing process. The finished product is rigid and flat.

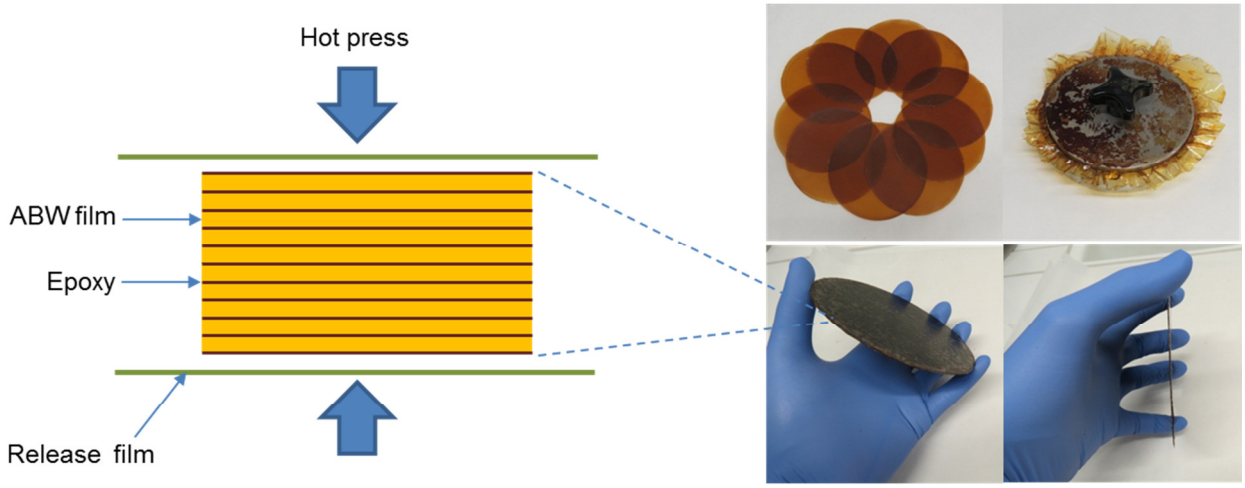

Figure 6.2 Schematic of the preparation process of a 10 layer laminate (ABW10L) with final thickness of 0.64 mm and volume fraction of 88.3%.

The control film (neat ABW) experienced 13% thickness reduction and a 10% weight loss compared to 'original ABW film'[19]. This weight loss needs to be considered when calculating the final volume fraction of the composites. The thickness reduction and weight loss was a result of the compaction pressure (1 ton), the curing temperature (180 °C), and longer consolidation time (6 h). Inevitably, this will affect our 'original ABW film' mechanical properties. Indeed the neat ABW has different tensile properties (E = 7.9 GPa, σ = 110.2, ε = 1.7%) compared to our 'original ABW film' (E = 6.9 GPa, σ = 204.4 MPa, ε = 5.3%). The increased modulus can be explained by the increased compaction of the fibers due to the higher compaction pressure, while the decrease in strength and strain is due to reduced flexibility of the fibers due to the removal of bound water at higher temperatures. The higher compaction pressure also resulted in a lower film porosity; it decreased from 58.9% to 42.5%.

Fracture surfaces of laminated composites are shown in Figure 6.3.

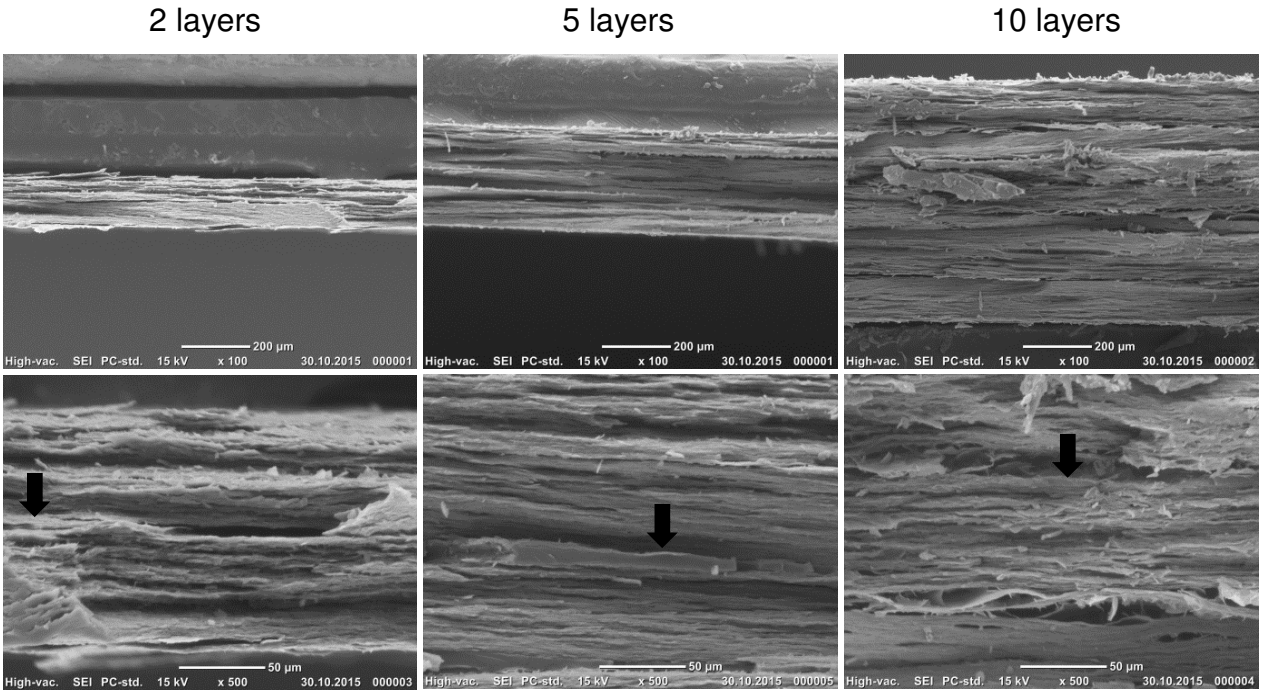

Figure 6.3 Fracture surface of ABW-epoxy laminates. Image at the bottom is a magnified section of top image. Arrows indicate epoxy resin layers.

[19] 'Original ABW film' represents mushroom film studied in Chapter 3, hot pressed under 5 kg, 120 °C for 3 h. Control film (or neat ABW) in this chapter (Chapter 6) was made by subjecting one 'original ABW film' to hot pressing parameter that is similar to laminate processing : 1 ton, 120 °C (2h) + 180 °C (2h) + 120 °C (2h).

The high compaction pressure compressed the ABW layers tightly together so it became hard to discern the individual films. Only small amounts of epoxy resin (indicated by arrows) can be seen between the layers, resulting in the high volume fraction of the laminated composites: 93.7%, 90.2%, and 88.3% for ABW2L, ABW5L, and ABW10L, respectively.

The fiber volume fraction (ν_f) increased as number of layer decreased because less resin was needed to impregnate the layers. The presence of a dense nanofibers network implies that ABW films are difficult to be impregnated by the rather viscous liquid epoxy resin melt. The surface of the film can be said to form a barrier and, therefore surplus resin is pressed out of the laminate during the compaction process, consequently leading to high ν_f composites. The difficulties of resin to impregnate a tight nanofibers network has also been demonstrated for cellulose nanopaper laminates [320].

6.2.2 Mechanical Properties of Chitin-Glucan Paper Based Composite Laminates

The tensile stress-stain curve behavior of our chitin paper base composite laminates is shown in Figure 6.4a and the corresponding data are summarized in Table 6.1. All laminates possessed a rather similar modulus of around 8 GPa, but the strength decreased with an increasing number of layers used to produce the composites. The constant modulus of the composites can be attributed to the fact that the resin did not impregnate the chitin films, hence, all measured moduli corresponds to the modulus of the control film itself.

The strength of the composite is affected, as any defects in the material will initiate cracks that lead to premature failure. An increase in specimen size will increase the likelihood of weakest links to be present in the material, which reduces its strength. This is generally true for brittle materials, such as epoxy based composites, a phenomenon commonly referred as the 'size effect' [321-323]. Although the negative size effect is prevalent in the composite field, it is possible to produce a positive size effect by removing the matrix/reinforcement interface, for instance in the case of all cellulose composites [324].

We can see from Figure 6.4a that thicker composite laminates (ABW10L) are more prone to delamination than thinner laminates, indicated by their intermittent stress drop before ultimate failure. This is an example of the discussed size effect associated with free-edge stresses produced when cutting thicker brittle specimen, which caused delamination in which crack

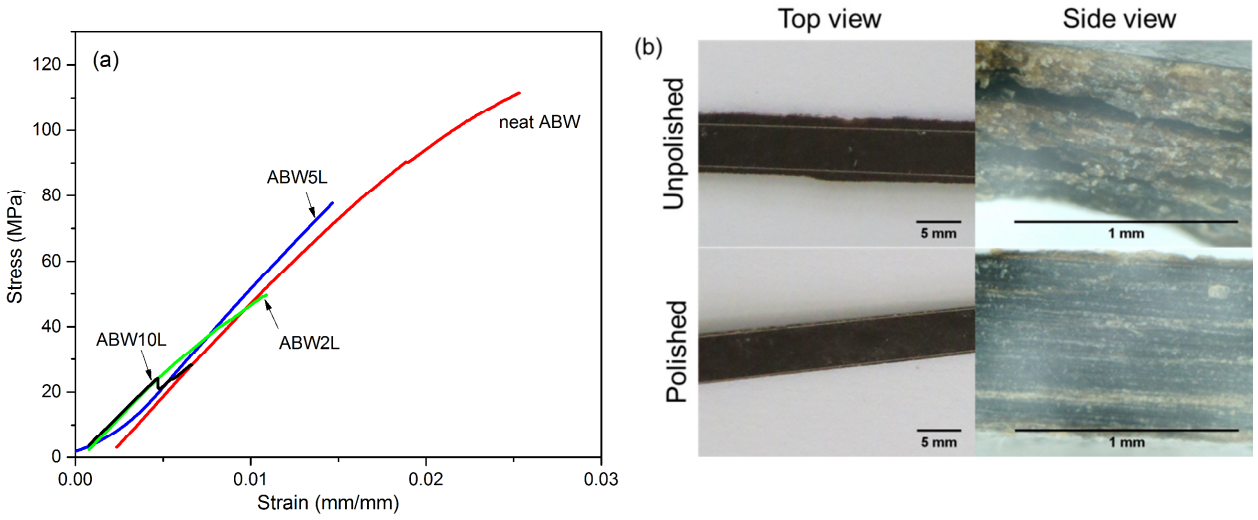

Figure 6.4 (a) typical stress-strain curves for chitin paper base composites laminates, (b) delamination in unpolished ABW10L compared with polished specimen.

Table 6.1 True density (ρ), porosity (P), reinforcement volume fraction (v_f) and tensile properties of investigated chitin film base composites.

Sample	ρ (g/cm^3)	P (%)	v_f (%)	Tensile strength (MPa)	Young modulus (GPa)	Elongation at break (%)	Tensile toughness (MJ/m^3)
Neat epoxy	1.167	–	–	74.0 ± 2.5	1.8 ± 0.2	8.8 ± 1.9	3.7 ± 0.4
Neat ABW	1.476	42.53	100.0	110.2 ± 7.9	7.9 ± 0.6	1.7 ± 0.1	0.9 ± 0.2
ABW2L	1.454	28.39	93.7	77.0 ± 4.4	8.0 ± 0.6	1.1 ± 0.1	0.4 ± 0.0
ABW5L	1.433	25.92	90.2	44.9 ± 3.8	7.8 ± 0.8	0.6 ± 0.1	0.2 ± 0.0
ABW10L	1.428	20.05	88.3	29.4 ± 4.2	8.0 ± 0.7	0.4 ± 0.1	0.1 ± 0.0

initiates at the laminate free edge and propagates inwards along the interface between two adjacent layers [325]. Figure 6.4b (unpolished) shows the state of ABW10L after being cut using our bench saw. Due to the brittle nature of the chitin film base composites, free edge delamination was observed. To minimize this effect, the cut specimens were polished with low grit sand paper. The polished samples were not cracked.

The theoretical performance of the chitin film base composite laminates can be predicted using the simple rule of mixture (ROM). Lee et al. [47] found that the ROM is a better predictor for high v_f nanocomposites (i.e. cellulose nanopaper) than the commonly used Cox-Krenchel

micromechanical model for randomly oriented short fiber composite. Figure 6.5 compares the measured with the predicted values of specific modulus and specific strength of our laminated composites with different v_f. The measured moduli were higher than predicted value. In fact it increases, albeit slightly, as v_f decreased. The strength follows the expected trend predicted by ROM; the strength decreased with decreasing v_f. The difference between predicted and measured strength increased when more chitin films were added in the final composite laminates. We attributed this phenomenon to the size effect discussed previously. For example the difference between ROM and measured strength ($\sigma_{ROM/actual}$) increased gradually by 1.4 times, 2.4 times, and 3.6 times for ABW2L, ABW5L and ABW10L respectively. This increase in $\sigma_{ROM/actual}$ is expected, as it is harder to cut thicker (and brittle) samples. Montrikittiphant et al. [320] already observed 1.6 times difference in $\sigma_{ROM/actual}$ value with only one layer of cellulose nanopaper in their laminated composite.

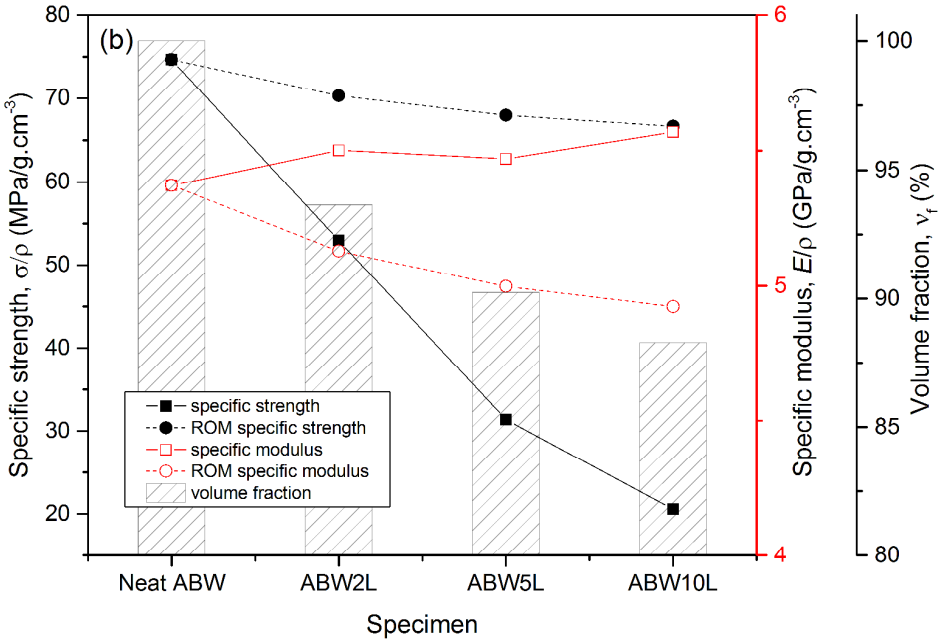

Figure 6.5 Specific strength and specific modulus of investigated specimens. Both experimental and predicted value from rule of mixture (ROM) is presented.

Table 6.2 summarizes the results of the flexural test of neat epoxy and ABW10L. Standard three point bending tests on neat ABW, ABW2L and ABW5L could not be performed because of their low thickness. In bending, significantly higher strength (105.4 MPa) was observed than in tension (29.4 MPa) because the probability of finding a critical defect is lower when less material volume is subjected to the maximum stress [326, 327]. The modulus (12.5 GPa), however, reflects the flexural properties of the chitin film base composite laminates rather than a material properties [328], thus a direct comparison with the tension modulus can be misleading. Both specimens failed catastrophically at maximum bending (deflection at maximum strength = strain to failure). In order to improve the strain, the matrix should isolate the fibers from each other, so that an external stress can be effectively transferred [329]. As the resin did not impregnate the film properly, the properties of individual ABW nanofibers could not be exploited [330].

Table 6.2 Flexural properties of neat epoxy and ABW10L sample[a]

Sample	ρ (g/cm^3)	P (%)	ν_f (%)	Flexural strength (MPa)	Flexural modulus (GPa)	Deflection at max strength (%)
Neat epoxy	1.167	–	0.0	129.9 ± 3.5	3.1 ± 0.2	7.1 ± 0.1
ABW10L	1.428	20.05	88.3	105.4 ± 4.6	12.5 ± 1.3	0.9 ± 0.1

[a]ρ, P, and ν_f represent true density, porosity, and volume fraction, respectively.

Evolution of specimen's storage modulus as a function of temperature is depicted in Figure 6.6. The neat cured epoxy resin has a storage modulus of 2–3 GPa. Upon passing the glass transition temperature the modulus dropped dramatically. The incorporation of ABW films in to the resin results in a significant increase in the bending storage modulus both below and most importantly above the glass transition temperature; the composite laminates maintain their storage modulus in bending over the whole temperature range. Because of the high reinforcement content, the influence of the matrix is significantly reduced. Because resin content in laminated composites is very low, there is not much difference between the storage modulus of the composites compared to ABW film.

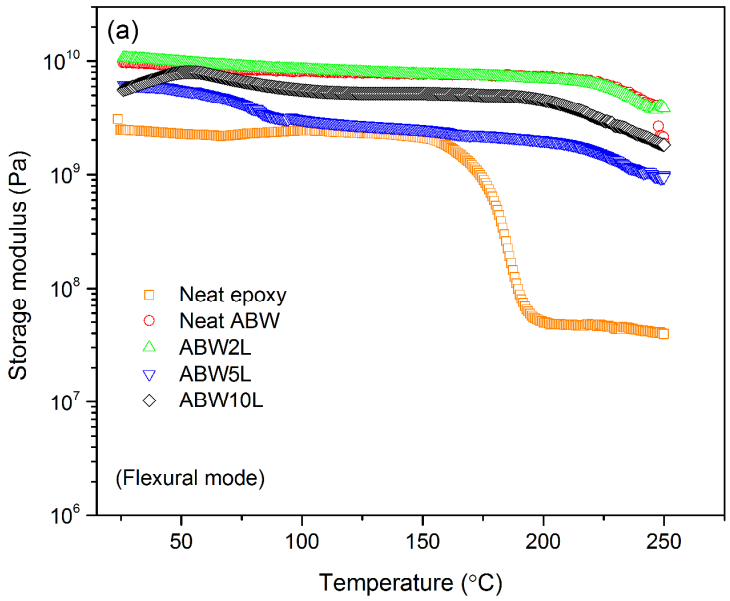

Figure 6.6 Evolution of storage modulus as a function of temperature in flexural mode; determined by DMTA

6.2.3 Thermal and Moisture Sorption of Chitin-Glucan Paper Based Composite Laminates

The cured epoxy resin has an onset degradation temperature at 10% weight loss ($T_{d,10\%}$) of 370 °C in both air and N_2 atmosphere. The addition of the resin should offer thermal protection to our neat ABW film, which possesses a lower $T_{d,10\%}$ ($T_{d,10\%,\ neat\ ABW}$: 270 °C). The low resin content and subsequent bleeding during the compaction process caused the laminate surfaces not to be fully covered. This led only to a minimal thermal protection as indicated by the small increase in $T_{d,10\%}$ for all laminated composites (see Table 6.3).

Table 6.3 Onset degradation temperature at 10% weight loss ($T_{d,10\%}$) by TGA analysis and moisture uptake of the laminates at 50% and 90% RH as determined by dynamic vapor sorption

Sample	$T_{d,10\%}$ (°C)		Moisture uptake (%)	
	air	N_2	50% RH	90% RH
Neat ABW	269	271	NA	NA
ABW2L	275	282	7.6	27.1
ABW5L	277	281	7.6	24.9
ABW10L	277	280	6.0	24.3

Although the epoxy does not fully encase the chitin films within the laminates, it did reduce the diffusion rate of water vapor into the composite specimens. The higher resin content of the thicker laminated composites resulted in a reduced moisture absorption rate and lower total moisture uptake. For example, at 50% RH, ABW10L took almost 24 h to equilibrate reaching a moisture content of 6.0%. In contrast, it took only 5 h for ABW5L to equilibrate reaching a higher moisture uptake of 7.6%. A similar trend was also observed at 90% RH.

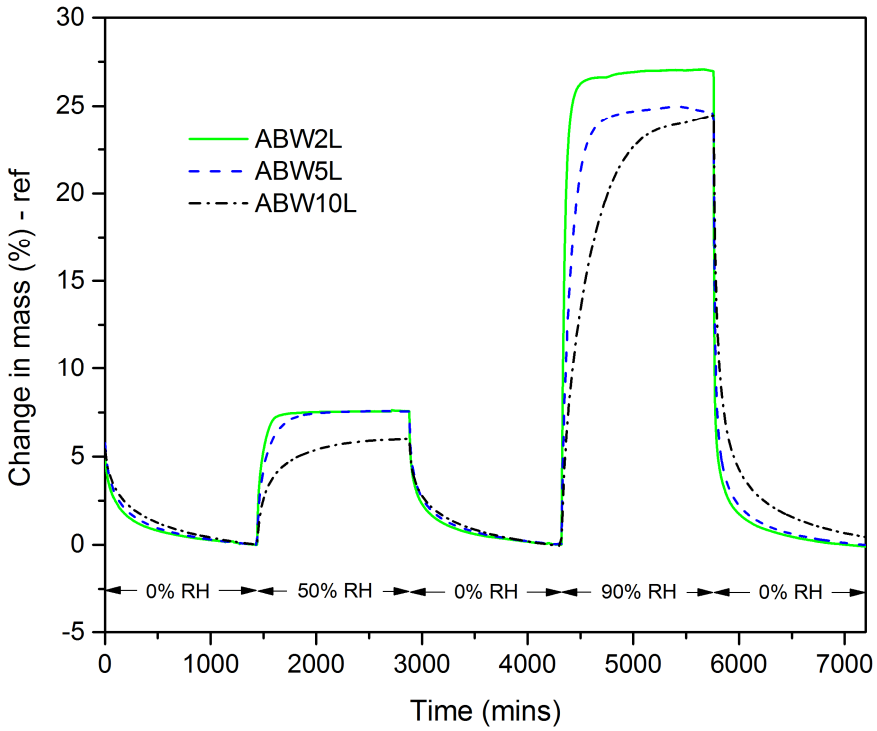

Figure 6.7 Moisture uptake profile for the laminates (ABW2L, ABW5L, and ABW10L) at 50% RH and 90% RH.

6.3 Nonwoven Flax Preforms Using Mushroom Chitin-Glucan Nanofibers as Binders

6.3.1 Nonwoven Flax Preforms: Preparation and Morphology

Binderless non-woven bio-based fiber mats can be formed without difficulties if the natural fibers are nano- or micrometer sized [178, 331, 332]. Because of the high surface area of the nanofibrils, extensive hydrogen bonds and fiber entanglements can be formed, hence keeping the structure intact and strong. However, nanofibrillation is very energy intensive [333], and this limit potential applications to thin materials (<0.5 mm), such as papers, membranes, and films. Moving to macroscale (i.e. wood chip, technical natural fiber) results in a reduction of the total available surface area and moreover, the resulting fibers entanglements are inadequate to produce strong nonwoven without the use of additional adhesive, called binders in this case. Binders, such as phenolic resin, are necessary to bind woodchips together for the production of fiberboard for instance. However, phenol formaldehyde resins with the associated formaldehyde emissions has triggered health concerns, and had prompted policy makers to regulate such emissions, which in turn initiated research into new adhesive and alternative binders for macroscale materials [334, 335]. In order for this to work, raw materials need to have high lignin content to serve as natural binder [336, 337] and additional pretreatments such as steam explosion [334] or mechanical beating [338] are often necessary to further soften the fibers. High pressure (normally >10 MPa) and temperatures (normally >180 °C) are used to consolidate the structure, and often the product need to have a considerable thickness (>5 mm) for them to be useful for load bearing applications. Herein we demonstrate a method to produce strong 1 mm thick nonwoven flax preforms using alternative nanofibrous binder via relatively mild hot pressing step (1 MPa pressure[20] at 120 °C for 3 h).

Figure 6.8a shows a non-woven flax preform without any binder. This preform was held together predominantly by fiber entanglements and fiber/fiber friction rather than lignin plasticization. This is based on the fact that the lignin content in used flax fibers was low (<3%) [289] and the temperature used during the consolidation step was below the temperature required to soften lignin allowing it to serve as effective binder, which normally occurs at temperature exceeding 150 °C [339, 340]. Extensive hydrogen bonding can also be ruled out since the used flax fibers were not refined, having average diameters in the range of 0.1–0.2 mm.

[20] Calculated based on 1 ton pressure applied onto 110 mm diameter specimen (= ~10^5 kg/m^2 or ~10 bar or ~150 psi).

In our procedure, the only pretreatment needed (to make neat flax preform) was to use loosed flax fibers that were soaked overnight in water with the aim to soften the fibers and to increase the number of macrofiber entanglements during the filtration process used to produce the fiber preforms. After hot pressing, the preform, at first, had a decent stiffness but was very susceptible to external stress. When the preform was slightly bended using thumb, the preform lost most of its initial stiffness and behaved like a pliable mat.

In an attempt to bind the fibers more effectively, the ABW nanofibers suspension was co-filtered with the flax fibers. A non-woven flax preform containing 10% ABW nanofibers (w/w) as an alternative binder is shown in Figure 6.8b. This ABW bound flax fiber network was stiff and moreover remained stiff even after repeated bending. The darker appearance of the ABW-Flax preform is not a byproduct of heat discoloration, but originated from natural pigmentation of ABW itself. This is the first report of chitin-based nanofibers used as a binder for loose natural fibers for the preparation of non-woven natural fiber preforms. Bacterial cellulose, nanofibrillated cellulose, and kraft pulps were previously reported to be effective binders for loose natural fibers [248, 341-343].

Figure 6.8 Nonwoven flax fiber preform before and after hot pressing (a) non-woven flax preform without any binder, (b) non-woven flax preform containing 10% ABW nanofibers as binder.

When a mixture of ABW suspension and flax fibers are poured together into a filtration funnel, ABW concentration gradient is expected to develop. This is expected to occur because the size difference between flax fibers and ABW nanofibers. The nanofibers should easily flow through the porous macro(flax)fibers network. This did continue until ABW nanofibers filtration

stopped by the formation of nanofiber filtercake below the flax fiber network. Gradient formation resulted in poor binder distribution throughout the thickness of the preform, which subsequently affected the overall mechanical properties of the fiber preform. To minimize this problem, we adopted the layer-by-layer filtration method suggested by Fortea-Verdejo et al. [248] which claimed to result in a 60% improvement in the tensile strength as compared to a fiber mat produced by a single-step filtration.

The layer-by-layer filtration process is schematically shown in Figure 6.9. Dewatering the first layer results in the consolidation of its top surface, providing a less porous base for the next successive layer.

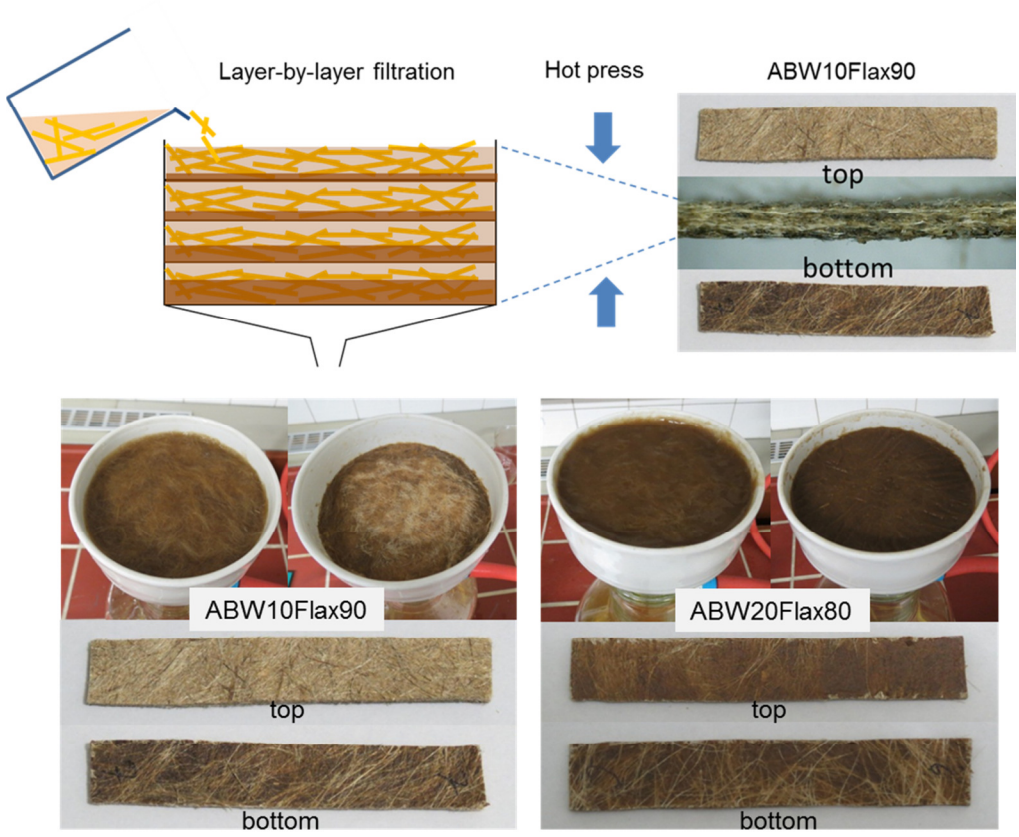

Figure 6.9 Schematic of layer-by-layer filtration and its dependence on ABW loading concentration.

Due to the nature of the filtration process, a higher concentration of ABW nanofibers can be found at the bottom than at the top surface of filtration cake. Moreover, ABW is of darker color compared to the flax fibers, which resulted in one side of the preform to be darker than the other. Although the gradient problem was not fully eliminated, a better binder distribution compared to the single step filtration method can be expected when using the layer-by-layer filtration method. This is indicated by an alternate dark-and-light band profile across the specimen thickness (see Figure 6.9).

It is worth noting that the problem of binder distribution within the fiber mat was reduced when higher binder concentrations were used. For example, when an ABW suspension with a concentration of 20% was used, the resulting fiber mat was saturated with nanofibers. This prevented ABW nanofibers from settling to the bottom, hence allowing for a better binder distribution throughout the preform. The fact is supported by the disappearance of the demarcation line between each subsequent filtration layer (i.e. alternate dark-and-light band) throught the hickness of the ABW20Flax80 specimen.

In term of color appearance, the top side surface of the preform containing 5% and 10% ABW was similar to the surface of the neat flax preform. Hence, the question might arise: is there any binder at all on the top side of ABW5Flax95 and ABW10Flax90? Figure 6.10 shows surface morphology of ABW5Flax95 and neat flax preforms.

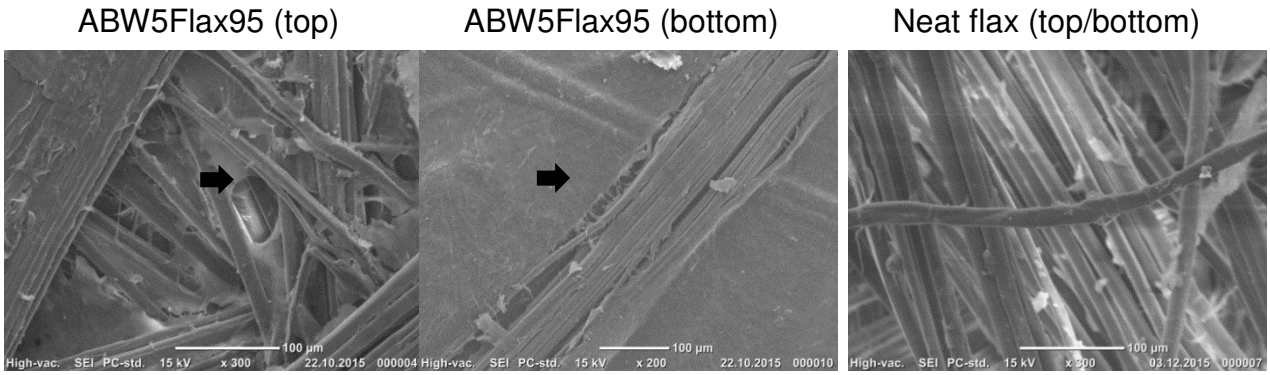

Figure 6.10 Surface morphology of neat flax and ABW5Flax95 preform. An arrow indicates presence of binder.

Even at low ABW loading, when the gradient problem should be greatest, there is still a considerable amount of ABW nanofiber binding the flax fibers together. However, as expected, denser nanofiber network can be seen at the bottom surface of the preform, where the entire flax fibers surfaces were covered by ABW nanofibers. In contrast when no binder was used at all, all fibers are loose suggesting that this preform structure were only held together mainly by physical fiber/fiber entanglements and the resulting interfibers friction.

The flax preforms bound with ABW nanofibers can easily be cut. Figure 6.11a shows a photograph contrasting a loose (binderless) flax fiber preform and an ABW bound fiber preform after cutting using a bench saw. Without binder, loose fibers were being pulled out by saw teeth, which results in hairy edge[21]. With binder however, the fibers were firmly held in its place and clean cut was produced. Figure 6.11b illustrates the ability of these fiber preforms to support a weight. A neat flax preform can only support minimal weight before it started to deform. In contrast, by using 10% ABW to bind the otherwise loose flax fibers stiffens the preform, allowing it to withstand 20 times more load than the loose flax fiber mat.

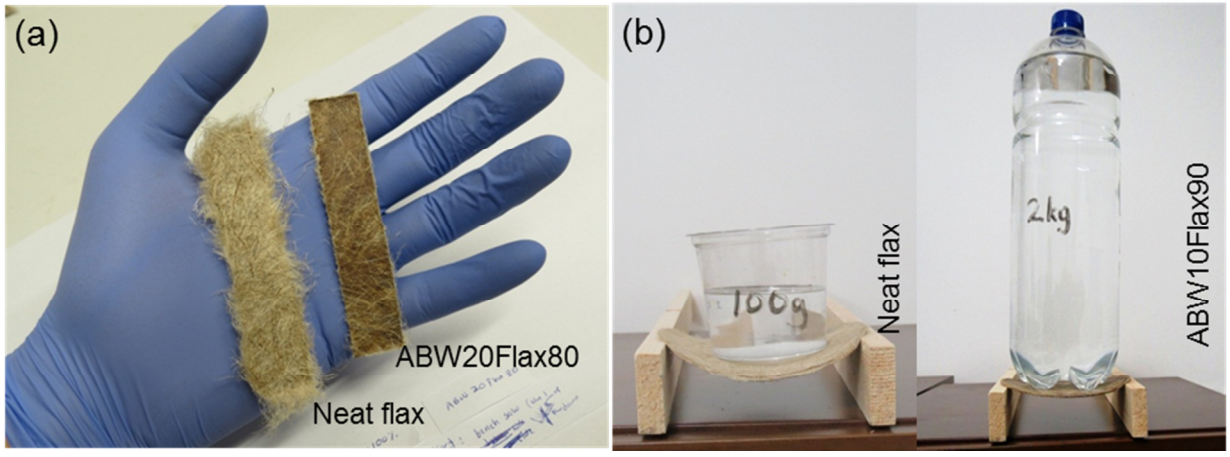

Figure 6.11 (a) appearances of loose and ABW bound flax preforms after being cut by a bench saw (b) preform ability to support weight. Both preform had a similar grammage and thickness: 1000 g/m^2 and ~1 mm, respectively.

[21] In order to obtain more defined dimension, all neat flax specimen used during mechanical test were cut by a scissors.

6.3.2 Mechanical Properties of Nonwoven Flax Fiber Preforms

Figure 6.12a shows typical uniaxial stress-strain curves for loose flax fiber preforms and ABW bound flax preforms. The corresponding data are tabulated in Table 6.4. With only 5% ABW as binder, the tensile strength and tensile modulus of neat flax preform increased by 4.4 times and 5.2 times, respectively. The binder held the flax fibers together allowing more stress to be transferred between the fibers than the entanglement friction does alone. The ABW binder prevented the flax fibers from slipping during the tensile test. Further addition of binder below 10% did not alter the preform mechanical properties by much. For example, when ABW concentration was doubled from 5% to 10%, the strength improved only by 2.2 MPa while the modulus remained constant. However, when ABW concentration doubled from 10% to 20%, a significant increase in mechanical properties was observed; the strength and modulus improved by 12.2 MPa and 1.9 GPa, respectively. We ascribe this to the saturation of the preform with binder. ABW20Flax80 had a much better binder distribution than ABW10Flax90 and thus better stress transfer at flax/binder/flax interface is expected. At this highest ABW concentration, ABW20Flax80 was 13.2 times stronger and 10.9 times stiffer (in tensile load) than the neat flax fiber preform.

Figure 6.12b shows typical flexural stress-strain curves for of the neat and ABW binder preforms. The corresponding data are tabulated in Table 6.5.

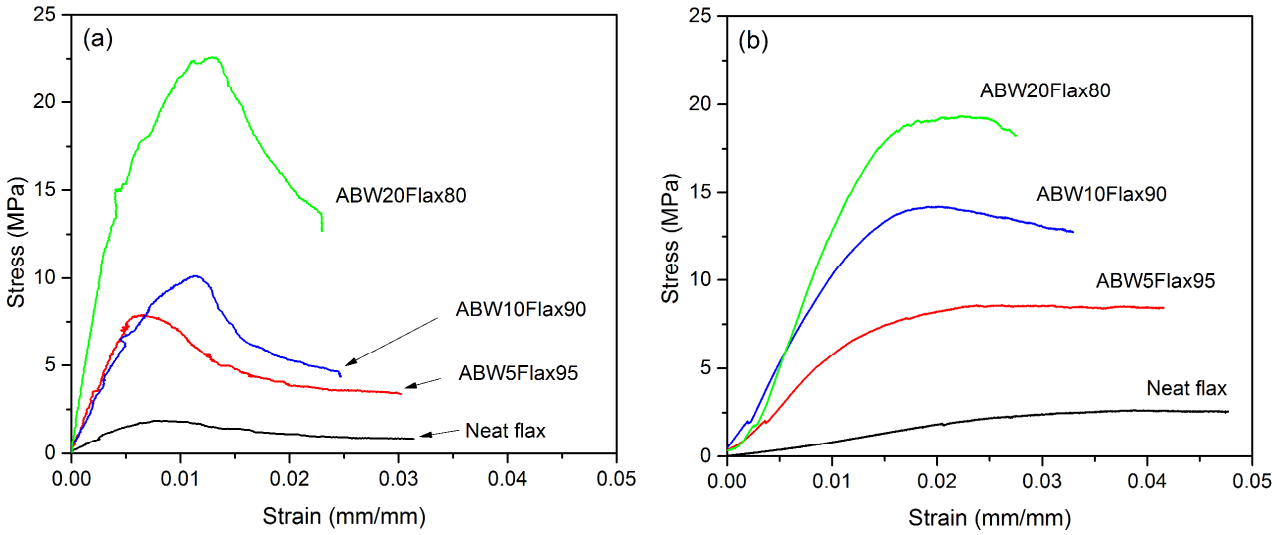

Figure 6.12 Typical stress-strain curve of preform in (a) tensile mode, (b) flexural mode.

Table 6.4 Physical and tensile properties of preforms[a]

Sample	ρ (g/cm^3)	P (%)	Tensile strength (MPa)	Young modulus (GPa)	Elongation at max strength (%)
Neat flax	1.566	73.64	1.6 ± 0.4	0.3 ± 0.1	0.8 ± 0.2
ABW5Flax95	1.552	63.38	7.2 ± 2.5	1.5 ± 0.5	0.6 ± 0.1
ABW10Flax90	1.543	62.27	9.4 ± 1.0	1.3 ± 0.1	1.0 ± 0.2
ABW20Flax80	1.519	60.33	21.6 ± 3.0	3.2 ± 0.7	1.1 ± 0.2

[a]ρ and P represent true density and porosity, respectively

Table 6.5 Flexural properties of preforms

Sample	Flexural strength (MPa)	Flexural modulus (GPa)	Deflection at max strength (%)
Neat flax	2.8 ± 0.4	0.1 ± 0.0	4.0 ± 0.3
ABW5Flax95	7.9 ± 1.4	0.6 ± 0.2	3.1 ± 0.6
ABW10Flax90	14.6 ± 1.9	2.0 ± 1.0	1.7 ± 0.5
ABW20Flax80	21.5 ± 3.9	2.3 ± 0.8	1.9 ± 0.3

With only 5% ABW as binder, the flexural strength and flexural modulus of neat flax preform improved by 2.8 times and 5.2 times, respectively. At highest ABW concentration, ABW20Flax80 was 7.7 times stronger and 19.5 times stiffer (in flexure) than the neat flax fiber preforms.

6.3.3 Thermal and Moisture Sorption Properties of Nonwoven Preforms

The pure ABW nanofiber film had a lower onset degradation temperature at 10% weight loss ($T_{d,10\%}$) than neat flax ($T_{d,10\%,ABWfilm}$: air = 246 °C, N_2 = 251 °C; $T_{d,10\%,flax}$: air = 298 °C, N_2 = 303 °C). However, when ABW was used as binder for flax it did not significantly affect the degradation behavior of flax $T_{d,10\%}$ (see Figure 6.13a and Table 6.6). For example, at 20% ABW, the preform only experience 20 °C drop in $T_{d,10\%}$, and the reduction of the degradation temperature was much lower at lower ABW concentrations.

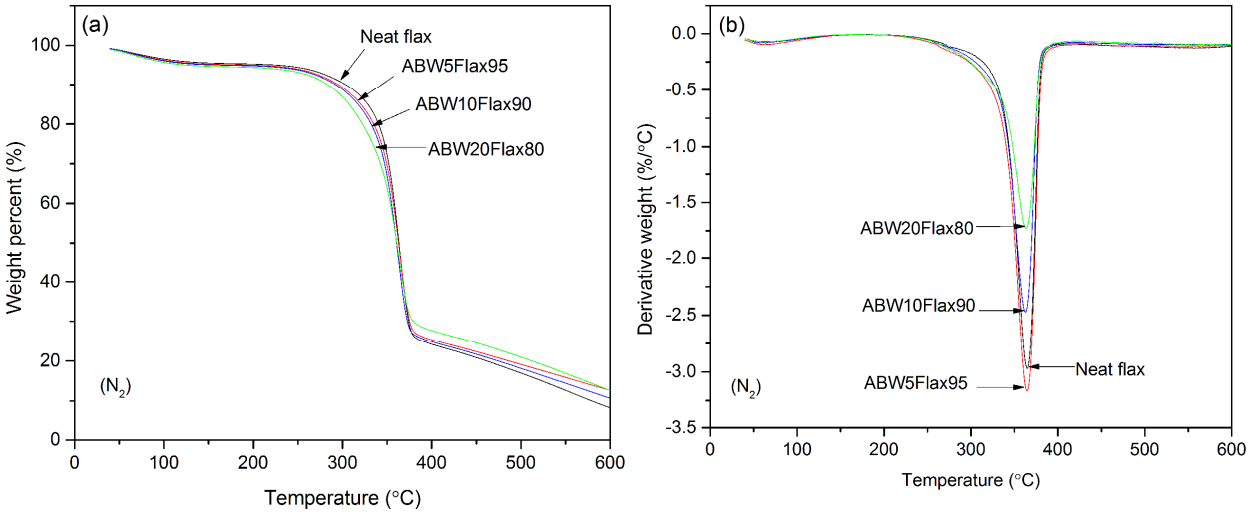

Figure 6.13 (a) TGA curve for preforms in N_2, (b) DTG curve for preforms in N_2

Table 6.6 Onset degradation temperature at 10% weight loss ($T_{d,10\%}$) by TGA analysis and moisture uptake for the laminates at 50% and 90% RH as determined by dynamic vapor sorption

Sample	$T_{d,10\%}$ (°C), film		Moisture uptake (%)	
	air	N_2	50% RH	90% RH
Neat flax	298	303	6.2	14.3
ABW5Flax95	290	295	6.4	15.2
ABW10Flax90	284	292	6.6	16.0
ABW20Flax80	279	283	6.9	17.3

Addition of ABW also did not affect the temperature at which the preform experienced the main weight loss during degradation process ($T_{DTG,peak}$ = 362 °C). In fact the rate of weight loss at $T_{DTG,peak}$ reduced with increasing ABW concentration (see Figure 6.13b).

Figure 6.14 depicts moisture uptake profile at 50% RH and 90% RH of the investigated preforms. The corresponding values are summarized in Table 6.6. Our flax fibers were not chemically pretreated, hence the moisture absorption of the neat flax (preform) was low due to presence of waxes and residual lignin. The moisture sorption of the flax preform gradually increased with increasing binder content. This was caused by the higher vapor sorption capacity of ABW (film) itself. The neat ABW (film) adsorbed more moisture (at 50% RH = 7.9% mass gain, at 90% RH = 32.7% mass gain) than the neat flax (at 50% RH = 6.2% mass gain, at 90% RH = 14.3% mass gain).

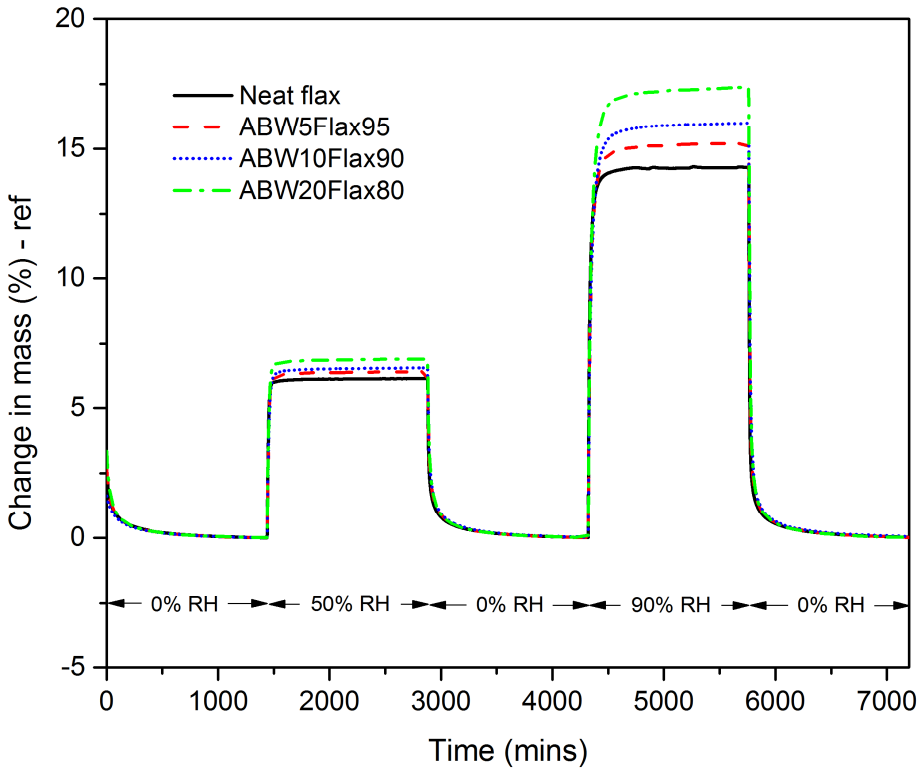

Figure 6.14 Moisture uptake profile for the preforms at 50% RH and 90% RH.

Nevertheless, an increase in moisture sorption capacity did not cause ABW-flax preform to lose its binding capability. Figure 6.15 illustrates the appearance of the neat flax preform and ABW10Flax90 after being immersed in 0.5 L water for 24 h. The neat flax fiber preform shows signs of disintegration and is unable to hold its own weight, whereas the ABW10Flax90 preform remained intact. Note also the color differences of water in which the preforms were immersed; extractives from flax leached out when no binder was present in the preform, turning the color of water yellowish. In contrast, no discoloration was observed in the spent water after the ABW10Flax90 preform was removed from it. Both samples, which were still wet, were subjected to a simple strength test. Wet neat flax preform was unable to sustain any weight because it was disintegrated. On the other hand, the wet ABW10Flax90 could hold 2.5 kg weight freely without any noticeable deformation of its structure, proving the water immersion of the preform did not affect the binding between ABW nanofibers and flax macrofibers.

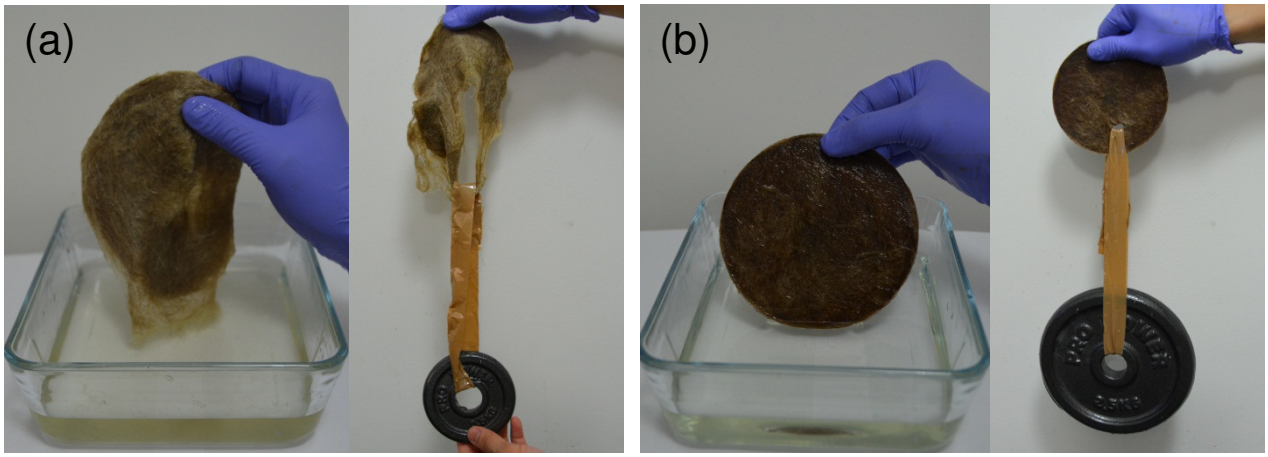

Figure 6.15 Condition of preform after being immersed in water for 24 h (a) flax preform without any binder, (b) flax preform with 10% ABW nanofiber as a binder.

CHAPTER SEVEN
CONCLUSIONS AND RECOMMENDATIONS FOR FUTURE WORK

7.1 Conclusions

In this study, the potential of fungal-based chitin nanofibers as an alternative to animal-based chitin nanofibers was investigated. Glucan associations with fungal chitin, although complicate the characterization process, provides a ready-made natural nanocomposite architecture that combine the strength and rigidity of chitin with the ductility of glucan. On the basis of our works, the following conclusions were drawn:

Chitin-Glucan Nanofibers from Common Mushrooms

1. Extract from common mushroom, *A. bisporus*, was found to be easily and readily disintegrated into uniform nanofibers 10–20 nm in width and several micrometers in length after chemical extraction without the need for any additional mechanical defibrillation process. The total extraction process takes less than 4 h and with sodium hydroxide being the only chemical used. The only pretreatment required is to blend the mushrooms in a blender for 5 min prior to chemical extraction. To the best of our knowledge, this is the fastest, simplest and mildest route used to extract chitin based nanofibers from natural materials.
2. The glucan to chitin ratio in common mushroom nanofibers is almost equal. Due to presence of glucan, mushroom nanofibers have excellent film forming ability. It was possible to prepare very thin (2 μm thick) free-standing chitin-glucan films without difficulty.
3. Films prepared from common mushroom nanofiber extract using the whole fruiting body had a tensile modulus (E) and strength (σ) of 6.9 GPa and 204.4 MPa, respectively. This is to date the highest tensile strength reported for chitin-based films. The measured tensile modulus for the chitin-glucan films compares favorably with the ~8 GPa, which is the highest modulus reported for chitin films in the literature (see Table 2.5 in Chapter 2 for the compilation of the mechanical properties of chitin films). The excellent mechanical

properties of the prepared chitin-glucan films can be ascribed to the mild conditions of the extraction processing which preserves most of the native nanofiber properties.

4. Irrespectively, from which part of the mushroom chitin-glucan nanofibers were extracted, the films have the same mechanical properties (E = ~5 GPa, σ = ~191 MPa). However, the films prepared from the nanofibers extracted from the mushroom stalk had a higher elongation at break (ε = 9.3%) compared to that prepared from the cap (ε = 7.4%). Both stalk and cap possess nanofibers with the same dimensions (10–20 nm width) but stalk nanofiber seemed to be longer and more oriented than cap nanofibers. Furthermore, the nanofibres extracted from the stalk had also a higher proportion of glucan to chitin compared to cap. We believe that the longer and more oriented nanofiber morphology and in addition to higher glucan to chitin ratio in stalk cause the films prepared from the stalk nanofibers to be tougher than that prepared from cap nanofibers (toughness: stalk film = 10.1 MJ/m^3, cap film = 8.0 MJ/m^3).
5. Films prepared from chitin-glucan nanofibers extracted from mushrooms had a higher water contact angle (θ = 66°) and lower total surface energy (γ^t = 52.5 mJ/m^2) than crustacean-based chitin films (θ = 24°, γ^t = 72.5 mJ/m^2). Thus, mushroom chitin films were more hydrophobic than crustacean chitin film.
6. The lower the grammage the lower were the mechanical properties of mushroom nanofiber films. This can be attributed to fact that the porosity of the films increased with decreasing grammage. The strength of fungal chitin based films with grammages of 2 g/m^2 and 5 g/m^2 were below 100 MPa but it peaked at around 190–200 MPa when the grammage ranged between 40 g/m^2 to 160 g/m^2 . The strength decreased again slightly to 181 MPa for films with a grammage of 240 g/m^2. The modulus, however, increased steadily with increasing film grammage, i.e. thickness from 2 GPa for 2 g/m^2 up to 9.2 GPa for 240 g/m^2.

Glucan Rich Microfibers Extracted from Tree Bracket Fungi

1. Tree bracket fungi, *D. confragosa,* cannot be disintegrated into nanofibers after chemical extraction. Further mechanical disintegration of the extract in a blender for 30 min does not result in further fibrillatation of the microfibers into nanofibers. Nevertheless, the microfibers are uniform in width (1-2 µm in width).

2. Chemically extracted microfibers (DCE) were more swollen and had smoother surfaces than mechanically extracted microfibers (DC), which lead to an increased accessibility of fiber surface functional groups. Films produced from chemically extracted microfibers had a lower porosity (50%) than DC (73%). The removal of impurities from the extracted nanofibers, mostly in the form of hydrophobic waxy materials, resulted in microfiber films with lower water contact angles ($\theta = 54°$) and a higher total surface energy ($\gamma^t = 55.7$ mJ/m^2) compared to DC ($\theta = 77°$, $\gamma^t = 44.5$ mJ/m^2).
3. DCE films had higher mechanical properties (E = 1.2 GPa, σ = 65.3 MPa, ε = 13.3%, toughness = 5.8 MJ/m^3) compared with DC films (E = 0.4 GPa, σ = 1.2 MPa, ε = 12.3%, toughness 1.8 MJ/m^3). The measured tensile strength and modulus was much lower compared to chitin-glucan nanofiber films made from nanofibres extracted from the common mushroom, but bracket fungi films had a much higher elongation at break. Chemical analysis revealed that bracket fungi consisted almost exclusively of glucan with only ~1% chitin being present. When investigating the chitin-glucan nanofibers extracted from common mushroom, we also saw that films prepared from the nanofibers extracted from stalk had a higher glucan to chitin ratio produces higher elongation at break. Thus, we concluded that in fungi, chitin offers strength and rigidity, while glucan offers toughness. This was further tested by preparing composite films using different ratios of common mushroom nanofibers (ABW) and bracket fungi microfibers. The more ABW nanofibers were added into the film, the stronger and stiffer were the composite but at the expanse of a lower toughness, i.e. a reduction in elongation at break.

Mushroom Chitin-Glucan Nanofibers as a Reinforcement for Laminated Composites & as a Binders for the Preparation of Flax Fiber Nonwovens

1. High volume fraction fungal chitin film base laminated composites (ν_f = 88–94%) were prepared by laminating mushroom chitin nanofiber films (ABW film) in presence of a small amount of epoxy resin followed by hot pressing. All laminated composites possess rather similar tensile moduli of about 8 GPa but the tensile strength decreased with increasing number of films being laminated, which was due to 'size effects' (strength: ABW2L = 77.1 MPa, ABW5L = 44.9 MPa, ABW10L = 29.4 MPa ; L represents number of laminates).

2. Mushroom chitin-glucan nanofibers not only found to be a useful binder for loose flax fibers, but can also improves the mechanical properties of resulting non-woven flax fiber preform. The addition of only 5% ABW nanofibers as a binder to flax fibers resulted in both tensile and flexural modulus to increase at least 5 times above the values of neat flax fiber preforms. The binding effect is remains intact even after the preform was soaked in water for 24 h.

7.2 Recommendations

1. **Preparation of long and highly oriented fungal chitin nanofibers**

   In this study we only focused on fungi fruiting bodies (i.e. stalk or cap or the whole fruiting body). For future work, it would be desirable to explore the use of fungal mycelium as raw material for the preparation of chitin nanofibers. It could be anticipated that when growing the mycelium in a capillary tube, it should be possible to produce longer and highly oriented chitin nanofibers, which could be extracted or used potentially directly as fiber. The growth of mycelium can also be regulated by creating a nutrient gradient during the solid state fermentation process. Based on our findings, films produced from chitin-glucan nanofibers extracted from mushroom stalks film possess a higher elongation at break, i.e. greater toughness, than cap chitin films. Thus, we predict that films made from directed growth mycelium will possess an even higher elongation at break. This will consequently improve the toughness of chitin-glucan films even further. The orientation of the nanofibers can be preserved if the extraction process is performed by, for instance, soaking the aligned mycelium in alkaline bath.

2. **Nanofibrillation of tree bracket fungi**

   In the present study it was only possible to extract microfibers from tree bracket fungi (DCE). It would be interesting to investigate whether it is feasible to further improve the mechanical properties of DCE fiber films, if it would be possible to produce DCE nanofibers.

3. **Investigation of chitin-glucan film properties**

   It was shown that mushroom chitin nanofibers, due to presence of glucan, have great film forming behavior. The chitin-glucan film forming ability could be a great asset if coatings should be produced. Investigation on film properties, such as water vapor transmision rate and permeability, or gas permeability is required in order to extend the applicability of mushroom chitin-glucan nanofibers.

4. **Preparation of transparent chitin-based films by adding decoloration step in the extraction process**

   Although the pigment of the common mushroom nanofiber extract was not removed, the resulting films still were quite transparent, albeit brownish in color. If a mild decoloration step would be included, for example by using ethanol, it might be possible to produce fully transparent films, which could prove useful as a substrate for printed electronics or the fabrication of transparent composites.

REFERENCES

1. Braconnot, H., *Sur la nature des champignons.* Annales de Chimie Physique, 1811. **79**: p. 265-304.
2. Rouget, C., *Des substances amylacées dans le tissue des animaux, spécialement les articulés (chitine).* Comptes Rendus de l'Académie des Sciences, 1959. **48**: p. 792-795.
3. Muzzarelli, R.A.A., *Chitin*. 1977: Pergamon Press.
4. Sietsma, J.H. and J.G.H. Wessels, *Evidence for Covalent Linkages between Chitin and β-Glucan in a Fungal Wall.* Journal of General Microbiology, 1979. **114**(Sep): p. 99-108.
5. Paillet, M. and A. Dufresne, *Chitin Whisker Reinforced Thermoplastic Nanocomposites.* Macromolecules, 2001. **34**(19): p. 6527-6530.
6. Payen, A., *Mémoire sur la composition du tissu propre des plantes et du ligneux.* Comptes Rendus Hebdomadaires des Séances de l'Académie des Sciences, 1838. **7**: p. 1052-1056.
7. Brown, A.J., *XIX. -The chemical action of pure cultivations of bacterium aceti.* Journal of the Chemical Society Transactions, 1886. **49**(0): p. 172-187.
8. Wuhrmann, K., A. Heuberger, and K. Mühlethaler, *Elektronenmikroskopische Untersuchungen an Zellulosefasern nach Behandlung mit Ultraschall.* Experientia, 1946. **2**(3): p. 105-107.
9. Gardner, K.H. and J. Blackwell, *Refinement of the Structure of β-Chitin.* Biopolymers, 1975. **14**(8): p. 1581-1595.
10. Minke, R. and J. Blackwell, *The Structure of α-Chitin.* Journal of Molecular Biology, 1978. **120**(2): p. 167-181.
11. Blackwell, J., et al., *Refinement of cellulose and chitin structures.* 1980.
12. Favier, V., et al., *Nanocomposite materials from latex and cellulose whiskers.* Polymers for Advanced Technologies, 1995. **6**(5): p. 351-355.
13. Hon, D.N.S., *Cellulose: a random walk along its historical path.* Cellulose, 1994. **1**(1): p. 1-25.
14. Muzzarelli, R.A.A., et al., *Current views on fungal chitin/chitosan, human chitinases, food preservation, glucans, pectins and inulin: A tribute to Henri Braconnot, precursor of the carbohydrate polymers science, on the chitin bicentennial.* Carbohydrate Polymers, 2012. **87**(2): p. 995-1012.
15. Roberts, G.A.F., *Thirthy Years of Progress in Chitin and Chitosan.* Progress on Chemistry and Application of Chitin, 2008. **13**: p. 7-15.
16. Muzzarelli, R.A.A., *Natural chelating polymers: alginic acid, chitin, and chitosan*. 1973: Pergamon Press.
17. Yamanaka, S., et al., *The structure and mechanical properties of sheets prepared from bacterial cellulose.* Journal of Materials Science, 1989. **24**(9): p. 3141-3145.
18. Henriksson, M., et al., *Cellulose nanopaper structures of high toughness.* Biomacromolecules, 2008. **9**(6): p. 1579-1585.
19. Sehaqui, H., et al., *Cellulose nanofiber orientation in nanopaper and nanocomposites by cold drawing.* ACS Appl Mater Interfaces, 2012. **4**(2): p. 1043-9.
20. Takai, M., et al., *Structure property relationship of alpha-chitin and beta-chitin.* Acs Symposium Series, 1992. **489**: p. 38-52.
21. Ifuku, S., et al., *Preparation of Chitin Nanofibers with a Uniform Width as alpha-Chitin from Crab Shells.* Biomacromolecules, 2009. **10**(6): p. 1584-1588.
22. Ifuku, S., et al., *Fibrillation of dried chitin into 10–20nm nanofibers by a simple grinding method under acidic conditions.* Carbohydrate Polymers, 2010. **81**(1): p. 134-139.
23. Ifuku, S., et al., *Method for producing chitin nanofibers, composite material and coating composition each containing chitin nanofibers, and method for producing chitosan nanofibers, composite material and coating composition each containing chitosan nanofibers.* U.S. Patent 8,940,881 B2, January 27, 2015.

24. Ifuku, S. and H. Saimoto, *Chitin nanofibers: preparations, modifications, and applications.* Nanoscale, 2012. **4**(11): p. 3308-18.
25. Ifuku, S., et al., *Preparation and characterization of optically transparent chitin nanofiber/(meth)acrylic resin composites.* Green Chemistry, 2011. **13**(7): p. 1708.
26. Mushi, N.E., et al., *Nanostructured membranes based on native chitin nanofibers prepared by mild process.* Carbohydrate Polymers, 2014. **112**: p. 255-263.
27. Turbak, A.F., F.W. Snyder, and K.R. Sandberg, *Microfibrillated cellulose.* U.S. Patent 4,374,702, February 22, 1983.
28. Helbert, W., J.Y. Cavaillé, and A. Dufresne, *Thermoplastic nanocomposites filled with wheat straw cellulose whiskers. Part I: Processing and mechanical behavior.* Polymer Composites, 1996. **17**(4): p. 604-611.
29. Dufresne, A., J.-Y. Cavaillé, and W. Helbert, *Thermoplastic nanocomposites filled with wheat straw cellulose whiskers. Part II: Effect of processing and modeling.* Polymer Composites, 1997. **18**(2): p. 198-210.
30. Dufresne, A. and M.R. Vignon, *Improvement of Starch Film Performances Using Cellulose Microfibrils.* Macromolecules, 1998. **31**(8): p. 2693-2696.
31. Dufresne, A., D. Dupeyre, and M.R. Vignon, *Cellulose microfibrils from potato tuber cells: Processing and characterization of starch–cellulose microfibril composites.* Journal of Applied Polymer Science, 2000. **76**(14): p. 2080-2092.
32. Morin, A. and A. Dufresne, *Nanocomposites of Chitin Whiskers from Riftia Tubes and Poly(caprolactone).* Macromolecules, 2002. **35**(6): p. 2190-2199.
33. Nair, K.G. and A. Dufresne, *Crab shell chitin whisker reinforced natural rubber nanocomposites. 1. Processing and swelling behavior.* Biomacromolecules, 2003. **4**(3): p. 657-665.
34. Nair, K.G. and A. Dufresne, *Crab shell chitin whisker reinforced natural rubber nanocomposites. 2. Mechanical behavior.* Biomacromolecules, 2003. **4**(3): p. 666-674.
35. Nair, K.G., et al., *Crab shell chitin whiskers reinforced natural rubber nanocomposites. 3. Effect of chemical modification of chitin whiskers.* Biomacromolecules, 2003. **4**(6): p. 1835-1842.
36. Matos Ruiz, M., et al., *Processing and characterization of new thermoset nanocomposites based on cellulose whiskers.* Composite Interfaces, 2000. **7**(2): p. 117-131.
37. Nakagaito, A.N. and H. Yano, *Novel high-strength biocomposites based on microfibrillated cellulose having nano-order-unit web-like network structure.* Applied Physics A-Materials Science & Processing, 2005. **80**(1): p. 155-159.
38. Nakagaito, A.N., S. Iwamoto, and H. Yano, *Bacterial cellulose: the ultimate nano-scalar cellulose morphology for the production of high-strength composites.* Applied Physics a-Materials Science & Processing, 2005. **80**(1): p. 93-97.
39. Yano, H. and S. Nakahara, *High strength material using cellulose microfibrils.* U.S. Patent 7,378,149 B2, May 27, 2008.
40. Shao, X., et al., *Chitin nanofibers/epoxy resin optically transparent nanocomposite films*, in *Advanced Materials Research*. 2013. p. 1479-1483.
41. Shibata, M., et al., *Bio-based epoxy/chitin nanofiber composites cured with amine-type hardeners containing chitosan.* Carbohydrate Polymers, 2016. **144**: p. 89-97.
42. Dufresne, A., *Nanocellulose: From Nature to High Performance Tailored Materials*. 2012: De Gruyter.
43. Eichhorn, S.J., et al., *Review: current international research into cellulose nanofibres and nanocomposites.* Journal of Materials Science, 2010. **45**(1): p. 1-33.
44. Klemm, D., et al., *Nanocelluloses: a new family of nature-based materials.* Angew Chem Int Ed Engl, 2011. **50**(24): p. 5438-66.
45. Isogai, A., *Wood nanocelluloses: Fundamentals and applications as new bio-based nanomaterials.* Journal of Wood Science, 2013. **59**(6): p. 449-459.
46. Lee, K.Y., et al., *More than meets the eye in bacterial cellulose: biosynthesis, bioprocessing, and applications in advanced fiber composites.* Macromol Biosci, 2014. **14**(1): p. 10-32.

47. Lee, K.-Y., et al., *On the use of nanocellulose as reinforcement in polymer matrix composites.* Composites Science and Technology, 2014. **105**: p. 15-27.
48. Oksman, K., et al., *Review of the recent developments in cellulose nanocomposite processing.* Composites Part A: Applied Science and Manufacturing, 2016. **83**: p. 2-18.
49. Raafat, D. and H.G. Sahl, *Chitosan and its antimicrobial potential - A critical literature survey.* Microbial Biotechnology, 2009. **2**(2 SPEC. ISS.): p. 186-201.
50. Foster, L.J.R. and J. Butt, *Chitosan films are NOT antimicrobial.* Biotechnology Letters, 2011. **33**(2): p. 417-421.
51. Guibal, E., *Interactions of metal ions with chitosan-based sorbents: a review.* Separation and Purification Technology, 2004. **38**(1): p. 43-74.
52. Crini, G. and P.M. Badot, *Application of chitosan, a natural aminopolysaccharide, for dye removal from aqueous solutions by adsorption processes using batch studies: A review of recent literature.* Progress in Polymer Science (Oxford), 2008. **33**(4): p. 399-447.
53. Wan Ngah, W.S., L.C. Teong, and M.A.K.M. Hanafiah, *Adsorption of dyes and heavy metal ions by chitosan composites: A review.* Carbohydrate Polymers, 2011. **83**(4): p. 1446-1456.
54. Kurita, K., *Controlled functionalization of the polysaccharide chitin.* Progress in Polymer Science, 2001. **26**(9): p. 1921-1971.
55. Blackwell, J., *Physical methods for the determination of chitin structure and conformation.* Methods in Enzymology, 1988. **161**: p. 435-442.
56. Raabe, D., et al., *Microstructure and crystallographic texture of the chitin–protein network in the biological composite material of the exoskeleton of the lobster Homarus americanus.* Materials Science and Engineering: A, 2006. **421**(1-2): p. 143-153.
57. Ifuku, S., et al., *Simple preparation method of chitin nanofibers with a uniform width of 10–20nm from prawn shell under neutral conditions.* Carbohydrate Polymers, 2011. **84**(2): p. 762-764.
58. Wang, Y., et al., *Crystalline structure and thermal property characterization of chitin from Antarctic krill (Euphausia superba).* Carbohydrate Polymers, 2013. **92**(1): p. 90-97.
59. Vincent, J.F.V. and U.G.K. Wegst, *Design and mechanical properties of insect cuticle.* Arthropod Structure & Development, 2004. **33**(3): p. 187-199.
60. Ifuku, S., et al., *Preparation of Chitin Nanofibers from Mushrooms.* Materials, 2011. **4**(12): p. 1417-1425.
61. Cabib, E. and J. Arroyo, *How carbohydrates sculpt cells: chemical control of morphogenesis in the yeast cell wall.* Nat Rev Microbiol, 2013. **11**(9): p. 648-55.
62. Beauvais, A., et al., *Aspergillus Cell Wall and Biofilm.* Mycopathologia, 2014.
63. Ogawa, Y., et al., *Crystal analysis and high-resolution imaging of microfibrillar α-chitin from Phaeocystis.* Journal of Structural Biology, 2010. **171**(1): p. 111-116.
64. Atkins, E.D.T., J. Dlugosz, and S. Foord, *Electron diffraction and electron microscopy of crystalline α-chitin from the grasping spines of the marine worm Sagitta.* International Journal of Biological Macromolecules, 1979. **1**(1): p. 29-32.
65. Kurita, K., et al., *Squid chitin as a potential alternative chitin source. Deacetylation behavior and characteristic properties.* Journal of Polymer Science, Part A: Polymer Chemistry, 1993. **31**(2): p. 485-491.
66. Ogawa, Y., et al., *X-ray texture analysis indicates downward spinning of chitin microfibrils in tubeworm tube.* Journal of Structural Biology, 2013. **184**(2): p. 212-216.
67. Ogawa, Y., S. Kimura, and M. Wada, *Electron diffraction and high-resolution imaging on highly-crystalline β-chitin microfibril.* Journal of Structural Biology, 2011. **176**(1): p. 83-90.
68. Sikorski, P., R. Hori, and M. Wada, *Revisit of alpha-Chitin Crystal Structure Using High Resolution X-ray Diffraction Data.* Biomacromolecules, 2009. **10**(5): p. 1100-1105.
69. Nishiyama, Y., Y. Noishiki, and M. Wada, *X-ray structure of anhydrous β-chitin at 1 Å resolution.* Macromolecules, 2011. **44**(4): p. 950-957.
70. Noishiki, Y., et al., *Alkali-induced conversion of beta-chitin to alpha-chitin.* Biomacromolecules, 2003. **4**(4): p. 896-899.

71. Saito, Y., et al., *Structural aspects of the swelling of beta chitin in HCl and its conversion into alpha chitin.* Macromolecules, 1997. **30**(13): p. 3867-3873.
72. Wada, M. and Y. Saito, *Lateral thermal expansion of chitin crystals.* Journal of Polymer Science, Part B: Polymer Physics, 2001. **39**(1): p. 168-174.
73. Nogi, M., et al., *Preparation of nanofibrillar carbon from chitin nanofibers.* Carbohydrate Polymers, 2010. **81**(4): p. 919-924.
74. Ogawa, Y., et al., *Elastic modulus in the crystalline region and the thermal expansion coefficients of α-chitin determined using synchrotron radiated X-ray diffraction.* Carbohydrate Polymers, 2011. **83**(3): p. 1213-1217.
75. Djahedi, C., L.A. Berglund, and J. Wohlert, *Molecular deformation mechanisms in cellulose allomorphs and the role of hydrogen bonds.* Carbohydrate Polymers, 2015. **130**: p. 175-182.
76. Rudall, K.M., *The Chitin/Protein Complexes of Insect Cuticles*, in *Advances in Insect Physiology.* 1963. p. 257-313.
77. Kobayashi, K., et al., *Crystal transition between hydrate and anhydrous β-chitin monitored by synchrotron X-ray fiber diffraction.* Carbohydrate Polymers, 2010. **79**(4): p. 882-889.
78. Rinaudo, M., *Chitin and chitosan: Properties and applications.* Progress in Polymer Science, 2006. **31**(7): p. 603-632.
79. Atkinson, A., et al., *A re-appraisal of the total biomass and annual production of Antarctic krill.* Deep Sea Research Part I: Oceanographic Research Papers, 2009. **56**(5): p. 727-740.
80. Jeuniaux, C. and M.F. Voss-Foucart, *Chitin biomass and production in the marine environment.* Biochemical Systematics and Ecology, 1991. **19**(5): p. 347-356.
81. Charoenvuttitham, P., J. Shi, and G.S. Mittal, *Chitin Extraction from Black Tiger Shrimp (Penaeus monodon) Waste using Organic Acids.* Separation Science and Technology, 2006. **41**(6): p. 1135-1153.
82. Kurita, K., *Chitin and chitosan: functional biopolymers from marine crustaceans.* Mar Biotechnol (NY), 2006. **8**(3): p. 203-26.
83. Muzzarelli, R.A.A., *Chitin Nanostructures in Living Organisms*, in *Chitin*, N.S. Gupta, Editor. 2011, Springer Netherlands. p. 1-34.
84. Vetter, J., *Chitin content of cultivated mushrooms Agaricus bisporus, Pleurotus ostreatus and Lentinula edodes.* Food Chemistry, 2007. **102**(1): p. 6-9.
85. Di Mario, F., et al., *Chitin and chitosan from Basidiomycetes.* Int J Biol Macromol, 2008. **43**(1): p. 8-12.
86. Wu, T., et al., *Chitin and chitosan - Value-added products from mushroom waste.* Journal of Agricultural and Food Chemistry, 2004. **52**(26): p. 7905-7910.
87. Novaes-Ledieu, M. and C.G. Mendoza, *The cell walls of Agaricus bisporus and Agaricus campestris fruiting body hyphae.* Canadian Journal of Microbiology, 1981. **27**(8): p. 779-787.
88. Mol, P.C. and J.G.H. Wessels, *Differences in wall structure between substrate hyphae and hyphae of fruit-body stipes in Agaricus bisporus.* Mycological Research, 1990. **94**(4): p. 472-479.
89. Shida, M., et al., *Structure of the alkali-insoluble skeletal glucan of Lentinus edodes.* Journal of Biochemistry, 1981. **90**(4): p. 1093-1100.
90. Synytsya, A., et al., *Glucans from fruit bodies of cultivated mushrooms Pleurotus ostreatus and Pleurotus eryngii: Structure and potential prebiotic activity.* Carbohydrate Polymers, 2009. **76**(4): p. 548-556.
91. Sietsma, J.H. and J.G.H. Wessels, *Chemical analysis of the hyphal wall of Schizophyllum commune.* Biochimica Et Biophysica Acta, 1977. **496**(1): p. 225-239.
92. Wu, T., et al., *Physicochemical properties and bioactivity of fungal chitin and chitosan.* Journal of Agricultural and Food Chemistry, 2005. **53**(10): p. 3888-3894.
93. Teng, W.L., et al., *Concurrent production of chitin from shrimp shells and fungi.* Carbohydrate Research, 2001. **332**(3): p. 305-316.
94. Cabib, E., et al., *The Yeast Cell Wall and Septum as Paradigms of Cell Growth and Morphogenesis.* Journal of Biological Chemistry, 2001. **276**(23): p. 19679-19682.

95. Nguyen, T.H., G.H. Fleet, and P.L. Rogers, *Composition of the cell walls of several yeast species.* Applied Microbiology and Biotechnology, 1998. **50**(2): p. 206-212.
96. Bartnicki-Garcia, S. and W.J. Nickerson, *Isolation, composition, and structure of cell walls of filamentous and yeast-like forms of Mucor rouxii.* Biochimica et Biophysica Acta, 1962. **58**(1): p. 102-119.
97. Zhang, X., W. Yang, and W. Blasiak, *Modeling study of woody biomass: Interactions of cellulose, hemicellulose, and lignin.* Energy and Fuels, 2011. **25**(10): p. 4786-4795.
98. Falk, M., et al., *Studies of chitan (β-(1→4)-linked 2-acetamido-2-deoxy-D-glucan) fibers of the diatom Thalassiosira fluviatilis Hustedt: II. Proton magnetic resonance, infrared, and X-ray studies.* Canadian Journal of Chemistry, 1966. **44**(19): p. 2269-2281.
99. Hackman, R.H., *Studies on Chitin IV. The Occurrence of Complexes in Which Chitin and Protein are Covalently Linked.* Australian Journal of Biological Sciences, 1960. **13**(4): p. 568-577.
100. Attwood, M.M. and H. Zola, *The association between chitin and protein in some chitinous tissues.* Comparative Biochemistry and Physiology, 1967. **20**(3): p. 993-998.
101. Kramer, K.J., T.L. Hopkins, and J. Schaefer, *Applications of solids NMR to the analysis of insect sclerotized structures.* Insect Biochemistry and Molecular Biology, 1995. **25**(10): p. 1067-1080.
102. Percot, A., C. Viton, and A. Domard, *Characterization of shrimp shell deproteinization.* Biomacromolecules, 2003. **4**(5): p. 1380-1385.
103. Kollar, R., et al., *Architecture of the yeast cell wall - beta(1->6)-glucan interconnects mannoprotein, beta(1-3)-glucan, and chitin.* Journal of Biological Chemistry, 1997. **272**(28): p. 17762-17775.
104. Hartland, R.P., et al., *The Linkage of (1-3)-B-Glucan to Chitin During Cell Wall Assembly in Saccharomyces cerevisiae.* Yeast, 1994. **10**(12): p. 1591-1599.
105. Heux, L., et al., *Solid state NMR for determination of degree of acetylation of chitin and chitosan.* Biomacromolecules, 2000. **1**(4): p. 746-751.
106. Sietsma, J.H. and J.G.H. Wessels, *Solubility of (1-3)-β-D/(1-6)-β-D-Glucan in Fungal Walls: Importance of Presumed Linkage between Glucan and Chitin.* Journal of General Microbiology, 1981. **125**(JUL): p. 209-212.
107. Surarit, R., P.K. Gopal, and M.G. Shepherd, *Evidence for a Glycosidic Linkage between Chitin and Glucan in the Cell Wall od Candida albicans.* Journal of General Microbiology, 1988. **134**: p. 1723-1730.
108. Fontaine, T., et al., *Molecular organization of the alkali-insoluble fraction of Aspergillus fumigatus cell wall.* Journal of Biological Chemistry, 2000. **275**(36): p. 27594-27607.
109. Stalhberger, T., et al., *Chemical organization of the cell wall polysaccharide core of Malassezia restricta.* J Biol Chem, 2014. **289**(18): p. 12647-56.
110. Synytsya, A. and M. Novak, *Structural diversity of fungal glucans.* Carbohydr Polym, 2013. **92**(1): p. 792-809.
111. Goodridge, H.S., A.J. Wolf, and D.M. Underhill, *β-glucan recognition by the innate immune system.* Immunological Reviews, 2009. **230**(1): p. 38-50.
112. Wasser, S.P., *Medicinal mushroom science: Current perspectives, advances, evidences, and challenges.* Biomedical Journal, 2014. **37**(6): p. 345-356.
113. Zhu, F., et al., *β-Glucans from edible and medicinal mushrooms: Characteristics, physicochemical and biological activities.* Journal of Food Composition and Analysis, 2015. **41**: p. 165-173.
114. Ruthes, A.C., F.R. Smiderle, and M. Iacomini, *Mushroom heteropolysaccharides: A review on their sources, structure and biological effects.* Carbohydrate Polymers, 2016. **136**: p. 358-375.
115. Roberson, R.W. and M.S. Fuller, *Ultrastructural Aspects of the Hyphal Tip of Sclerotium rolfsii Preserved by Freeze Substitution.* Protoplasma, 1988. **146**(2-3): p. 143-149.
116. Latge, J.P., *The cell wall: a carbohydrate armour for the fungal cell.* Mol Microbiol, 2007. **66**(2): p. 279-90.

117. Karimi, K. and A. Zamani, *Mucor indicus: Biology and industrial application perspectives: A review.* Biotechnology Advances, 2013. **31**(4): p. 466-481.
118. Kollar, R., et al., *Architecture of the Yeast Cell Wall: The Linkage between Chitin and B(1-3)-Glucan.* Journal of Biological Chemistry, 1995. **270**(3): p. 1170-1178.
119. Shimahara, K. and Y. Takiguchi, *Preparation of Crustacean Chitin.* Methods in Enzymology, 1988. **161**: p. 417-423.
120. Versali, M.F., et al., *Cell wall derivatives from biomass and preparation thereof.* U.S. Patent 7,556,946 B2, July 7, 2009.
121. Shively, J.E. and H.E. Conrad, *Stoichiometry of the Nitrous Acid Deaminative Cleavage of Model Amino Sugar Glycosides and Glycosaminoglycuronans.* Biochemistry, 1970. **9**(1): p. 33-&.
122. Hackman, R.H., *Studies on Chitin V. The Action of Mineral Acids on Chitin.* Australian Journal of Biological Sciences, 1962. **15**(3): p. 526-537.
123. Percot, A., C. Viton, and A. Domard, *Optimization of chitin extraction from shrimp shells.* Biomacromolecules, 2003. **4**(1): p. 12-18.
124. Foster, A.B. and R.H. Hackman, *Application of ethylenediaminetetra-acetic acid in the isolation of crustacean chitin.* Nature, 1957. **180**(4575): p. 40-1.
125. Sannan, T., K. Kurita, and Y. Iwakura, *Studies on chitin, 2. Effect of deacetylation on solubility.* Die Makromolekulare Chemie, 1976. **177**(12): p. 3589-3600.
126. Tomihata, K. and Y. Ikada, *In vitro and in vivo degradation of films of chitin and its deacetylated derivatives.* Biomaterials, 1997. **18**(7): p. 567-575.
127. Li, J., J.F. Revol, and R.H. Marchessault, *Effect of degree of deacetylation of chitin on the properties of chitin crystallites.* Journal of Applied Polymer Science, 1997. **65**(2): p. 373-380.
128. Chatelet, C., O. Damour, and A. Domard, *Influence of the degree of acetylation on some biological properties of chitosan films.* Biomaterials, 2001. **22**(3): p. 261-268.
129. Younes, I., et al., *Chitin and chitosan preparation from shrimp shells using optimized enzymatic deproteinization.* Process Biochemistry, 2012. **47**(12): p. 2032-2039.
130. Ifuku, S., et al., *Preparation of a protein-chitin nanofiber complex from crab shells and its application as a reinforcement filler or substrate for biomineralization.* RSC Advances, 2015. **5**(79): p. 64196-64201.
131. Arbia, W., et al., *Chitin extraction from crustacean shells using biological methods -A review.* Food Technology and Biotechnology, 2013. **51**(1): p. 12-25.
132. Jung, W.J., et al., *Production of chitin from red crab shell waste by successive fermentation with Lactobacillus paracasei KCTC-3074 and Serratia marcescens FS-3.* Carbohydrate Polymers, 2007. **68**(4): p. 746-750.
133. Pacheco, N., et al., *Structural characterization of chitin and chitosan obtained by biological and chemical methods.* Biomacromolecules, 2011. **12**(9): p. 3285-90.
134. Sannan, T., K. Kurita, and Y. Iwakura, *Studies on chitin, 1. Solubility change by alkaline treatment and film casting.* Die Makromolekulare Chemie, 1975. **176**(4): p. 1191-1195.
135. Kurita, K., T. Sannan, and Y. Iwakura, *Studies on chitin, 4. Evidence for formation of block and random copolymers of N-acetyl-D-glucosamine and D-glucosamine by hetero- and homogeneous hydrolyses.* Die Makromolekulare Chemie, 1977. **178**(12): p. 3197-3202.
136. Muzzarelli, R.A.A., *Carboxymethylated chitins and chitosans.* Carbohydrate Polymers, 1988. **8**(1): p. 1-21.
137. Zeng, J.B., et al., *Chitin whiskers: an overview.* Biomacromolecules, 2012. **13**(1): p. 1-11.
138. Kaya, M., et al., *Physicochemical Properties of Chitin and Chitosan Produced from Medicinal Fungus (Fomitopsis pinicola).* Food Biophysics, 2014: p. 1-7.
139. Chen, C., et al., *Optically transparent biocomposites: Polymethylmethacrylate reinforced with high performance chitin nanofibers.* Bioresources, 2012. **7**(4): p. 5960-5971.
140. Ezekiel Mushi, N., et al., *Nanopaper membranes from chitin-protein composite nanofibers-structure and mechanical properties.* Journal of Applied Polymer Science, 2014. **131**(7): p. n/a-n/a.

141. Wijesena, R.N., et al., *A method for top down preparation of chitosan nanoparticles and nanofibers.* Carbohydr Polym, 2015. **117**: p. 731-8.
142. Ifuku, S., et al., *Preparation of high-strength transparent chitosan film reinforced with surface-deacetylated chitin nanofibers.* Carbohydr Polym, 2013. **98**(1): p. 1198-202.
143. Ifuku, S., et al., *Control of mechanical properties of chitin nanofiber film using glycerol without losing its characteristics.* Carbohydr Polym, 2014. **101**: p. 714-7.
144. Ifuku, S., et al., *Nanofibrillation of Dry Chitin Powder by Star Burst System.* Journal of Nanomaterials, 2012. **2012**: p. 1-7.
145. Shams, M.I., et al., *Fabrication of optically transparent chitin nanocomposites.* Applied Physics A, 2011. **102**(2): p. 325-331.
146. Shams, M.I. and H. Yano, *Simplified Fabrication of Optically Transparent Composites Reinforced with Nanostructured Chitin.* Journal of Polymers and the Environment, 2013. **21**(4): p. 937-943.
147. Lu, Y., et al., *Fabrication and characterisation of α-chitin nanofibers and highly transparent chitin films by pulsed ultrasonication.* Carbohydrate Polymers, 2013. **98**(2): p. 1497-1504.
148. Barber, P.S., et al., *Electrospinning of chitin nanofibers directly from an ionic liquid extract of shrimp shells.* Green Chemistry, 2013. **15**(3): p. 601.
149. Biswas, S., et al., *Flexible and transparent chitin/acrylic nanocomposite films with high mechanical strength.* Fibers and Polymers, 2015. **16**(4): p. 774-781.
150. Abe, K., et al., *Preparation of tough hydrogels based on β-chitin nanofibers via NaOH treatment.* Cellulose, 2013. **21**(1): p. 535-540.
151. Fan, Y., T. Saito, and A. Isogai, *Preparation of chitin nanofibers from squid pen beta-chitin by simple mechanical treatment under acid conditions.* Biomacromolecules, 2008. **9**(7): p. 1919-1923.
152. Zhong, C., et al., *A facile bottom-up route to self-assembled biogenic chitin nanofibers.* Soft Matter, 2010. **6**(21): p. 5298-5301.
153. Zhong, C., et al., *A Chitin Nanofiber Ink for Airbrushing, Replica Molding, and Microcontact Printing of Self-assembled Macro-, Micro-, and Nanostructures.* Advanced Materials, 2011. **23**(41): p. 4776-4781.
154. Salaberria, A.M., et al., *Processing of α-chitin nanofibers by dynamic high pressure homogenization: Characterization and antifungal activity against A. niger.* Carbohydrate Polymers, 2015. **116**: p. 286-291.
155. Zhao, H.P., X.Q. Feng, and H. Gao, *Ultrasonic technique for extracting nanofibers from nature materials.* Applied Physics Letters, 2007. **90**(7).
156. Chakraborty, A., M. Sain, and M. Kortschot, *Cellulose microfibrils: A novel method of preparation using high shear refining and cryocrushing.* Holzforschung, 2005. **59**(1): p. 102-107.
157. Bragd, P.L., H. van Bekkum, and A.C. Besemer, *TEMPO-mediated oxidation of polysaccharides: survey of methods and applications.* Topics in Catalysis, 2004. **27**(1-4): p. 49-66.
158. Isogai, A., T. Saito, and H. Fukuzumi, *TEMPO-oxidized cellulose nanofibers.* Nanoscale, 2011. **3**(1): p. 71-85.
159. Saito, T., et al., *Homogeneous suspensions of individualized microfibrils from TEMPO-catalyzed oxidation of native cellulose.* Biomacromolecules, 2006. **7**(6): p. 1687-1691.
160. Saito, T. and A. Isogai, *TEMPO-mediated oxidation of native cellulose. The effect of oxidation conditions on chemical and crystal structures of the water-insoluble fractions.* Biomacromolecules, 2004. **5**(5): p. 1983-1989.
161. Muzzarelli, R.A.A., et al., *6-Oxychitins, novel hyaluronan-like regiospecifically carboxylated chitins.* Carbohydrate Polymers, 1999. **39**(4): p. 361-367.
162. Kato, Y., et al., *TEMPO-mediated oxidation of chitin, regenerated chitin and N-acetylated chitosan.* Carbohydrate Polymers, 2004. **58**(4): p. 421-426.
163. Fan, Y., T. Saito, and A. Isogai, *TEMPO-mediated oxidation of β-chitin to prepare individual nanofibrils.* Carbohydrate Polymers, 2009. **77**(4): p. 832-838.

164. Fan, Y., T. Saito, and A. Isogai, *Chitin nanocrystals prepared by TEMPO-mediated oxidation of alpha-chitin.* Biomacromolecules, 2008. **9**(1): p. 192-198.
165. Fan, Y., T. Saito, and A. Isogai, *Individual chitin nano-whiskers prepared from partially deacetylated α-chitin by fibril surface cationization.* Carbohydrate Polymers, 2010. **79**(4): p. 1046-1051.
166. Uddin, A.J., et al., *Outstanding reinforcing effect of highly oriented chitin whiskers in PVA nanocomposites.* Carbohydrate Polymers, 2012. **87**(1): p. 799-805.
167. Ma, B., et al., *Structure and properties of chitin whisker reinforced chitosan membranes.* Int J Biol Macromol, 2014. **64**: p. 341-6.
168. Ifuku, S., et al., *Preparation of zwitterionically charged nanocrystals by surface TEMPO-mediated oxidation and partial deacetylation of α-chitin.* Carbohydrate Polymers, 2015. **122**: p. 1-4.
169. Zhang, C., et al., *Chitin nanowhisker-supported sulfonated poly(ether sulfone) proton exchange for fuel cell applications.* Carbohydrate Polymers, 2016. **140**: p. 195-201.
170. Kadokawa, J.-i., et al., *Preparation of chitin nanowhiskers using an ionic liquid and their composite materials with poly(vinyl alcohol).* Carbohydrate Polymers, 2011. **84**(4): p. 1408-1412.
171. Sriupayo, J., et al., *Preparation and characterization of α-chitin whisker-reinforced poly(vinyl alcohol) nanocomposite films with or without heat treatment.* Polymer, 2005. **46**(15): p. 5637-5644.
172. Junkasem, J., R. Rujiravanit, and P. Supaphol, *Fabrication of α-chitin whisker-reinforced poly(vinyl alcohol) nanocomposite nanofibres by electrospinning.* Nanotechnology, 2006. **17**(17): p. 4519-4528.
173. Goodrich, J.D. and W.T. Winter, *alpha-Chitin nanocrystals prepared from shrimp shells and their specific surface area measurement.* Biomacromolecules, 2007. **8**(1): p. 252-257.
174. Revol, J.F. and R.H. Marchessault, *In vitro chiral nematic ordering of chitin crystallites.* International Journal of Biological Macromolecules, 1993. **15**(6): p. 329-335.
175. Marchessault, R.H., F.F. Morehead, and N.M. Walter, *Liquid Crystal Systems from Fibrillar Polysaccharides.* Nature, 1959. **184**(4686): p. 632-633.
176. Roman, M. and W.T. Winter, *Effect of Sulfate Groups from Sulfuric Acid Hydrolysis on the Thermal Degradation Behavior of Bacterial Cellulose.* Biomacromolecules, 2004. **5**(5): p. 1671-1677.
177. Dong, X.M., J.F. Revol, and D.G. Gray, *Effect of microcrystallite preparation conditions on the formation of colloid crystals of cellulose.* Cellulose, 1998. **5**(1): p. 19-32.
178. Fan, Y., et al., *Comparative characterization of aqueous dispersions and cast films of different chitin nanowhiskers/nanofibers.* Int J Biol Macromol, 2012. **50**(1): p. 69-76.
179. Kataoka, S. and T. Ando, *Regenerated Chitin Film from the Solution of Trichloroacetic Acid Systems.* Kobunshi Ronbunshu, 1979. **36**(3): p. 175-181.
180. Hassanzadeh, P., et al., *Mechanical properties of self-assembled chitin nanofiber networks.* Journal of Materials Chemistry B, 2014. **2**(17): p. 2461.
181. Jin, J., et al., *Chitin Nanofiber Transparent Paper for Flexible Green Electronics.* Advanced Materials, 2016: p. n/a-n/a.
182. Joffe, I. and H.R. Hepburn, *Observations on regenerated chitin films.* Journal of Materials Science, 1973. **8**(12): p. 1751-1754.
183. Duan, B., et al., *High strength films with gas-barrier fabricated from chitin solution dissolved at low temperature.* Journal of Materials Chemistry A, 2013. **1**(5): p. 1867.
184. Yusof, N.L., L.Y. Lim, and E. Khor, *Flexible chitin films: structural studies.* Carbohydr Res, 2004. **339**(16): p. 2701-11.
185. Saïd Azizi Samir, M.A., et al., *Tangling Effect in Fibrillated Cellulose Reinforced Nanocomposites.* Macromolecules, 2004. **37**(11): p. 4313-4316.

186. Salaberria, A.M., J. Labidi, and S.C.M. Fernandes, *Chitin nanocrystals and nanofibers as nano-sized fillers into thermoplastic starch-based biocomposites processed by melt-mixing.* Chemical Engineering Journal, 2014. **256**: p. 356-364.
187. Lu, Y., L. Weng, and L. Zhang, *Morphology and properties of soy protein isolate thermoplastics reinforced with chitin whiskers.* Biomacromolecules, 2004. **5**(3): p. 1046-1051.
188. Zhang, Q., et al., *Effect of surface acetylated-chitin nanocrystals on structure and mechanical properties of poly(lactic acid).* Journal of Applied Polymer Science, 2014. **131**(2): p. n/a-n/a.
189. Rizvi, R., et al., *Fabrication and characterization of melt-blended polylactide-chitin composites and their foams.* Journal of Cellular Plastics, 2011. **47**(3): p. 283-300.
190. Uddin, A.J., et al., *Interfacial interaction and mechanical properties of chitin whisker-poly(vinyl alcohol) gel-spun nanocomposite fibers.* Polymer International, 2012. **61**(6): p. 1010-1015.
191. Huang, J., et al., *New waterborne polyurethane-based nanocomposites reinforced with low loading levels of chitin whisker.* Express Polymer Letters, 2011. **5**(4): p. 362-373.
192. Qin, A., et al., *Preparation and characterization of nano-chitin whisker reinforced PVDF membrane with excellent antifouling property.* Journal of Membrane Science, 2015. **480**: p. 1-10.
193. Mathew, A.P., M.-P.G. Laborie, and K. Oksman, *Cross-Linked Chitosan/Chitin Crystal Nanocomposites with Improved Permeation Selectivity and pH Stability.* Biomacromolecules, 2009. **10**(6): p. 1627-1632.
194. Rubentheren, V., et al., *Processing and analysis of chitosan nanocomposites reinforced with chitin whiskers and tannic acid as a crosslinker.* Carbohydrate Polymers, 2015. **115**: p. 379-387.
195. Araki, J., Y. Yamanaka, and K. Ohkawa, *Chitin-chitosan nanocomposite gels: reinforcement of chitosan hydrogels with rod-like chitin nanowhiskers.* Polymer Journal, 2012. **44**(7): p. 713-717.
196. Ma, B., et al., *Bioinspired design and chitin whisker reinforced chitosan membrane.* Materials Letters, 2014. **120**: p. 82-85.
197. Villares, A., et al., *Chitin nanocrystal-xyloglucan multilayer thin films.* Biomacromolecules, 2014. **15**(1): p. 188-94.
198. Qin, Y., et al., *Effects of chitin nano-whiskers on the antibacterial and physicochemical properties of maize starch films.* Carbohydrate Polymers, 2016. **147**: p. 372-378.
199. Naseri, N., A.P. Mathew, and K. Oksman, *Electrospinnability of bionanocomposites with high nanocrystal loadings: The effect of nanocrystal surface characteristics.* Carbohydrate Polymers, 2016. **147**: p. 464-472.
200. Hariraksapitak, P. and P. Supaphol, *Preparation and properties of α-chitin-whisker-reinforced hyaluronan-gelatin nanocomposite scaffolds.* Journal of Applied Polymer Science, 2010: p. n/a-n/a.
201. Wu, J., H. Lin, and J.C. Meredith, *Poly(ethylene oxide) bionanocomposites reinforced with chitin nanofiber networks.* Polymer, 2016. **84**: p. 267-274.
202. Chen, C., et al., *Properties of polymethyl methacrylate-based nanocomposites: Reinforced with ultra-long chitin nanofiber extracted from crab shells.* Materials & Design, 2014. **56**: p. 1049-1056.
203. Ifuku, S., et al., *Preparation of polysilsesquioxane-urethaneacrylate copolymer film reinforced with chitin nanofibers.* Carbohydr Polym, 2012. **89**(3): p. 865-9.
204. Shankar, S., et al., *Preparation, characterization, and antimicrobial activity of chitin nanofibrils reinforced carrageenan nanocomposite films.* Carbohydrate Polymers, 2015. **117**: p. 468-475.
205. Shams, M.I. and H. Yano, *Doubly curved nanofiber-reinforced optically transparent composites.* Scientific Reports, 2015. **5**.
206. Anraku, M., et al., *Surface-deacetylated chitin nano-fiber/hyaluronic acid composites as potential antioxidative compounds for use in extended-release matrix tablets.* International Journal of Molecular Sciences, 2015. **16**(10): p. 24707-24717.
207. Kadokawa, J.-i., T. Setoguchi, and K. Yamamoto, *Preparation of highly flexible chitin nanofiber-graft-poly(γ-l-glutamic acid) network film.* Polymer Bulletin, 2013. **70**(12): p. 3279-3289.

208. Chen, C., et al., *A three-dimensionally chitin nanofiber/carbon nanotube hydrogel network for foldable conductive paper.* Carbohydrate Polymers, 2015. **134**: p. 309-313.
209. Hatanaka, D., K. Yamamoto, and J.-i. Kadokawa, *Preparation of chitin nanofiber-reinforced carboxymethyl cellulose films.* International Journal of Biological Macromolecules, 2014. **69**: p. 35-38.
210. Chang, P.R., et al., *Starch-based composites reinforced with novel chitin nanoparticles.* Carbohydrate Polymers, 2010. **80**(2): p. 420-425.
211. Herrera, N., et al., *Functionalized blown films of plasticized polylactic acid/chitin nanocomposite: Preparation and characterization.* Materials & Design, 2016. **92**: p. 846-852.
212. Salaberria, A.M., et al., *Role of chitin nanocrystals and nanofibers on physical, mechanical and functional properties in thermoplastic starch films.* Food Hydrocolloids, 2015. **46**: p. 93-102.
213. Robles, E., et al., *Self-bonded composite films based on cellulose nanofibers and chitin nanocrystals as antifungal materials.* Carbohydrate Polymers, 2016. **144**: p. 41-49.
214. Mushi, N.E., S. Utsel, and L.A. Berglund, *Nanostructured biocomposite films of high toughness based on native chitin nanofibers and chitosan.* Frontiers in chemistry, 2014. **2**: p. 99-99.
215. Wang, B., et al., *Thermo-mechanical properties of the composite made of poly (3-hydroxybutyrate-co-3-hydroxyvalerate) and acetylated chitin nanocrystals.* Carbohydrate Polymers, 2013. **95**(1): p. 100-106.
216. Watthanaphanit, A., et al., *Fabrication, structure, and properties of chitin whisker-reinforced alginate nanocomposite fibers.* Journal of Applied Polymer Science, 2008. **110**(2): p. 890-899.
217. Sriupayo, J., et al., *Preparation and characterization of α-chitin whisker-reinforced chitosan nanocomposite films with or without heat treatment.* Carbohydrate Polymers, 2005. **62**(2): p. 130-136.
218. Zhu, L., K. Liang, and Y. Ji, *Prominent reinforcing effect of chitin nanocrystals on electrospun polydioxanone nanocomposite fiber mats.* Journal of the Mechanical Behavior of Biomedical Materials, 2015. **44**: p. 35-42.
219. Ji, Y., X. Wang, and K. Liang, *Regulating the mechanical properties of poly(1,8-octanediol citrate) bioelastomer via loading of chitin nanocrystals.* RSC Advances, 2014. **4**(78): p. 41357-41363.
220. Wongpanit, P., et al., *Preparation and characterization of chitin whisker-reinforced silk fibroin nanocomposite sponges.* European Polymer Journal, 2007. **43**(10): p. 4123-4135.
221. Butchosa, N., et al., *Nanocomposites of bacterial cellulose nanofibers and chitin nanocrystals: fabrication, characterization and bactericidal activity.* Green Chemistry, 2013. **15**(12): p. 3404.
222. Ang-atikarnkul, P., A. Watthanaphanit, and R. Rujiravanit, *Fabrication of cellulose nanofiber/chitin whisker/silk sericin bionanocomposite sponges and characterizations of their physical and biological properties.* Composites Science and Technology, 2014. **96**: p. 88-96.
223. de Sousa Mol, A. and R.L. Oréfice, *Preparation of chitin nanofibers (whiskers) and their application as property-recovery agents in re-processed polypropylene.* Polymer Bulletin, 2016. **73**(3): p. 661-675.
224. Herrera, N., et al., *Plasticized polylactic acid nanocomposite films with cellulose and chitin nanocrystals prepared using extrusion and compression molding with two cooling rates: Effects on mechanical, thermal and optical properties.* Composites Part A: Applied Science and Manufacturing, 2016. **83**: p. 89-97.
225. Liu, H., et al., *Electrospun composite nanofiber membrane of poly(l-lactide) and surface grafted chitin whiskers: Fabrication, mechanical properties and cytocompatibility.* Carbohydrate Polymers, 2016. **147**: p. 216-225.
226. Zeng, M., et al., *Preparation and Characterization of Nanocomposite Films from Chitin Whisker and Waterborne Poly(ester-urethane) With or Without Ultra-Sonification Treatment.* Journal of Macromolecular Science, Part A, 2010. **47**(8): p. 867-876.
227. Huang, Y., et al., *Effects of Chitin Whiskers on Physical Properties and Osteoblast Culture of Alginate Based Nanocomposite Hydrogels.* Biomacromolecules, 2015. **16**(11): p. 3499-3507.

228. Yan, W., et al., *Chitin nanocrystal reinforced wet-spun chitosan fibers.* Journal of Applied Polymer Science, 2014. **131**(19): p. n/a-n/a.
229. Huang, Y., et al., *Structure and Properties of Cellulose Films Reinforced by Chitin Whiskers.* Macromolecular Materials and Engineering, 2013. **298**(3): p. 303-310.
230. Corvaglia, S., et al., *Chitin whiskers reinforced carrageenan films as low adhesion cell substrates.* International Journal of Polymeric Materials and Polymeric Biomaterials, 2016. **65**(11): p. 574-580.
231. Saralegi, A., et al., *Shape-memory bionanocomposites based on chitin nanocrystals and thermoplastic polyurethane with a highly crystalline soft segment.* Biomacromolecules, 2013. **14**(12): p. 4475-82.
232. Li, Z., et al., *Structure and properties of chitin whisker reinforced papers for food packaging application.* BioResources, 2015. **10**(2): p. 2995-3004.
233. Ma, Z., et al., *Graphene oxide/chitin nanofibril composite foams as column adsorbents for aqueous pollutants.* Carbohydrate Polymers, 2016. **144**: p. 230-237.
234. De Sousa Mol, A., I. Martins, and R.L. Oréfice, *Surface-pegylated chitin whiskers as an effective additive to enhance the mechanical properties of recycled ABS.* Journal of Applied Polymer Science, 2015. **132**(35).
235. Stephan, A.M., et al., *Chitin-Incorporated Poly(ethylene oxide)-Based Nanocomposite Electrolytes for Lithium Batteries.* The Journal of Physical Chemistry B, 2009. **113**(7): p. 1963-1971.
236. Liu, M., et al., *Tough and highly stretchable polyacrylamide nanocomposite hydrogels with chitin nanocrystals.* International Journal of Biological Macromolecules, 2015. **78**(0): p. 23-31.
237. Ji, Y.-l., et al., *Preparation of chitin nanofibril/polycaprolactone nanocomposite from a nonaqueous medium suspension.* Carbohydrate Polymers, 2012. **87**(3): p. 2313-2319.
238. Muzzarelli, R.A.A., et al., *Chitin nanofibrils/chitosan glycolate composites as wound medicaments.* Carbohydrate Polymers, 2007. **70**(3): p. 274-284.
239. Hassanzadeh, P., et al., *Ultrastrong and flexible hybrid hydrogels based on solution self-assembly of chitin nanofibers in gelatin methacryloyl (GelMA).* Journal of Materials Chemistry B, 2016. **4**(15): p. 2539-2543.
240. Jin, J., et al., *A biomimetic composite from solution self-assembly of chitin nanofibers in a silk fibroin matrix.* Adv Mater, 2013. **25**(32): p. 4482-7.
241. Qi, Z.D., et al., *Multifunctional coating films by layer-by-layer deposition of cellulose and chitin nanofibrils.* Biomacromolecules, 2012. **13**(2): p. 553-8.
242. Blackwell, M., *The fungi: 1, 2, 3 ... 5.1 million species?* American Journal of Botany, 2011. **98**(3): p. 426-438.
243. Taylor, A., et al., *Removal of Escherichia coli from synthetic stormwater using mycofiltration.* Ecological Engineering, 2014.
244. Stamets, P., *Mycelium Running: How Mushrooms Can Help Save the World*. 2005: Ten Speed Press.
245. Lopata, A.L., R.E. O'Hehir, and S.B. Lehrer, *Shellfish allergy.* Clinical and Experimental Allergy, 2010. **40**(6): p. 850-858.
246. European Food Safety, A., *Scientific Opinion on the safety of 'Chitin-glucan' as a Novel Food ingredient.* EFSA Journal, 2010. **8**(7): p. 1687.
247. Khor, E., *Chitin: Fulfilling a Biomaterial Promise*. 2001: Elsevier.
248. Fortea-Verdejo, M., et al., *Upgrading flax nonwovens: Nanocellulose as binder to produce rigid and robust flax fibre preforms.* Composites Part A: Applied Science and Manufacturing, 2016. **83**: p. 63-71.
249. Patterson, A.L., *The Scherrer Formula for X-Ray Particle Size Determination.* Physical Review, 1939. **56**.

250. Duarte, M.L., et al., *An optimised method to determine the degree of acetylation of chitin and chitosan by FTIR spectroscopy.* International Journal of Biological Macromolecules, 2002. **31**(1-3): p. 1-8.
251. Troger, J., et al., *Determination of the surface tension of microporous membranes using wetting kinetics measurements.* Colloids and Surfaces a-Physicochemical and Engineering Aspects, 1998. **134**(3): p. 299-304.
252. Schultz, J., L. Lavielle, and C. Martin, *The Role of the Interface in Carbon Fibre-Epoxy Composites.* The Journal of Adhesion, 1987. **23**(1): p. 45-60.
253. Topalovic, T., et al., *Analysis of the effects of catalytic bleaching on cotton.* Cellulose, 2007. **14**(4): p. 385-400.
254. McGarry, A. and K.S. Burton, *Mechanical properties of the mushroom, Agaricus bisporus.* Mycological Research, 1994. **98**(2): p. 241-245.
255. Jolivet, S., et al., *Agaricus bisporus browning: a review.* Mycological Research, 1998. **102**: p. 1459-1483.
256. Hubbe, M.A., R.A. Venditti, and O.J. Rojas, *What happens to cellulosic fibers during papermaking and recycling? A review.* BioResources, 2007. **2**(4): p. 739-788.
257. Welinder, B.S., *The crustacean cuticle - I. Studies on the composition of the cuticle.* Comparative Biochemistry and Physiology, 1974. **47**(2-A): p. 779-787.
258. Welinder, B.S., *The crustacean cuticle-III. Composition of the individual layers in Cancer pagurus cuticle.* Comparative Biochemistry and Physiology a-Physiology, 1975. **52**(4): p. 659-663.
259. Shahidi, F. and J. Synowiecki, *Isolation and Characterization of Nutrients and Value-Added Products from Snow Crab (Chinoecetes opilio) and Shrimp (Pandalus borealis) Processing Discards.* Journal of Agricultural and Food Chemistry, 1991. **39**(8): p. 1527-1532.
260. Sagheer, F.A.A., et al., *Extraction and characterization of chitin and chitosan from marine sources in Arabian Gulf.* Carbohydrate Polymers, 2009. **77**(2): p. 410-419.
261. Smiderle, F.R., et al., *Polysaccharides from Agaricus bisporus and Agaricus brasiliensis show similarities in their structures and their immunomodulatory effects on human monocytic THP-1 cells.* BMC Complementary and Alternative Medicine, 2011. **11**.
262. Patyshakuliyeva, A., et al., *Carbohydrate utilization and metabolism is highly differentiated in Agaricus bisporus.* BMC Genomics, 2013. **14**(1): p. 1-14.
263. Uetani, K. and H. Yano, *Nanofibrillation of Wood Pulp Using a High-Speed Blender.* Biomacromolecules, 2010. **12**(2): p. 348-353.
264. Chen, W., et al., *Revealing the structures of cellulose nanofiber bundles obtained by mechanical nanofibrillation via TEM observation.* Carbohydrate Polymers, 2015. **117**: p. 950-956.
265. Rojo, E., et al., *Comprehensive elucidation of the effect of residual lignin on the physical, barrier, mechanical and surface properties of nanocellulose films.* Green Chemistry, 2015. **17**(3): p. 1853-1866.
266. Focher, B., et al., *Alkaline N-deacetylation of chitin enhanced by flash treatments. Reaction kinetics and structure modification.* Carbohydrate Polymers, 1990. **12**(4): p. 405-418.
267. Zhang, Y., et al., *Determination of the degree of deacetylation of chitin and chitosan by X-ray powder diffraction.* Carbohydr Res, 2005. **340**(11): p. 1914-7.
268. Segal, L., et al., *An empirical method for estimating the degree of crystallinity of native cellulose using the X-ray diffractometer.* Textile Research Journal, 1959. **29**(10): p. 786-794.
269. Park, S., et al., *Cellulose crystallinity index: measurement techniques and their impact on interpreting cellulase performance.* Biotechnol Biofuels, 2010. **3**: p. 10.
270. Torres-Rendon, J.G., et al., *Mechanical performance of macrofibers of cellulose and chitin nanofibrils aligned by wet-stretching: a critical comparison.* Biomacromolecules, 2014. **15**(7): p. 2709-17.

271. Salmon, S. and S.M. Hudson, *Crystal morphology, biosynthesis, and physical assembly of cellulose, chitin, and chitosan.* Journal of Macromolecular Science, Part C: Polymer Reviews, 1997. **37**(2): p. 199-276.
272. Wessels, J.G.H., *Hydrophobins: Proteins that Change the Nature of the Fungal Surface*, in *Advances in Microbial Physiology*, R.K. Poole, Editor. 1996, Academic Press. p. 1-45.
273. Baltazar-y-Jimenez, A. and A. Bismarck, *Wetting behaviour, moisture up-take and electrokinetic properties of lignocellulosic fibres.* Cellulose, 2007. **14**(2): p. 115-127.
274. Ylä-Mäihäniemi, P.P., et al., *Inverse gas chromatographic method for measuring the dispersive surface energy distribution for particulates.* Langmuir, 2008. **24**(17): p. 9551-9557.
275. Shah, U.V., et al., *Decoupling the contribution of surface energy and surface area on the cohesion of pharmaceutical powders.* Pharmaceutical Research, 2015. **32**(1): p. 248-259.
276. Ho, R., et al., *Effect of milling on particle shape and surface energy heterogeneity of needle-Shaped crystals.* Pharmaceutical Research, 2012. **29**(10): p. 2806-2816.
277. Belgacem, M.N., A. Blayo, and A. Gandini, *Surface Characterization of Polysaccharides, Lignins, Printing Ink Pigments, and Ink Fillers by Inverse Gas Chromatography.* Journal of Colloid and Interface Science, 1996. **182**(2): p. 431-436.
278. Shi, B., et al., *Surface characterization of chitin by inverse gas chromatography.* Carbohydrate Polymers, 2007. **67**(3): p. 398-402.
279. Cunha, A.G., et al., *What Is the Real Value of Chitosan's Surface Energy?* Biomacromolecules, 2008. **9**(2): p. 610-614.
280. Bismarck, A., et al., *Electrokinetic and contact angle measurements of grafted carbon fibers.* Colloid and Polymer Science, 1998. **276**(12): p. 1110-1116.
281. Stana-Kleinschek, K., et al., *Reactivity and electrokinetical properties of different types of regenerated cellulose fibres.* Colloids and Surfaces A: Physicochemical and Engineering Aspects, 2001. **195**(1–3): p. 275-284.
282. Stawski, D., et al., *Thermogravimetric analysis of chitins of different origin.* Journal of Thermal Analysis and Calorimetry, 2008. **93**(2): p. 489-494.
283. Wanjun, T., W. Cunxin, and C. Donghua, *Kinetic studies on the pyrolysis of chitin and chitosan.* Polymer Degradation and Stability, 2005. **87**(3): p. 389-394.
284. I'Anson, S.J. and W.W. Sampson, *Competing Weibull and stress-transfer influences on the specific tensile strength of a bonded fibrous network.* Composites Science and Technology, 2007. **67**(7–8): p. 1650-1658.
285. I'Anson, S.J., W.W. Sampson, and S. Savani, *Density dependent influence of grammage on tensile properties of handsheets.* Journal of Pulp and Paper Science, 2008. **34**(3): p. 182-189.
286. King, A. and R. Watling, *Paper made from bracket fungi.* Mycologist, 1997. **11**(2): p. XI-54.
287. Novák, M., et al., *Yeast β(1-3),(1-6)-d-glucan films: Preparation and characterization of some structural and physical properties.* Carbohydrate Polymers, 2012. **87**(4): p. 2496-2504.
288. Stana-Kleinschek, K., S. Strnad, and V. Ribitsch, *Surface characterization and adsorption abilities of cellulose fibers.* Polymer Engineering and Science, 1999. **39**(8): p. 1412-1424.
289. Mohanty, A.K., M. Misra, and G. Hinrichsen, *Biofibres, biodegradable polymers and biocomposites: An overview.* Macromolecular Materials and Engineering, 2000. **276-277**: p. 1-24.
290. Ververis, C., et al., *Fiber dimensions, lignin and cellulose content of various plant materials and their suitability for paper production.* Industrial Crops and Products, 2004. **19**(3): p. 245-254.
291. Pandey, K.K., *A study of chemical structure of soft and hardwood and wood polymers by FTIR spectroscopy.* Journal of Applied Polymer Science, 1999. **71**(12): p. 1969-1975.
292. Garvey, C.J., I.H. Parker, and G.P. Simon, *On the interpretation of X-ray diffraction powder patterns in terms of the nanostructure of cellulose I fibres.* Macromolecular Chemistry and Physics, 2005. **206**(15): p. 1568-1575.
293. French, A.D., *Idealized powder diffraction patterns for cellulose polymorphs.* Cellulose, 2014. **21**(2): p. 885-896.

294. Jelsma, J. and D.R. Kreger, *Observations on the cell-wall compositions of the bracket fungi Laetiporus sulphureus and Piptoporus betulinus.* Archives of Microbiology, 1978. **119**(3): p. 249-255.
295. Harada, T., et al., *Effect of heating on formation of curdlan gels.* Carbohydrate Polymers, 1994. **24**(2): p. 101-106.
296. Tamura, N., M. Wada, and A. Isogai, *TEMPO-mediated oxidation of (1 → 3)-β-d-glucans.* Carbohydrate Polymers, 2009. **77**(2): p. 300-305.
297. Henriksson, M. and L.A. Berglund, *Structure and properties of cellulose nanocomposite films containing melamine formaldehyde.* Journal of Applied Polymer Science, 2007. **106**(4): p. 2817-2824.
298. Wu, C., et al., *Structural characterization and properties of konjac glucomannan/curdlan blend films.* Carbohydrate Polymers, 2012. **89**(2): p. 497-503.
299. Sun, Y., et al., *Preparation and characterization of novel curdlan/chitosan blending membranes for antibacterial applications.* Carbohydrate Polymers, 2011. **84**(3): p. 952-959.
300. Ahmad, M., N.P. Nirmal, and J. Chuprom, *Blend film based on fish gelatine/curdlan for packaging applications: spectral, microstructural and thermal characteristics.* RSC Advances, 2015. **5**(120): p. 99044-99057.
301. Schulz, D., U. Rau, and F. Wagner, *Characteristics of films prepared from native and modified branched β-1,3-d-glucans.* Carbohydrate Polymers, 1992. **18**(4): p. 295-299.
302. Blahovec, J., et al., *Tensile properties of microbial β-glucan films.* Polymer Engineering & Science, 2011. **51**(12): p. 2564-2570.
303. Hejlová, A. and J. Blahovec, *Stress relaxation and activation volume in tension in β-glucan and chitosan films.* Polymer Engineering & Science, 2014: p. n/a-n/a.
304. Kawahara, Y. and A. Koganemaru, *Development of novel film using paramylon prepared from Euglena gracilis.* Journal of Applied Polymer Science, 2006. **102**(4): p. 3495-3497.
305. Shibakami, M., et al., *Preparation of transparent self-standing thin films made from acetylated euglenoid β-1,3-glucans.* Carbohydrate Polymers, 2015. **133**: p. 421-428.
306. Skendi, A., et al., *Structure and rheological properties of water soluble β-glucans from oat cultivars of Avena sativa and Avena bysantina.* Journal of Cereal Science, 2003. **38**(1): p. 15-31.
307. Ying, R., et al., *Hydration and mechanical properties of arabinoxylans and β-d-glucans films.* Carbohydrate Polymers, 2013. **96**(1): p. 31-38.
308. González, I., et al., *From paper to nanopaper: evolution of mechanical and physical properties.* Cellulose, 2014. **21**(4): p. 2599-2609.
309. Siqueira, G., J. Bras, and A. Dufresne, *New process of chemical grafting of cellulose nanoparticles with a long chain isocyanate.* Langmuir, 2010. **26**(1): p. 402-411.
310. Rjiba, N., et al., *A study of the surface properties of cotton fibers by inverse gas chromatography.* Journal of Colloid and Interface Science, 2007. **314**(2): p. 373-380.
311. Papirer, E., et al., *Inverse gas chromatography investigation of the surface properties of cellulose.* Journal of Adhesion Science and Technology, 2000. **14**(3): p. 321-337.
312. Bismarck, A., M.E. Kumru, and J. Springer, *Characterization of several polymer surfaces by streaming potential and wetting measurements: Some reflections on acid-base interactions.* Journal of Colloid and Interface Science, 1999. **217**(2): p. 377-387.
313. Bismarck, A., et al., *Surface characterization of natural fibers; surface properties and the water up-take behavior of modified sisal and coir fibers.* Green Chemistry, 2001. **3**(2): p. 100-107.
314. Bismarck, A., et al., *Characterization of several modified jute fibers using zeta-potential measurements.* Colloid and Polymer Science, 2000. **278**(3): p. 229-235.
315. Bismarck, A., et al., *Surface characterization of flax, hemp and cellulose fibers; Surface properties and the water uptake behavior.* Polymer Composites, 2002. **23**(5): p. 872-894.
316. Bellmann, C., et al., *Electrokinetic properties of natural fibres.* Colloids and Surfaces A: Physicochemical and Engineering Aspects, 2005. **267**(1–3): p. 19-23.

317. Jonoobi, M., et al., *Different preparation methods and properties of nanostructured cellulose from various natural resources and residues: a review.* Cellulose, 2015. **22**(2): p. 935-969.
318. Sehaqui, H., et al., *Wood cellulose biocomposites with fibrous structures at micro- and nanoscale.* Composites Science and Technology, 2011. **71**(3): p. 382-387.
319. Papirer, E., et al., *Comparison of the surface properties of graphite, carbon black and fullerene samples, measured by inverse gas chromatography.* Carbon, 1999. **37**(8): p. 1265-1274.
320. Montrikittiphant, T., et al., *Bacterial Cellulose Nanopaper as Reinforcement for Polylactide Composites: Renewable Thermoplastic NanoPaPreg.* Macromolecular Rapid Communications, 2014.
321. Zweben, C., *Is there a size effect in composites?* Composites, 1994. **25**(6): p. 451-454.
322. Wisnom, M.R., *Size effects in the testing of fibre-composite materials.* Composites Science and Technology, 1999. **59**(13): p. 1937-1957.
323. Scheider, I., et al., *Size effects in short fibre reinforced composites.* Engineering Fracture Mechanics, 2013. **100**: p. 17-27.
324. Dormanns, J.W., et al., *Positive size and scale effects of all-cellulose composite laminates.* Composites Part A: Applied Science and Manufacturing, 2016. **85**: p. 65-75.
325. Wang, A.S.D., *Fracture mechanics of sublaminate cracks in composite materials.* Composites technology review, 1984. **6**(2): p. 45-62.
326. Wisnom, M.R., *The Relationship between Tensile and Flexural Strength of Unidirectional Composites.* Journal of Composite Materials, 1992. **26**(8): p. 1173-1180.
327. Bullock, R.E., *Strength Ratios of Composite Materials in Flexure and in Tension.* Journal of Composite Materials, 1974. **8**(2): p. 200-206.
328. Zweben, C., W.S. Smith, and M.W. Wardle, *Test methods for fiber tensile stregth, composite flexural modulus, and properties of fabric-reinforced laminates.* ASTM Special Technical Publication, 1979(674): p. 228-262.
329. Messiry, M.E., *Theoretical analysis of natural fiber volume fraction of reinforced composites.* Alexandria Engineering Journal, 2013. **52**(3): p. 301-306.
330. Zweben, C., *Fracture mechanics and composite materials: A critical analysis.* ASTM Special Technical Publication, 1972: p. 65-97.
331. Mtibe, A., et al., *A comparative study on properties of micro and nanopapers produced from cellulose and cellulose nanofibres.* Carbohydrate Polymers, 2015. **118**: p. 1-8.
332. Yousefi, H., et al., *Comparative study of paper and nanopaper properties prepared from bacterial cellulose nanofibers and fibers/ground cellulose nanofibers of canola straw.* Industrial Crops and Products, 2013. **43**: p. 732-737.
333. Spence, K.L., et al., *A comparative study of energy consumption and physical properties of microfibrillated cellulose produced by different processing methods.* Cellulose, 2011. **18**(4): p. 1097-1111.
334. Pintiaux, T., et al., *Binderless materials obtained by thermo-compressive processing of lignocellulosic fibers: A Comprehensive review.* BioResources, 2015. **10**(1): p. 1915-1963.
335. Zhang, D., A. Zhang, and L. Xue, *A review of preparation of binderless fiberboards and its self-bonding mechanism.* Wood Science and Technology, 2015. **49**(4): p. 661-679.
336. Okuda, N., K. Hori, and M. Sato, *Chemical changes of kenaf core binderless boards during hot pressing (I): influence of the pressing temperature condition.* Journal of Wood Science, 2006. **52**(3): p. 244-248.
337. Okuda, N., K. Hori, and M. Sato, *Chemical changes of kenaf core binderless boards during hot pressing (II): effects on the binderless board properties.* Journal of Wood Science, 2006. **52**(3): p. 249-254.
338. Arévalo, R. and T. Peijs, *Binderless all-cellulose fibreboard from microfibrillated lignocellulosic natural fibres.* Composites Part A: Applied Science and Manufacturing, 2016. **83**: p. 38-46.
339. Anglès, M.N., et al., *Binderless composites from pretreated residual softwood.* Journal of Applied Polymer Science, 1999. **73**(12): p. 2485-2491.

340. Bouajila, J., et al., *Lignin plasticization to improve binderless fiberboard mechanical properties.* Polymer Engineering & Science, 2005. **45**(6): p. 809-816.
341. Pommet, M., et al., *Surface modification of natural fibers using bacteria: Depositing bacterial cellulose onto natural fibers to create hierarchical fiber reinforced nanocomposites.* Biomacromolecules, 2008. **9**(6): p. 1643-1651.
342. Lee, K.-Y., et al., *Hierarchical composites reinforced with robust short sisal fibre preforms utilising bacterial cellulose as binder.* Composites Science and Technology, 2012. **72**(13): p. 1479-1486.
343. Lee, K.Y., et al., *Manufacturing of robust natural fiber preforms utilizing bacterial cellulose as binder.* Journal of Visualized Experiments, 2014(87).

APPENDIX A

Compliance Determination during Mechanical Testing

1. Theory:

1) Due to atomic interspacing of any material, any testing equipment will be subjected to compliance however tiny. The use of extensometer for strain measurement will solve this problem (as in Chapter 6). However, for small test specimens (as in Chapter 4 & Chapter 5), when this cannot be done, the strain can be measured by its crosshead movement using high resolution photo encoder/laser, or by means of system compliance.
2) For compliance measurement, the system can be viewed as 2 springs in series resulting to total stiffness, $k_{total,}$ which is sum of specimen stiffness, k_{sample}, and stiffness outside of the sample, $k_{machine}$. Compliance is inverse of stiffness and thus:

$$\frac{1}{k_{total}} = \frac{1}{k_{machine}} + \frac{1}{k_{sample}} \quad (1)$$

$$C_{\text{total}} = C_{\text{machine}} + C_{\text{sample}} \quad (2)$$

3) Using Hooke Law, one can formulate expression relating C_{sample} to sample properties: gage length (l_0), cross-section area (A), and modulus (E) :

$$E = \frac{\sigma}{\varepsilon} = \frac{F/A}{\Delta l/l_0} = \frac{Fl_0}{A\Delta l} = k_{sample}\frac{l_0}{A} = \frac{l_0}{C_{sample}\,A} \quad (3)$$

Combining (2) and (3):

$$C_{total} = C_{machine} + \frac{l_0}{E\,A} \quad (4)$$

Equation (4) is equation of line, y = mx +c, where sample gage length, l_0 is independent variable and C_{total} is dependent variable. 1/EA is line slope and C_{machine} is y intercept of best linear fit. The modulus of sample can be calculated by solving equation (4) for E :

$$E = \frac{l_0}{(C_{total} - C_{machine})A} \quad (5)$$

Reference:

1. Kant, M. and Hay, J.(2011). *Measurement of System Compliance Using Template Grip Technique and Agilent T150*, Agilent Technologies Application Notes.
2. ASTM C1557-14

2. Compliance Determination

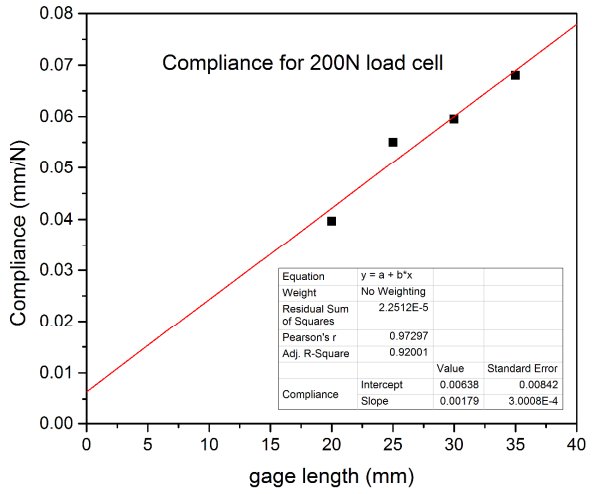

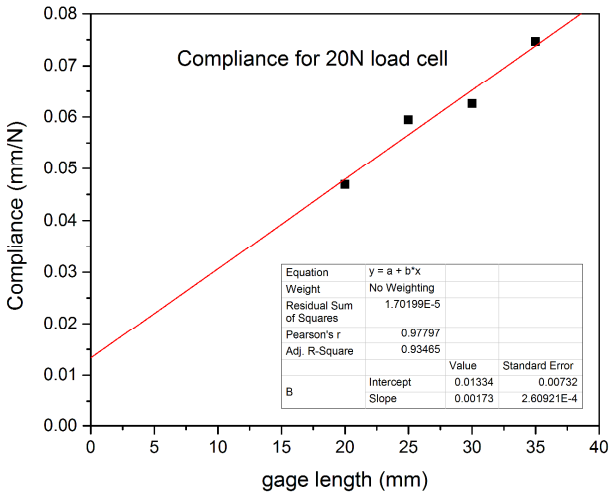

(200N load cell) system/machine compliance

Equipment : Microtester TST350 (Linkam Scientific Instruments, Surrey, UK)
Test Date : 5 March 2014/ Wan

Load cell : 200N
Crosshead speed : 1 mm/min
Specimens : polyimide film having thickness of 0.0023 mm and width approximately 2.2 mm at different gage length, (20mm, 25mm, 30mm, and 35mm). Five specimens were tested per different gage length.

Machine Compliance : **6.38×10^{-3} mm/N**

(20N load cell) system/machine compliance

Equipment : Microtester TST350 (Linkam Scientific Instruments, Surrey, UK)
Test Date : 17 December 2014/ Wan

Load cell : 20N
Crosshead speed : 1 mm/min
Specimens : polyimide film having thickness of 0.0023 mm and width approximately 2.2 mm at different gage length, (20mm, 25mm, 30mm, and 35mm). Five specimens were tested per different gage length.

Machine Compliance : **1.33×10^{-2} mm/N**

APPENDIX B

How Much Nanofibers are there in 1 kg Mushrooms?

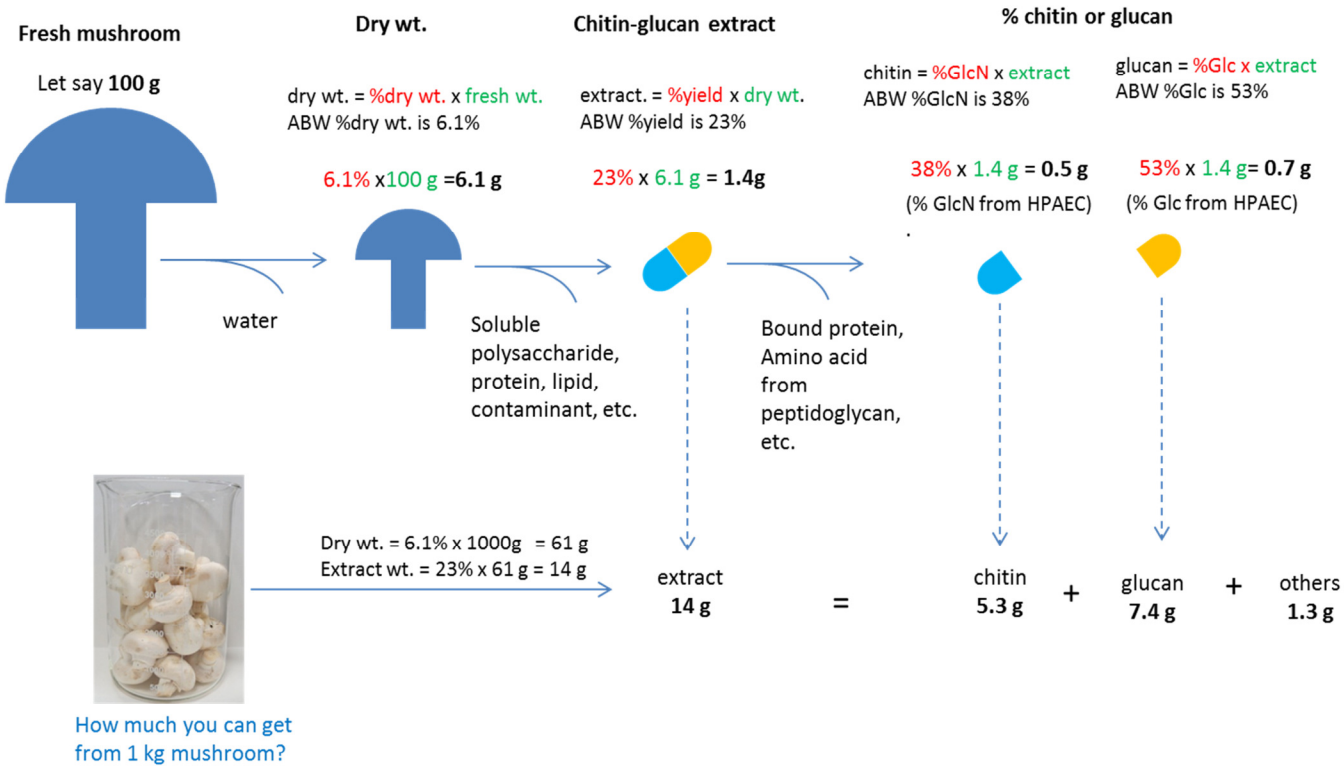

%dry wt. = refer p.60, "…water made up around 94% of their fresh body mass"
In this study, water content in common mushroom was measured by oven dry method, and dry mass obtained were as follows:
Stalk only = 6.05%
Cap only = 7.44%
Whole fruiting body = 6.14%

%yield = refer p.61, see Table 4.1 under yield column
%GlcN = refer p.62; for whole fruit body of common mushroom, take average chitin value for stalk and cap ; e.g. chitin: (36% + 41%) / 2 = 38%
%Glc = refer p.62; for whole fruit body of common mushroom, take average glucan value for stalk and cap; e.g. glucan: (56% + 50%) / 2 = 53%

Notes: the value of % GlcN and %Glc is calculated by taking its proportion per total sugar in Table 4.2, e.g. GlcN for stalk = (29.8 / 83.6) x100 = 36%
